From Research to Applied Geotechnics
N.P. López-Acosta et al. (Eds.)


doi:10.3233/ASMGE190004

# Geotechnical Engineering in Spatially Variable Soft Soils. *The Case of Mexico City.* The 9th Arthur Casagrande Lecture

# Ingeniería geotécnica en suelos blandos con variación espacial. *El caso de la Ciudad de México.* La 9.ª Conferencia Arthur Casagrande

by

Gabriel Y. AUVINET
*Professor, Instituto de Ingeniería,*
*Universidad Nacional Autónoma de México,*
*Mexico City, Mexico*
GAuvinetG@iingen.unam.mx

prepared for

XVI Pan-American Conference on Soil Mechanics and Geotechnical Engineering
Cancún, Mexico
November, 2019

# The 9th Arthur Casagrande Lecture

**Gabriel Y. AUVINET**

Gabriel Auvinet obtained a Doctor degree in Engineering from UNAM, Mexico in 1986. He is a Researcher at Instituto de Ingeniería (Institute of Engineering), UNAM (National University of Mexico) and Faculty member of UNAM Postgraduate program. He was a guest Professor in the French Universities of Grenoble (1986), Nancy (1993-1994) and Clermont (2003-2004). He has directed a large number of professional, master and doctoral theses and is author of 367 papers in Journals and National and International Conferences and 248 research reports. He is presently Head of the Geotechnical Computing Laboratory of Institute of Engineering, UNAM. He has dedicated his research work to Soil Mechanics with emphasis on special foundations and tunnels in consolidating soft soils. Simultaneously, he has developed new techniques for application of probabilistic and geostatistical methods in Civil Engineering. He has been involved as a consultant in many large projects in Mexico, Central and South America and Europe. He performed geostatistical and geomechanical analyses for the design of award-winning Rion-Antirion bridge foundation in Greece. Professor Auvinet has been President of the Mexican Society for Soil Mechanics (SMIG, 1992-1993) and Vice President for North America of International Society for Soil Mechanics and Geotechnical Engineering (ISSMGE, 2009-2013). He has received a number of teaching and research awards in Mexico, France and South America. From 2001 to 2009 he chaired ISSMGE's Technical Committee TC36: "Foundation Engineering in difficult soft soils conditions". In 2002 he delivered the Sixteenth "Nabor Carrillo" Lecture: "Uncertainty in Geotechnical Engineering". He is a member of the Mexican Science Academy, and National Engineering Academy of Mexico. In 2015, He received a Doctor Honoris Causa degree from Universidad Nacional de Córdoba. Argentina. He is author of the updated version (2017) of the internationally known book "The subsoil of Mexico City".

## Table of contents

## List of Tables



## List of Figures

# The 9th Casagrande Lecture Presentation and Biographical Sketch of Professor Gabriel Auvinet Guichard

Efraín OVANDO SHELLEY[a,1]
[a] *Research Professor, Instituto de Ingeniería, Universidad Nacional Autónoma de México, Mexico*

Today we meet again to honour the memory of Professor Arthur Casagrande, as we did on eight previous occasions. We pride ourselves that the memory of Casagrande is honoured like this in Mexico, a country that Casagrande knew as a geotechnician, a country where he unselfishly displayed his wit and knowledge, a place that profited from that display. In previous Panamerican conferences the lecture bearing his name has always been of the highest quality, given by colleagues of the highest level. Our lecturer today is by no means the exception.

Professor Gabriel Auvinet obtained the title of civil engineer from the *Ecole Spéciale des Travaux Publics de Paris.* Later, he got a diploma as a specialist in prestressed concrete from the *Centre des Hautes Etudes de la Construction*, also in Paris. He has been living in Mexico since 1968. He joined the Graduate School of Engineering at UNAM where he got his master´s and doctoral degrees. The totality of his career as a research engineer has taken place at the *Instituto de Ingeniería* of UNAM, which he joined formally in 1970. There, he benefited from the influence of Raúl J. Marsal, Daniel Reséndiz, Jesús Alberro and Emilio Rosenblueth who backed him at the beginning of his career. He has been the Coordinator of the Geotechnics Section and Sub-Director at the Institute, as well as head of the Civil Engineering Department at the Graduate School of Engineering at UNAM.

In his study of granular media, Gabriel Auvinet put forth an original description of discrete media with which a continuous link between the granular scale and the scale of continua can be established by means of the concept of the *geometric scale effect*, expressed in terms of probabilities. This allowed him, for example, to provide an answer to the problem of Soritos, posed by the ancient Greeks, i. e. "*How many particles in a group of grains are required to have a mass of sand?"* In developing these concepts, he pondered on their practical implications in Geotechnics, such as the definition of soil mixtures having the minimum possible porosity, the design of filters and the selection and control of materials for earth structures, the evaluation of the hydraulic conductivity of porous media and the mechanical behaviour of discrete media. His algorithms have also been used by specialists of other fields, especially in connection to the interpretation of the mechanical behaviour of metallic dusts.

His most important contributions in the field of numerical and analytical modelling are related to the analysis of deep foundations in Mexico City's difficult soil conditions. Early in his career, he developed graphical, numerical and analytical elasticity-based solutions relevant for the analysis of foundations. Later he developed an interest in the analysis of piled foundations in soils undergoing a consolidation process, as in Mexico

[1] Research Professor, Instituto de Ingeniería, UNAM. Email: EOvandoS@iingen.unam.mx

City. Using load cells of his own and novel design, he measured the development of negative friction on point bearing and friction piles in Lake Texcoco. With analytical and numerical models, he interpreted the behaviour of those piles and was able to elucidate the complex interaction mechanism between piles, substructure and soil in deep foundations. After the 1985 earthquakes, he performed and published meticulous interpretations of the behaviour of foundations during that event. He participated in the project for the correction of differential settlements in Mexico City's Metropolitan Cathedral putting forth an original method for analysing a system of rigid inclusions to control soil settlements. In view of his contributions in this field, he coordinated the team responsible for drafting the new regulations for the design of foundations in Mexico City.

Auvinet has actively promoted the application of the probabilistic approach to geotechnical engineering. Using it, he has made significant contributions to the development of new methods to consider uncertainty in soil mechanics analyses. Combined with Geographical Information Systems, he has continuously been using these tools for more nearly three decades to improve on the geotechnical description of the subsoil in the Basin of Mexico. This knowledge has allowed him to develop a geotechnical zoning map present in the city's building code.

On the other hand, Gabriel Auvinet has also come up with a rational interpretation of the fissures that so often appear in Mexico City's lacustrine clays. Using field observations and fracture mechanics, he proposed crack generation and propagation criteria that have been used after the 19 September 2017 earthquake. These criteria are presently being applied under Auvinet´s supervision in the southern portion of the Basin of Mexico, to define confinement and reinforcement techniques with which such a problematic phenomenon can be mitigated or even avoided.

He has also pioneered the development and application of the *stochastic finite element method* with which uncertainties related to the mechanical parameters of soils can be accounted for. He has developed simple, time efficient and innovative techniques for solving three dimensional seepage problems using the Monte Carlo Method, as well as new methods for the assessment of geotechnical risks that can also be used to estimate the reliability of foundations, dams, slopes, trenches, retaining walls and culverts.

He developed the geostatistic model of the foundation soil of the Rion-Antirion bridge on the Gulf of Corynth, in Greece, one of the largest of the world, collaborating with such specialists as Professors Ralph B. Peck, Ricardo Dobry and Alain Pecker. His contributions in this field have been recognized by his peers in the international geotechnical community. Recently, application of geostatistics in the project of the new airport for Mexico City in Texcoco proved to be a most useful tool for developing a comprehensive stratigraphical model at that site. His contributions in that project were also paramount in analysing the behaviour of airport infrastructure in the short and long terms.

Dr. Auvinet´s knowledge and research into earth and rockfill dams led him to participate as a consultant in the design, construction and behaviour assessments of many such works not only in Mexico but also in France, Central and South America. He co-authored the seminal book in Spanish on this subject, *"Presas de tierra y enrocamientos*" edited by R. J. Marsal and D. Reséndiz which was awarded the Javier Barros Sierra prize by the *Colegio de Ingenieros Civiles de México*. He was awarded that prize again as a co-author of a manual for Geotechnical construction published by the Mexican Society for Geotechnical Engineering (SMIG).

Professor Auvinet has been President of the Mexican Society for Soil Mechanics (SMIG, 1992-1993) and Vice President for North America of ISSMGE (2009-2013). He has received a number of teaching and research awards in Mexico, France and South America. From 2001 to 2009, he chaired ISSMGE's Technical Committee TC36: "Foundation Engineering in difficult soft soils conditions". In 2002, he delivered the Sixteenth "Nabor Carrillo" Lecture: "Uncertainty in Geotechnical Engineering". He is a member of the Mexican Science Academy, and National Engineering Academy of Mexico. In 2015, he received a Doctor Honoris Causa degree from *Universidad Nacional de Córdoba. Argentina*. He is author of the updated version (2017) of the internationally known book "The subsoil of Mexico City".

Direct beneficiaries of his research work at the Instituto de Ingeniería and in French universities are the 172 students that have up to now received their bachelors, masters, and doctoral degrees under his tutorship. The rest of us have profited from his publications, lectures, informal talks and his humour.

Gabriel Auvinet´s broader interests overlap Geotechnical Engineering. He is also a historian, a profound connoisseur and also a joyful one, of a large part of Mexican History and of the history of Mexico City. His incursions into historical research are known only by a few and it is only needed that more get to know them to be more recognized in this field, as in Geotechnics. He is also an art lover and appreciates good food at least as much as History or Soil Mechanics. In that I declare and confess that I have been his occasional accomplice.

It is not enough goodness, nor fine manners, nor the appreciation for the good things of life, nor historiographic rigour, nor the love for his adoptive country to justify his designation as the ninth Casagrande Lecturer. My words, those of a friend, are of little use to argue on his behalf, in attention to objectivity, which in this case I can´t pretend to have, nor do I wish to have. His career as a researcher and a teacher says very much more, at times as a field engineer and on other occasions as a mender of geotechnical misdemeanours, as a rigorous practitioner of Soil Mechanics, an art that, without science, ceases to be in art, as shown by the richness of our lecturer's work.

# Geotechnical Engineering in Spatially Variable Soft Soils.

## *The Case of Mexico City.*

## The 9th Arthur Casagrande Lecture

# Ingeniería geotécnica en suelos blandos con variación espacial.

## *El caso de la Ciudad de México.*

## La 9.ª Conferencia Arthur Casagrande

Gabriel Y. AUVINET[a,2]

[a] *Professor, Instituto de Ingeniería, Universidad Nacional Autónoma de México, Mexico*

**Abstract.** Many large cities such as Tokyo, Bangkok, Río de Janeiro, Recife, Bogota and, of course, Mexico City, to name only a few, were built and are still being developed on soft soils. In many cases, these cities also experience regional subsidence induced by pumping of groundwater from deep local aquifers. Among the sources of uncertainty prevailing in the geotechnical characterization of these sites, soil properties spatial variability is one of the most difficult to deal with since the associated uncertainty cannot be eliminated only by improving laboratory and field-testing techniques. For an accurate evaluation of the subsoil conditions, spatial variations of the soil profile and mechanical properties together with the groundwater conditions must be assessed by performing a sufficient number of soil explorations, processing a generally large amount of data and developing either deterministic or probabilistic models of these variations. The techniques available to develop such models and some difficulties encountered to implement them are examined in this lecture. Some geotechnical analysis and design methods that take into account soft soils spatial variations are also reviewed together with constructions techniques aimed at mitigating consequences of soil variability.

The above considerations are illustrated with reference to Mexico City's highly compressible volcanic lacustrine clays. Models of the spatial variability of these materials developed over the years for different projects using traditional and geostatistical techniques are presented. Some of the geotechnical analysis and construction methods used by geotechnical engineers to deal with soil spatial variability in this megacity once called by Terzaghi "the paradise of soil mechanics", are also discussed.

[2] Dr. Gabriel Y. Auvinet, Laboratorio de Geoinformática, Instituto de Ingeniería, Universidad Nacional Autónoma de México, Torre de Ingeniería, 2º nivel, Ciudad Universitaria, 04510, Ciudad de México, Mexico; e-mail: GAuvinetG@iingen.unam.mx

**Keywords.** Soft soils, geotechnical characterization, spatial variations, deterministic models, probabilistic models, geostatistics, analysis, design, reliability.

**Resumen.** Un gran número de ciudades tales como Tokio, Bangkok, Río de Janeiro, Recife, Bogotá y, por supuesto, la Ciudad de México, para nombrar solamente algunas, han sido construidas y siguen desarrollándose sobre suelos blandos. En muchos casos estos sitios están también afectados por subsidencia regional inducida por el bombeo de agua desde acuíferos profundos locales. Entre las fuentes principales de incertidumbre para la caracterización geotécnica de estos sitios, la variación espacial de las propiedades del suelo es una de las más difíciles de tomar en cuenta porque no puede eliminarse simplemente mejorando la calidad de los ensayes de campo y de laboratorio. Para una satisfactoria evaluación de las condiciones del subsuelo, las variaciones espaciales de la estratigrafía y de las propiedades mecánicas del subsuelo y de las condiciones piezométricas deben ser determinadas mediante un número suficiente de exploraciones, procesando grandes cantidades de datos y desarrollando modelos deterministas o probabilistas que representen estas variaciones. En esta conferencia se examinan las diferentes técnicas existentes para desarrollar tales modelos y las dificultades que comúnmente se encuentran para implementarlas. Se discuten asimismo algunos métodos de análisis y diseño geotécnico y técnicas constructivas que permiten mitigar las consecuencias de las variaciones espaciales del suelo.

Las consideraciones anteriores se ilustran tomando como referencia principal el caso de las arcillas volcánicas altamente compresibles de la ciudad de México. Se presentan algunos modelos que han sido desarrollados para representar las variaciones espaciales de estos materiales recurriendo a técnicas tradicionales y geoestadísticas. Se presentan asimismo algunos métodos de análisis y diseño empleados por los ingenieros geotecnistas para tomar en cuenta la variación espacial del suelo en esta ciudad que fue alguna vez llamada por Terzaghí “el paraíso de la mecánica de suelos”.

**Palabras clave.** Suelos blandos, caracterización geotécnica, variaciones espaciales, modelos deterministas, modelos probabilistas, geoestadística, análisis, diseño, confiabilidad.

## 1. Introduction

Throughout the world, many large cities have been built and are still being developed on soft ground. Large projects are being developed on sites that were previously considered as unfit for construction due to the high compressibility and low shear strength of the soft subsoil. This constitutes a serious challenge for geotechnical engineers.

Foundations of constructions on soft materials must be designed taking into account that they should not be loaded significantly beyond their yielding stress. This is a condition particularly difficult to achieve when the soil characteristics present spatial variations due to their formation process and to local anomalies due to geological or anthropic factors.

Spatial variations of the soil must be assessed by performing a sufficient number of soil explorations, processing a generally large amount of data and developing deterministic or probabilistic models of these variations that can be introduced in geotechnical analyses.

A wide variety of models can be developed, depending on the available information and the problem to be solved. As asserted in the famous sentence attributed to Einstein these models should be “as simple as possible but not more simple”. These models can be deterministic or probabilistic.

In this lecture, the techniques available to develop appropriate models and some difficulties encountered to implement them in practice are examined. Geotechnical analysis and design methods that take into account soft soils spatial variations are also reviewed together with some construction techniques aimed at mitigating consequences of soil variability.

The above considerations are illustrated with reference to the Mexico City's highly compressible volcanic lacustrine clays. Models of the spatial variability of these materials developed over the years for different projects using traditional and geostatistical techniques are presented. Some of the geotechnical analysis and construction methods used by local geotechnical engineers to deal with soil spatial variability in this megacity, which was called by Terzaghi "the paradise of soil mechanics", are also discussed.

## 2. Soft soils

### *2.1. Classification of soft soils*

As asserted by Ladd and DeGroot in a previous Casagrande lecture (2003 [1]), and according to the Unified Soil Classification System (USCS), soft soils are generally clays (CL and CH), silts (ML and MH) and organic soils (OL and OH) that were deposited in an alluvial, lacustrine or marine environment and are essentially saturated.

The Unified Soil Classification System (USCS), an outgrowth of the Airfield Classification system developed by Casagrande (1948 [2]), has remained along the years as the main reference frame for soft soils classification for geotechnical purposes.

Resiliency of USCS is in fact somewhat surprising if it is considered that, as far as soft soils are concerned, this system was probably not based on the best physical and index properties available.

Consider for example soil gravimetric water content, $w$, defined since the early stages of soil mechanics as:

$$w = \frac{W_{\mathrm{w}}}{W_{\mathrm{S}}} \tag{1}$$

where $W_{\mathrm{w}}$ = weight of water in sample, and $W_{\mathrm{S}}$ = weight of solids in sample.

The original argument for using definition of Eq. (1) was apparently that it allowed describing in a simple way the variations of water content and volumetric changes of soils for a given (constant) amount of solids (Spangler and Handy, 1982 [3]). This advantage becomes however a drawback when dealing with soft soil spatial variability. It can in fact be argued that this was a poorly chosen descriptive property, especially for heterogeneous soft soils with high water content. As shown in Appendix I, the parameter defined by Eq. (1) is very unstable for small samples and for high water content soils. Strictly speaking, it cannot be averaged on a volume. Averaging local water contents introduces a bias and overestimates the actual water content of the whole sample (Appendix I). Water content as defined by Eq. (1) can thus be considered as ill-fitted for statistical analyses. Note that Atterberg's limits $w_{\mathrm{L}}$ (liquid limit) and $w_{\mathrm{P}}$ (plasticity limit) are also gravimetric water contents based on Eq. (1).

To avoid these difficulties, water content can be defined differently switching for example to another gravimetric definition adopted in most fields of science:

$$w' = \frac{W_W}{W_T} \tag{2}$$

where $W_T$ = total weight of sample ($= W_W + W_S$).

A volumetric definition of water content can also be adopted:

$$w'' = \frac{V_W}{V_T} \tag{3}$$

where $V_W$ = volume of water in sample, and $V_T$ = total volume of sample.

The merits of these alternative definitions are evaluated in Appendix I.

Some objections to the plasticity chart introduced by Casagrande as a central element of USCS (Figure 1) have also been presented (Gutiérrez García, 2006 [4]).

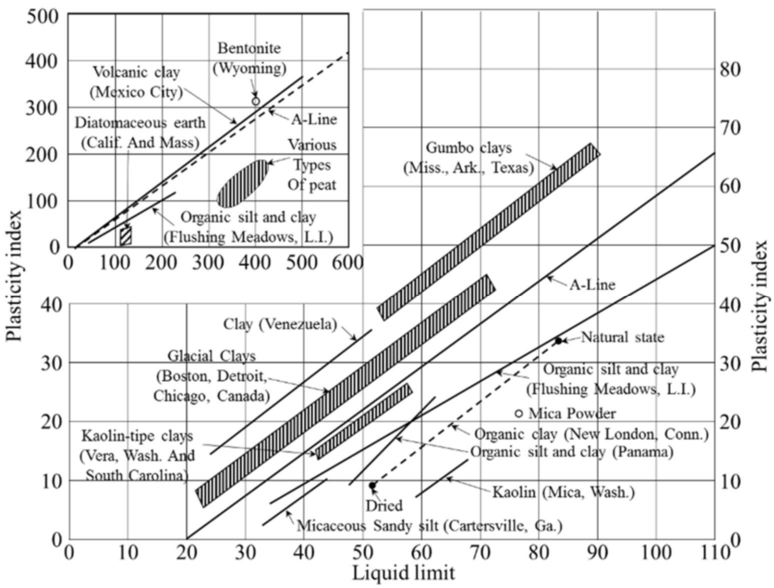


**Figure 1.** Relation between Liquid limit and Plasticity index for typical soils (Casagrande, 1948 [2]).

In this chart, the same variable $w_L$, is present on both the abscissae (Liquid limit, $w_L$) and ordinates (Plasticity Index, PI = $w_L$-$w_P$) axes. This condition introduces a spurious correlation between PI and $w_L$ that explains to some degree why Casagrande observed that all the soils he had studied could be represented along straight lines practically parallel to the A-Line. This objection is not so serious since, apparently, Casagrande was not trying to establish linear correlations between PI and $w_L$ for different soils. He was only looking for a practical way to define a partition of the Atterberg's limits space into disjoint subsets where different types of soils could be classified without ambiguity.

Some proposals have also been published to modify clays classification (Moreno-Maroto and Alonso-Azcárate, 2018 [5]). The advantages of these new concepts have yet to be assessed.

The original USCS system did had to be modified to provide a more detailed classification of organic soils based on Atterberg limits after oven drying (ASTM D2487-85, D2488-84, 1989 [6]). Other modifications based on Von Post humidification tests reflecting the state of the fiber structure of the organic matter have also been proposed (Perrin, 1974 [7]; Magnan, 1980 [8]).

Notwithstanding the above observations, Casagrande's USCS has proven to be a very robust system that has been extremely useful worldwide to myriads of geotechnical engineers during the last 71 years.

### *2.2. Typical soft soil deposits*

A large number of soft soil deposits have been described in the technical literature and the difficulties encountered to deal with them from a geotechnical engineering point of view have been exposed.

Akagi (2004 [9]) refers to the soft clayey ground of Tokyo Bay where most underground structures are constructed. Large settlements of the soft ground around the tunnels were observed due to consolidation originating from excess pore water pressure induced by reclaimed soil and other construction works such as pumping of underground water. 3-D finite element simulations of the interaction between soil and tunnels with flexible joints were performed.

According to Phien-wej *et al.* (2009 [10]), the city of Bangkok is founded on a soft marine clay, 12 to 18m in thickness, followed by thin layers of medium and stiff clay of the same origin overlying a sand layer typically found at a depth of 20 to 22m. Land subsidence due to deep well pumping has affected the area reaching a rate as high as 12cm/year in the early 1980's. In spite of measures that were exerted to mitigate the phenomenon, ground surface in some parts of the city has sunk below the mean sea level, which makes flood drainage more difficult and costly.

Kempfert and Raithel (2005 [11]) presented experiences on dike foundations and landfills on very soft soils for the extension of an airplane dockyard in Hamburg, Germany. These and other experiences were the basis for the preparation of an excellent monograph on excavations and foundations in soft soils (Kempfert, 2006 [12]).

As far as the Americas are concerned, Mitchell and Countinho (1991 [13]) presented a general overview of "Occurrence, geotechnical properties and special problems of some soil in America" that included many soft soil sites in the U.S. and Canada but also in Mexico, Ecuador and Brazil.

Coutinho and Oliveira (2005 [14]) described the soft clay and organic soil deposits that can be found in about fifty percent of the lowland of the urban area of the city of Recife on the Northeastern coast of Brazil. Comprehensive program of laboratory and in situ tests have been performed in two research sites. Databases have been developed to support foundation design and as a pedagogical tool.

Almeida *et al.* (2004 [15]) also discussed the geotechnical properties and behavior of ten deposits of soft to medium clays situated in industrialized and residential areas of Rio de Janeiro City and Río de Janeiro State. A summary describing index properties, compressibility, stress history and undrained and drained strengths was presented.

As exposed by Martínez (1991 [16]) and Caicedo *et al.* (2018 [17]), the city of Bogotá (Colombia) is located on a high plateau of the Andes Mountains at 2550 m above sea level. More than 60% of the area of this city with 9 million of inhabitants is located on soft soil deposits. At some sites of the plateau, the depth of the lacustrine deposit can reach 586m. Shallow deposits of soil from 5 m to 10 m deep are overconsolidated, but in deeper layers, the soil can reach extreme values for some geotechnical properties: consistency index lower than 0.5, water content higher than 200%, liquid limit up to 400%, void ratio as high as 5, and high diatomaceous percentage.

It is noteworthy to observe that in the presentation of most of these different soft soil sites, scant attention was given to the description of spatial variations of the soil properties in statistical of probabilistic terms. This reflects the still prevalent reluctance of many geotechnical engineers to using these tools in spite of the wide diffusion they have received (Whitman, 1996 [18]; Lacasse and Nadim, 1996 [19]; Fenton, 1997 [20]; Phoon and Kulhawy, 1999 [21]; Auvinet, 2001 [22], 2002 [23]; Baecher and Christian, 2003 [24]; Huber, 2013 [25]).

### *2.3. The lacustrine clays of Mexico City*

Geologically, the so-called valley of Mexico is actually a closed basin located in the highest part and southern end of the Mexican plateau. It is located between parallels 19°00' and 20°12' north and meridians 98°10' and 99°33' west. It is bounded on the north by the mountains of Tepozotlan, Tezontlalpan and Pachuca, east by the plains of Apan and the Sierra Nevada, south by the mountains of Chichinautzin and Ajusco and west by Sierras de Las Cruces, Monte Alto and Monte Bajo. Its surface is about 9600 km$^2$, of which only 30% is flat. The geology of the Valley of Mexico has been the subject of many studies, from the first surveys of Del Castillo and Ordoñez (1893 [26]) to those presented more recently by Mooser *et al.* (1978 [27]; 1996 [28], 2018 [29]) and other geologists. Physiographically, the Basin of Mexico belongs to the Neovolcanic belt, an awesome volcanic range that crosses the Mexican territory from east to west.

The metropolitan area of Mexico City (Figure 2, Auvinet *et al.*, 2017 [30]) is limited by large topographic elevations. Two major volcanic units dominate the East part of the valley: Popocatepetl and Iztaccihuatl. Within the valley, some isolated volcanic domes such as Peñon de los Baños, Peñon del Marqués, Cerro de la Estrella and those forming Sierra de Santa Catarina protrude from the lacustrine area. The Valley of Mexico is mainly formed by volcanic and pyroclastic materials interspersed with alluvial deposits covered in the center of the valley by lacustrine clays. According to Mooser (1978 [27]), before the Pleistocene, the basin drained south to the Amacuzac River by two deep ravines passing through Cuautla and Cuernavaca. During the late Pliocene, fractures occurred predominantly in the WE direction in the area of Puebla and south of Toluca, and large outpourings of basalt formed the Sierra de Chichinautzin in the Quaternary. According to paleomagnetic measurements, massive eruptions occurred during the last 700.000 years. These events transformed the valley into a closed basin. The Sierra de Chichinautzin, lying between Sierra de Zempoala in the West and Popocatepetl in the East, and resting in the center on the Tepozteco massif formed a huge natural barrier that dammed the valley of Mexico.

Until the end of the XVIIIth century, the valley of Mexico remained a closed basin, with a number of shallow lakes. Mexico City (then Tenochtitlán) was founded in a small island of the Texcoco Lake. The valley became an open basin when the Nochistongo cut was completed in 1789. During the XXth century, the lakes were drained through the Tequisquiac tunnel, completed in 1900, and the Deep Drainage tunnel (Emisor Central), built in 1967. A new drainage tunnel (Túnel Emisor Oriente), 7m in diameter and 62 km long is expected to be finished by the date of the present lecture. Today, with the exception of small remaining bodies of water, the lakes have practically disappeared.

A large part of the city was thus built on lacustrine sediments in the lower part of the basin with a surface of some 2050km$^2$. These are highly compressible soft clays interbedded with layers of silt, sand and sandy gravels of alluvial origin. With a growing population now exceeding 20 million inhabitants, the metropolitan area of Mexico Valley is one of the largest urban conglomerates in the world.

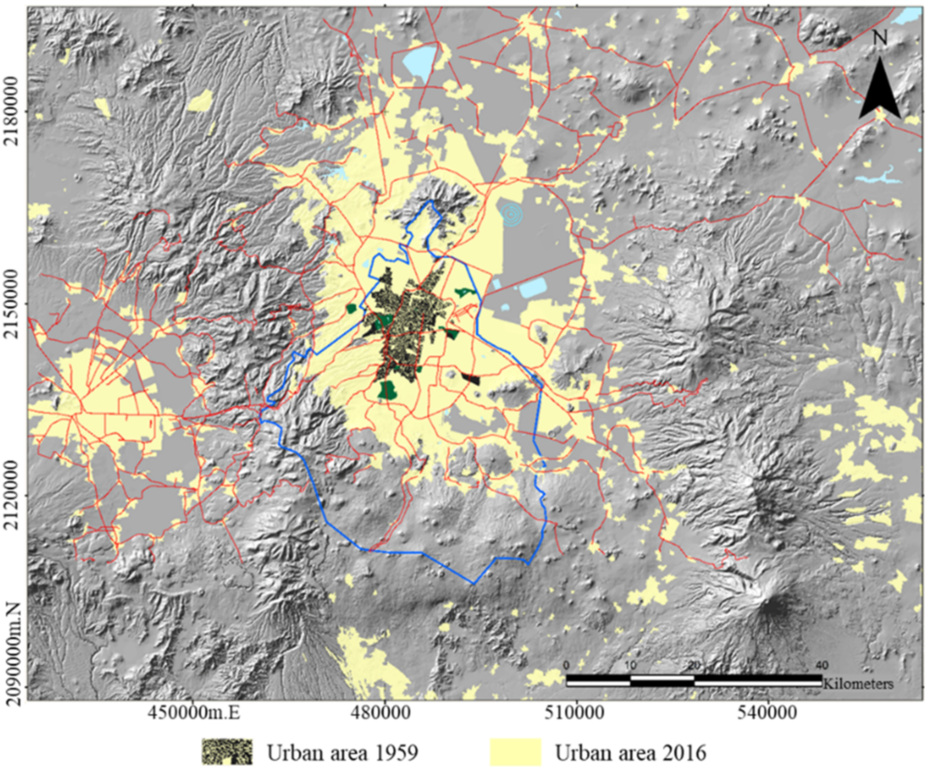


**Figure 2.** Urban area of Mexico City and surroundings neighborhoods.

## 3. Soft soils characterization

### *3.1. Soil stratigraphy, ground water conditions and mechanical parameters*

For identification of the soil type of successive layers, a number of rapidly evolving field techniques have become available. Semi continuous penetration tests such as CPT (Cone Penetration Test), CPTu (Cone Penetration Test with pore pressure measurement, also called piezocone test) or DMT (Marchetti Dilatometer test) are now generally preferred to SPT (Standard Penetration Test) (Robertson, 2009 [31]; 2012 [32]).

The SPT approach has the advantage of providing split spoon samples for visual classification and obtaining index properties such as water content that are very useful to assess spatial variations. On the other hand, CPTu tests can readily differentiate between free draining lenses and the soft soil matrix, and it is often considered that piezocone soundings provide the most rapid and detailed approach for soil profiling. The continuous nature of the CPTu results provides valuable information about soil variability that is difficult to match with sampling and laboratory testing, because the CPT obtains more channels of data (typically 3) at more frequent intervals (typically every 20 to 50 mm). Performing a well-balanced combination of SPT and CPTu tests seems the best way to go, although simple direct-push samplers can also be used to obtain small (typically 25 to 50 mm in diameter) disturbed soil samples of similar size to that obtained from SPT. Charts are used for definition of soil type descriptions derived from CPTu data. Note that the zones in these charts are imprecise compared to the Unified Soil Classification System (USCS) and thus it is highly advisable that the site investigation include sampling for final classification of soft cohesive strata. As recommended by Ladd and De Groot (2003 [1]), the final developed soil profile should always include the USCS designation for each soil type.

When performing CPT tests, shear strength is estimated in terms of the net tip resistance as:

$$s_u = \frac{q_c - \sigma_0}{N_k} \tag{4}$$

where $s_u$ = undrained shear strength, $q_c$ = tip resistance in CPT test, $\sigma_0$ = total vertical stress at the level of the measurement, and $N_k$ = cone factor.

A large number of increasingly sophisticated relationships between CPT results and parameters such as the Over Consolidation Ratio (*OCR*), yield stress $\sigma'_p$, shear wave velocity $V_S$, small strain shear modulus $G_0$ as well as coefficient of volumetric compressibility $m_v$ have also been established (Robertson, 2012 [32]).

Geotechnical practitioners are sometimes puzzled by the refinements introduced in the coefficients or exponents of the proposed relationships between CPT tests results and soil properties, some of them with no evident physical meaning. In all cases, formal statistical analyses indicating clearly the soil population to which they are applicable and showing the scattering of the data around the established relationships should always be presented.

Ground water conditions assessment through piezometric measurements is also an important part of the characterization of any soft soil deposit, since the original effective state of stress within the medium can only be known when a full knowledge of water table location (and variations) has been achieved and possible drawdown conditions due to deep pumping have been evaluated.

Laboratory tests on high quality samples laboratory tests must also be performed. Consolidation tests will provide compression index, $C_v$ and swelling index, $C_s$ as well as yield stress $\sigma'_p$. Triaxial shear tests will furnish value of undrained shear strength, $s_u$. Using advanced soft soil constitutive laws in geotechnical analyses, many based on the modified Cam-clay model implicit in most modern geotechnical software, may require assessing additional parameters.

In seismic areas, dynamic parameters such as shear modulus, damping ratio and seismic wave velocity will also be required in order to evaluate seismic site effects and performing dynamic soil-structure analyses. Some of this information can be obtained through CPT tests but performing geophysical field tests and cyclic laboratory tests may also be required.

### 3.2. Practice of soft soil characterization in Mexico City

The main reference regarding geotechnical characterization of Mexico City clays is still "The Subsoil of Mexico City" by Marsal and Mazari (2017 [33]), an encyclopedic work initially published in 1959, that presents an impressive number of laboratory and field tests results. Casagrande used to refer to this book as "The Bible". This publication was recently updated with a third volume summarizing more recent works on this topic (Auvinet *et al.*, 2017 [30]). Valuable information is also found in Zeevaert (1972 [34]). Additional laboratory and field tests results have been presented by Santoyo *et al*. (2005 [35]) and Ovando (2011 [36]).

The unique properties of Mexico City clay have been evaluated in a number of studies performed to assess their mineral composition and structure (Zeevaert, 1952 [37]; Marsal and Mazari, 1959 [33]; Leonards and Girault, 1961 [38]; Girault, 1964 [39]; Lo, 1962 [40]; Mesri, Rokhsar and Bohor, 1975 [41]; Peralta y Fabi, 1973 [42]; Díaz-Rodríguez *et al.*, 2003 [43]). Most of these studies are inconclusive. This heterogeneous volcanic lacustrine clay appears to be a complex mixture of clayey and non-clayey minerals with microorganisms, dissolved salts and organic components. The presence of microfossils such as ostracods and diatoms could explain some of the properties of the material including its high water content.

Note that when the plasticity chart of USCS was established (Casagrande, 1948 [2]), Mexico City clay was "expelled" together with various types of peat and Wyoming bentonite, from the main chart due to their high water content (and liquid limit) (Figure 1). This was in fact a consequence of the definition adopted for water content (Eq. (1)). Figure 3 shows a plasticity chart in which a more conventional definition of water content ($w$', Eq. (2)) was adopted. In this chart, Mexico City clay is reunited with the large family of fine-grained soils.

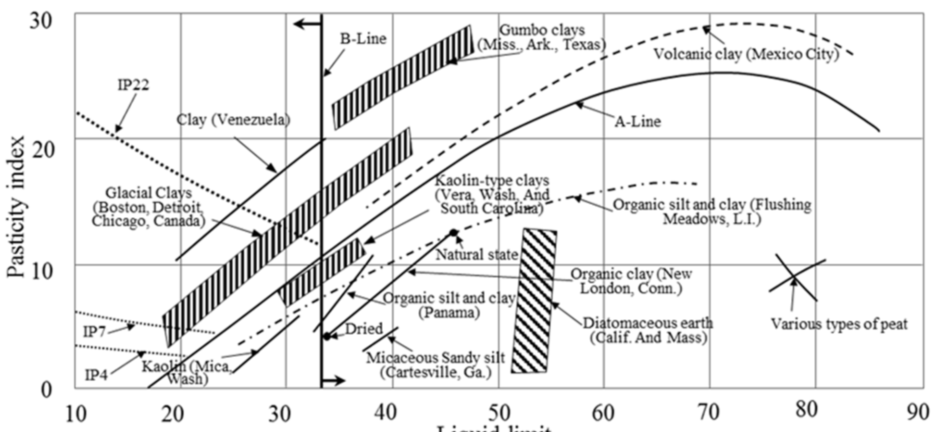


**Figure 3.** Plasticity chart based on water content $w$' defined by Eq. (2).

A discussion has been going on regarding whether Mexico City clay should be classified as a "highly organic material" as suggested by some authors (Mesri *et al.*, 1975 [41]). This opinion has been reinforced by the fact that when CPT tests are performed, the behavior of Mexico City clay seems typical of organic materials (Cruz and Mayne, 2006 [44]; Mayne, 2019 [45]). This should be clarified since Marsal and Mazari (1959 [33]) carried out measurements of the organic content of the fine soils of Mexico City based on the carbonate content, that indicate that these soils have a medium to low percentage (5% percent as an average) of organic components. The highest percentages correspond to the upper part of the clayey series (between 5 and 15m deep). In a recent study (Rangel *et al.*, 2019 [46]), the organic content has been determined using the Walkley and Black method (1934 [47]). All soils samples tested presented a low organic content. The same authors are currently performing additional tests on materials obtained from the former Texcoco Lake (water with high salt content) and Xochimilco Lake (fresh water).

Materials from the clayey deposits of Mexico City subsoil are characterized by their extraordinary compressibility. Coefficient of compressibility $a_v$, defined as the quotient between the decrement of void ratio and the respective increment of applied pressure may reach values as high as 6 cm$^2$/kg (0.06 m$^2$/kN). The clay shear strength is higher than what could be expected taking into account the exceptionally high water content of this material, showing that it is highly structured. However, average values of 40 kN/m$^2$ are not uncommon, with extreme values as low as 15 kN/m$^2$.

Mexico City clay is commonly described as an elasto-plastic material. The initial yielding surface of typical Mexico City clay samples was defined performing a number of triaxial tests following distinct different stress paths (Díaz-Rodríguez *et al*. 1992 [48]). Wheeler (2003 [49]) adjusted the model presented in Figure 4 to these results.

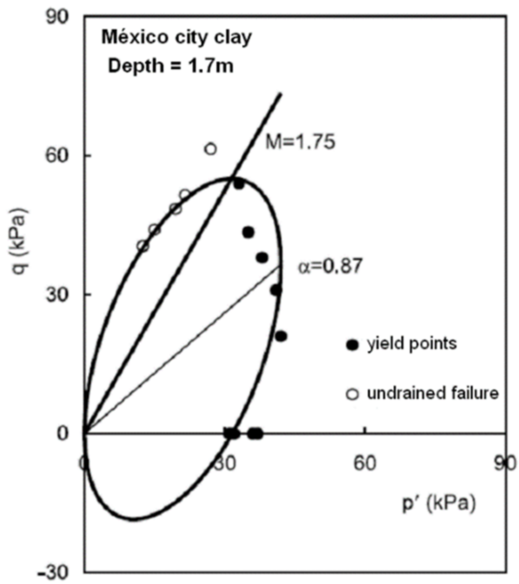


**Figure 4.** Initial yielding surface for typical Mexico City clay.

Field-tests techniques commonly used for Mexico City soft soil characterization have been extensively described by Santoyo (2010 [50]). To illustrate the present Mexican practice, reconnaissance and laboratory tests that were performed recently on a site considered at some point for developing a new airport in Mexico City (NAICM) are presented in Tables 1 and 2 (Mendoza *et al.*, 2018 [51]).

**Table 1.** Geotechnical borings performed from 2013 to 2016 (NAICM).

| Type | Preliminary exploration (2013) | Test embankments (2014a) | Terminal Building area (2014b) | Terminal Building and Control Tower area (2015) | Runways, platforms and taxiways (2016) | Test embank ments (2016) | Total |
|---|---|---|---|---|---|---|---|
| Test pits (PCA) | | 19 | 10 | | 261 | | 290 |
| Dynamic cone penetrometer (PND) | | 72 | | | 323 | | 395 |
| Standard Penetration Test (SPT) | 3 | | 7 | | 90 | | 100 |
| Mixed boring (SM) | 66 | | | 20 | 90 | 7 | 183 |
| Continuous sampling (SC) | | 12 | 1 | | 2 | | 15 |
| Selective sampling (SS) | 14 | 6 | 3 | | 54 | | 77 |
| Cone penetration test (CPT) | | 11 | 7 | | 13 | | 31 |
| Cone penetration test with pore pressure measurement (CPTu) | | | 3 | 30 | 177 | 7 | 217 |
| Suspension PS logging (Sds) | | 6 | | 6 | | | 12 |
| Dilatometer (DMT) | | | 2 | | 20 | | 22 |
| Seismic dilatometer (SDMT) | | | 1 | | | | 1 |
| Vane shear test (VST) | | | | | 30 | | 30 |
| Total | 83 | 126 | 34 | 56 | 1060 | 14 | 1373 |

**Table 2.** Laboratory tests (NAICM).

| Type | Preliminary reconnaissance (2013) | Test embankments | Terminal Building and Control Tower area. | Runways, platforms and taxiways | Total |
|---|---|---|---|---|---|
| Water content | 1512 | 1190 | 4504 | 34961 | 42167 |
| Atterberg limits | | 208 | 131 | 855 | 1194 |
| % of fines | | 208 | 136 | 850 | 1194 |
| Specific gravity of solids | | 25 | 118 | 744 | 887 |
| Triaxial UU | 21 | 31 | 60 | 308 | 420 |
| Triaxial CU | | | 46 | 274 | 320 |
| Consolidation | 41 | 12 | 69 | 363 | 485 |
| Total | 1574 | 1674 | 5064 | 38355 | 46667 |

In this project, the portable dynamic cone penetrometer (Panda) was useful to assess the thickness and mechanical characteristics of the crust of desiccated soils topping the clay deposits. Standard Penetration Tests (SPT) were performed mainly to obtain representative samples for soil classification and water content determination. Undisturbed samples were obtained using Shelby type or special samplers for laboratory tests. A large number of Cone Penetration Tests (CPT and CPTu) and a limited number of Vane Shear Tests (VST), formerly a much more popular test, were also performed. To assess shear wave velocity, the suspension PS logging technique was preferred to other geophysical methods. In the lakebed area soft clay deposits, shear wave velocity ranges from 40 to 90 m/s. Silt and sand lenses interspersed in the clay as well as the hard crust and the superficial fills topping the clay may however present a much higher velocity.

Regarding characterization of Mexico City clay shear strength from CPT tests, an empirical relation has proven to provide better estimates than the classic Eq. (4). This relation is considered to be of general applicability for the Basin of Mexico clays (Santoyo *et al*., 1989 [52]):

$$s_u = \frac{q_c}{N_k} \tag{5}$$

where $s_u$ = undrained shear strength, $q_c$ = tip resistance in CPT test, and $N_k$ = cone factor.

A large number of field and laboratory determinations showed that a very good agreement between shear strength estimated with Eq. (5) and actual laboratory measurements (UU tests) is obtained when $N_\mathrm{k}$ = 13 (Alanís, 2003 [53]). However, evidences suggesting a significant influence of Over Consolidation Ratio (*OCR*) on the cone factor have also been presented (Montañez, 1983 [54]).

For modelling of deep foundations, tunnels, and other geotechnical structures in Mexico City clay, the Soft-Soil model (Plaxis software) has been extensively used in Mexico City with satisfactory results (Rodríguez, 2011 [55]). The Hardening soil model is however generally preferred for modelling excavations where the soil is submitted to unloading. To take into account the anisotropic behavior apparent in Figure 3, models such as the S-Clay1 are preferred. Visco-elastic behavior of Mexico City clay has also been assessed and the results are being incorporated into new constitutive models (Ossa, 2004 [56]).

Experimental investigations have shown that the dynamic response of Mexico City clays strongly depends on the strain level induced. At low deformations, the response is relatively linear, the clay has low capacity to dissipate energy and degradation with the number of stress cycle applications is negligible. For large deformations, the response is strongly non-linear, damping increases notably and stiffness degradation may be important. The threshold shear strain between linear and non-linear behavior of clays depends on clay characteristics. It has been shown that of all factors that affect the degree of non-linearity of clay behavior, the most important appears to be the plasticity index, PI. The upper bound seems to be given by the highly plastic clays of Mexico City (PI > 200 %). The behavior of these clays remains practically elastic with low damping up to an angular strain level of the order of 0.5%. This contributes to explain the large site effects registered in the lake zone of Mexico City during earthquakes (Romo and Auvinet, 1992 [57]). For large amplitude cyclic strains, the clay structure degrades continuously causing pore water pressure variations and reductions in stiffness and strength.

## 4. Spatial variations

### *4.1. Factors contributing to soft soils spatial variations*

Spatial variations of soft soils properties can be induced by many factors. The formation process of soft soils, especially lacustrine soils, generally leads to a stratified structure with strong vertical variations and smooth horizontal differences. Many natural anomalies can however be present in soft soil deposits due to interference with other geological formations and to anthropic factors, including the land use and loading history of the area that affect significantly the properties of the subsoil, especially in urban areas.

To detect topographical anomalies suggesting local variations of soil characteristics and to assess subsidence, new remote sensing techniques such as LiDAR (light detection and ranging, or laser radar; GPS based), InSAR (Interferometric Synthetic Aperture Radar) or DinSAR (Differential Synthetic Aperture Radar Interferometry) techniques have proven to be extremely useful (Auvinet *et al.*, 2017 [30]).

*4.2. Spatial variations within the lacustrine zone of Mexico City*

In Mexico City, large spatial variations of the subsoil are observed at different scales.

The urban area of Mexico Valley is usually divided in three main geotechnical zones (Marsal, 1975 [58]): Foothills (Zone I), Transition (Zone II) and Lake (Zone III). Figure 5 shows the three zones as defined in the present building code (GDCMX, 2017a [59]). In the foothills, very compact but heterogeneous volcanic soils and lava are found. These materials contrast with the highly compressible soft soils of the Lake Zone. Generally, in between, a Transition Zone is found where clayey layers of lacustrine origin alternate with sandy alluvial deposits.

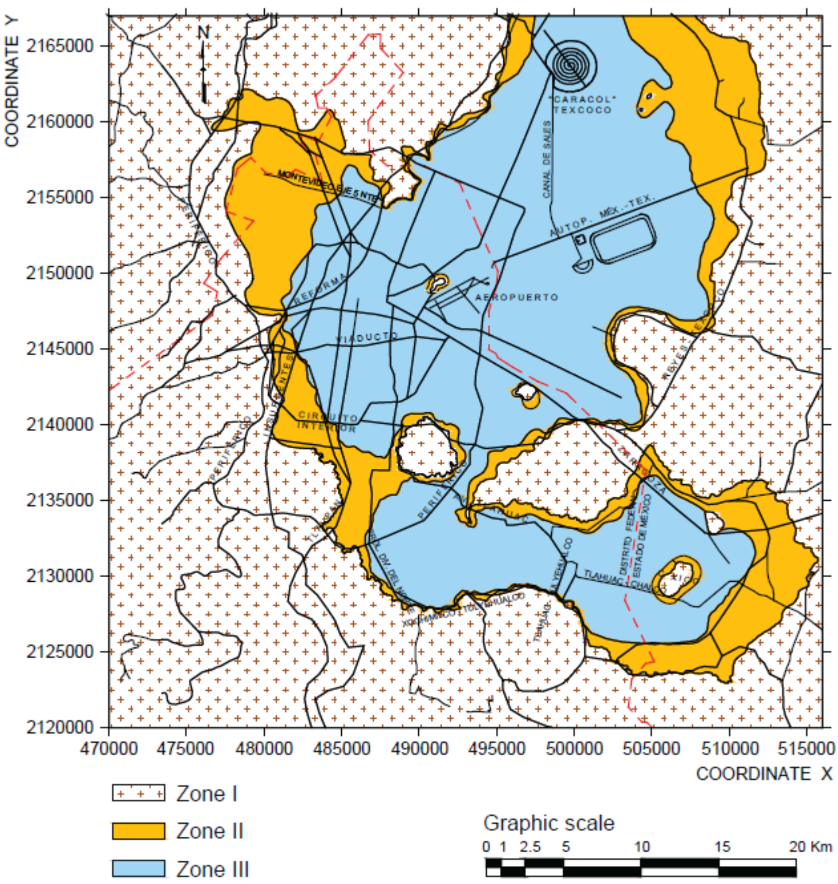


**Figure 5.** Geotechnical zoning of Mexico City and surrounding areas (GCDMX, 2017a [59]).

In Figure 6, typical soil profiles are presented (Marsal, 1975 [58]). Borehole Pc-28 corresponds to the Lake Zone. The water table is close to the surface. Three clayey layers are to be distinguished, denominated upper clay formation (Formación Arcillosa Superior, FAS), lower clay formation (Formación Arcillosa Inferior, FAI) and deep deposits (Depósitos Profundos, DP). The clays of FAS are separated from FAI by a hard layer (Capa Dura, CD), a sandy clayey stratum, generally less than 3m thick, found at a typical depth of 30 to 35m. In most sites, FAS is topped by a desiccated crust and/or artificial fills several meters thick.

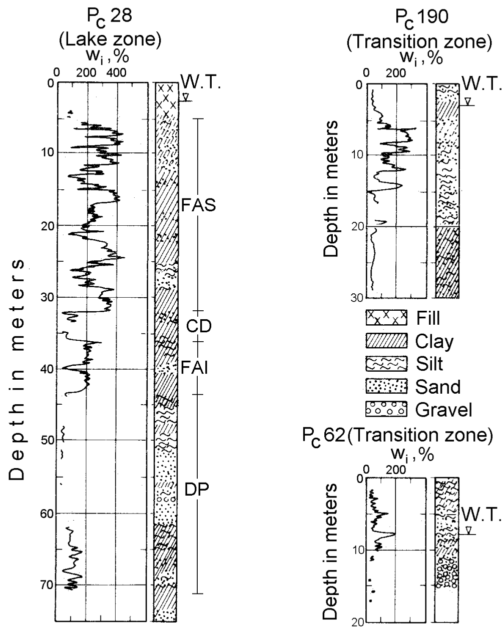


**Figure 6.** Typical soil profile for the different geotechnical zones.

Typical values of index properties for borehole Pc 28 are presented in Table 3. In some areas of the lacustrine zone, the water content of this exceptional material can indeed be higher than the value indicated in Table 3. The highest water contents in the city lake area are found in the upper part of the upper clay formation, down to a depth of about 20m.

**Table 3.** Typical values of index properties in the Lake Zone (Borehole Pc 28, Marsal, 1975 [58]).

| Property | FAS | CD | FAI |
|---|---|---|---|
| Water content, % (Eq.(1)) | 270 | 58 | 191 |
| Liquid limit $w_L$, % | 300 | 59 | 288 |
| Plastic limit, $w_P$, % | 86 | 45 | 68 |
| Density of solids, $G_s$ | 2.30 | 2.58 | 2.31 |
| Initial void ratio, $e_0$ | 6.17 | 1.36 | 4.53 |
| Unconfined compressive strength, $q_u$, kN/m$^2$ | 85 | 24 | 160 |

At a small scale, spatial water content variations within the soft soil deposits are also observed. Marsal (1959, [33]) determined the water content of Mexico City clays at different points of horizontal cross-sections of samples obtained using a thin wall Shelby sampler (Figure 7)

The scattering of the values obtained locally looks surprisingly high and raises the question of what the true water content of the sample really is. Most of the scattering is however due to the definition of water content *w* given by Eq. (1). The standard deviation of the *w* data presented in Figure 7 is 28.5% and the coefficient of variation is 7%. Switching to the definition of Eq. (2), the standard deviation of *w*' is 1.1 % and the coefficient of variation is only 1.4%. Finally, using definition of Eq. (3) the standard deviation of *w*'' is 1.6% and the coefficient of variation decreases further to .6%.

As can be expected in lacustrine materials, horizontal variations of the material are in fact hardly significant.

As mentioned earlier in this lecture, averaging the local values as suggested by Marsal in Figure 7 overestimates the true water content of the whole sample. The magnitude of the overestimation can be obtained as described in Appendix I. A simple calculation shows that in this case the true global value of water content *w*' (Eq. (1)) for the whole sample is of the order of 404.8%, only slightly inferior to the average value indicated in Figure 7. The variations of water content observed in Figure 7 will be examined further in this lecture (Figure 19).

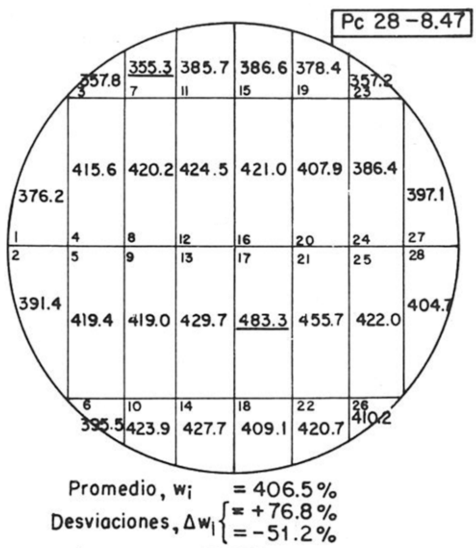


**Figure 7.** Variations of water content *w* (Eq. (1)) in a cross-section of a Mexico City clay sample.

In some areas of Mexico valley and especially in former Texcoco Lake (eastern part of the lacustrine area) the salinity of the soil is particularly high. In its central and northern zones, it can reach 54,000 mg/l in the first 60 m. It decreases gradually with depth and diminishes towards the edge of the former lake area and towards the south. Maximum concentrations of salt in former Texcoco Lake may be as large as 18%, according to data provided by Murillo and Morales (1991 [60]). Presence of salt leads to a significantly smaller apparent water content that can be corrected to account for the presence of dissolved minerals following Marsal and Graue (1969 [61]):

$$w = \frac{w_{ap}}{1 - cw_{ap}} \tag{6}$$

where $c$ = salt concentration in %, $w_{ap}$ = apparent water content (including salt in solids, Eq. (1), and $w$ = actual water content.

Differences between the apparent and true water content are significant. This is mainly due to the definition of water content given in Eq. (1). When definition of Eq. (2) is adopted, differences are much smaller. In that case, the actual water content $w'$ can be obtained as:

$$w' = \frac{w'_{ap}}{1 + (1 - c)\, w'_{ap}} \tag{7}$$

where $w'_{ap}$ = apparent water content (including salt in solids, Eq. (2)).

When using definition of Eq. (3), no correction is needed.

At a larger scale, Figure 7 presents a typical soil profile for the Lake Zone clays that includes water content, CPT tip resistance, SPT blow count number and undrained shear strength (Rodríguez, 2011 [55]).

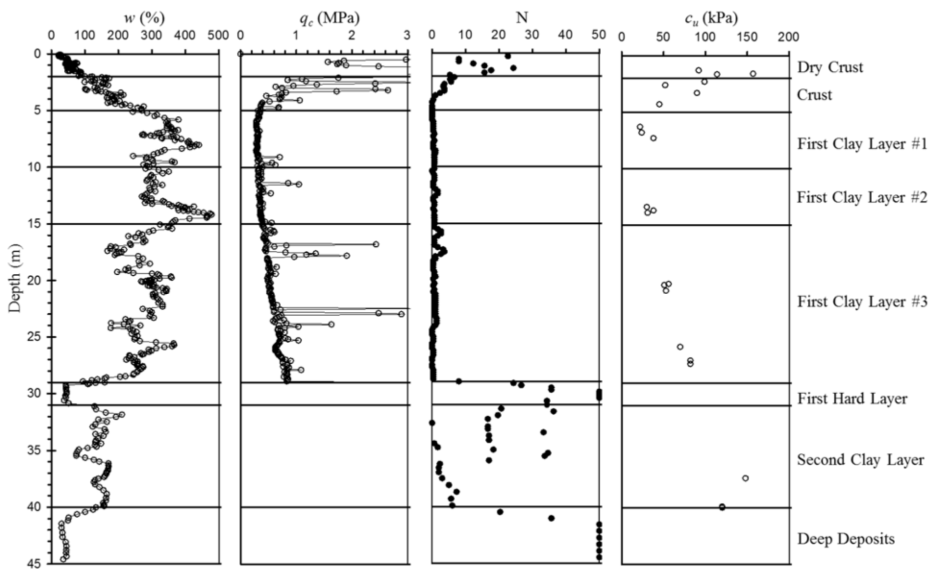


(a)

**Figure 8.** (a) Typical soil profile, San Juan de Aragón site, Lake Zone, (b) Zoom on water content of the 5 to 15m deep layer.

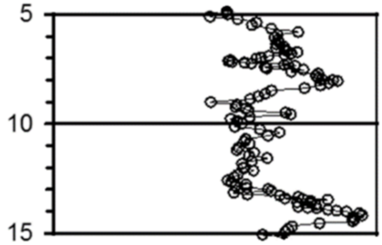


(b)

**Figure 8.** (*continued*) (a) Typical soil profile, San Juan de Aragón site, Lake Zone, (b) Zoom on water content of the 5 to 15m deep layer.

As observed on the soil profiles of Figures 6 and 8, in the Lake Zone, the water content of the clays presents wild variations on short vertical distances. This is generally attributed to a complex history of successive volcanic eruptions as well as to flooding and drying episodes.

It can however be observed that water content variations are not matched by equivalent variations of the CPT tip resistance $q_c$, except at the elevation of sand lenses interspersed within the clay. A large part of the apparently strong variations of the water content within the clay layers observed in Figures 6 and 8 should in fact be traced to the definition of water content itself.

Focusing the analysis on the water content measured in the 5 to 15m deep layer (Figure 8b), the statistical results presented on Table 4 are obtained.

**Table 4.** Statistical analysis of water content and void ratio for the 5 to 15m deep layer of Figure 8b.

| | *w*, % | *w*', % | *w*'', % | *e* |
|---|---|---|---|---|
| Average | 366.1 | 77.1 | 89.3 | 9.15 |
| STD | 240.9 | 5.5 | 2.7 | 6.02 |
| CV, % | 65.8 | 7.1 | 3.0 | 65.8 |
| True value | 333.8 | 76.9 | 89.3 | 8.34 |
| Bias | 32.3 | 0.2 | 0 | 0.81 |

The scattering of the values of water content *w* is high. The standard deviation of the *w* data in this layer is 240.5% and the coefficient of variation is 65.8%. Most of the scattering is however due to the definition of water content *w* given by Eq. (1). Switching to the definition of Eq. (2), the standard deviation of *w*' is 5.5 % and the coefficient of variation is only 7.1%. Finally, using definition of Eq. (3) the standard deviation of *w*'' is 2.7% and the coefficient of variation decreases further to 3%.

As mentioned earlier in this paper, averaging the local values overestimates the true water content of the whole population. The magnitude of the overestimation can be obtained as described in Appendix I. A simple calculation shows that the true value of water content *w*' (Eq. (1)) for the whole population is of the order of 333.8%, clearly inferior to the average value of 366.1%.

In the same way, it can be observed that the scattering of the void ratio is very high. The average value of the *e* data in this layer is 9.15, the standard deviation is 6.02 and the coefficient of variation is 65.8%. However, this is basically due to the definition of void ratio adopted in geotechnical engineering. Switching to porosity (in this case equal to *w*'') the coefficient of variation is only 3%. Note also that averaging the void ratio local values leads to a value of 9.15 when the true global value is 8.34. Characterizing a layer by the average values of void ratio, *e*, and water content, *w*, can be a source of significant errors for this type of soil, in particular for settlements computations.

Figure 9 shows three water content profiles corresponding to the same site (Runway 6, NAICM) and presented using the alternative definitions of water content corresponding to Eqs. (1) to (3). With the gravimetric definition referred to the total weight of the sample (Eq. (2)) (centre of Figure 9), differences between water contents at distinct elevations within the upper clay formation are no longer so conspicuous, especially at depth between 0 and 20m. The profile is even smoother when the volumetric definition of water content (Eq. (3)) is used (right hand side of Figure 9). It can then be concluded that different definitions of water content provide quite different descriptions of the soil. Profiles based on water content defined by Eq. (1) suggest that large variations in the composition the soil occur when in fact these variations correspond to small changes in the amount of water and solids in the soil. This is due to the high non-linearity of the relation between *w* and weight of solids $W_s$ in Eq. (1) (Appendix I).

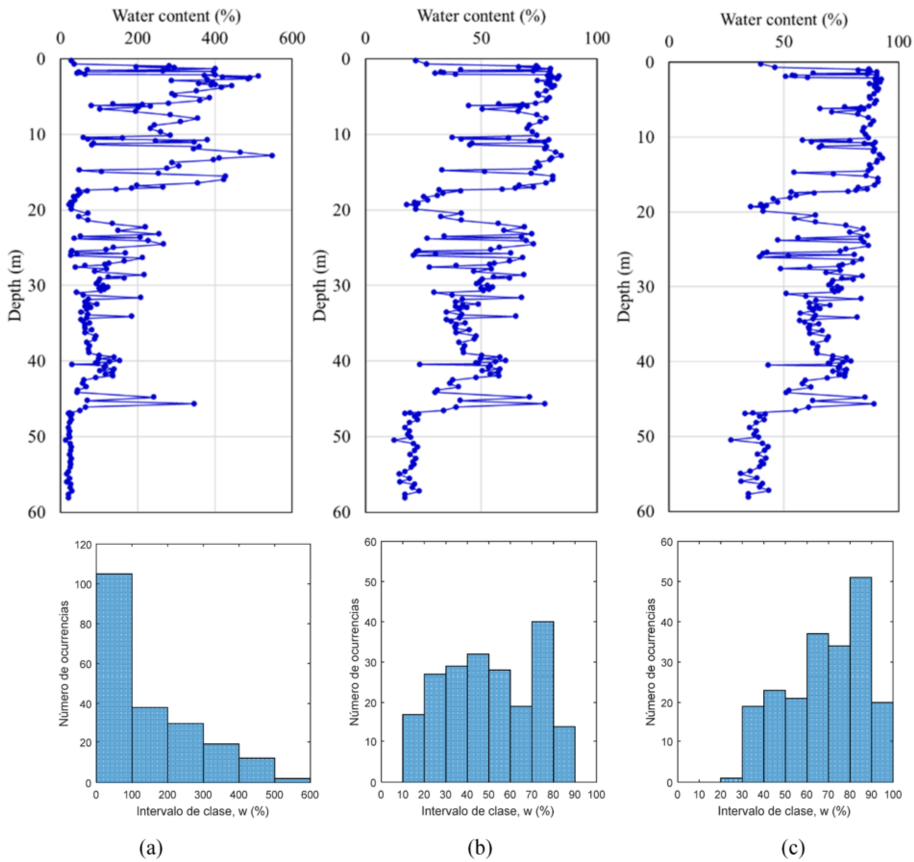


**Figure 9.** Water content profiles in a Lake Zone site established using different definitions of water content (a) Eq. (1), (b) Eq. (2), (c) Eq. (3) and corresponding histograms.

The shape of the water content histograms corresponding to different definitions of water content is extremely variable. The histogram corresponding to the second definition (Eq. (2)) of water content is slightly bimodal but approximately Gaussian, a condition favorable for geostatistical analyses (Appendix II). The other histograms are strongly skewed respectively to the left (Eq. (1)) and to the right (Eq. (3)). In all cases, geostatistical analyses would benefit from a transformation by *anamorphosis* of the corresponding random field of water content to a Gaussian field (Appendix II).

Local variations are only one aspect of the heterogeneity of the Lake Zone soft clay deposits. Zone III (Figure 5) is far from being homogeneous. Many natural and anthropomorphic anomalies leading to geotechnical variations have been encountered in the valley as shown on Figure 10 (Méndez *et al*., 2010 [62]; Auvinet *et al.*, 2017 [30]).

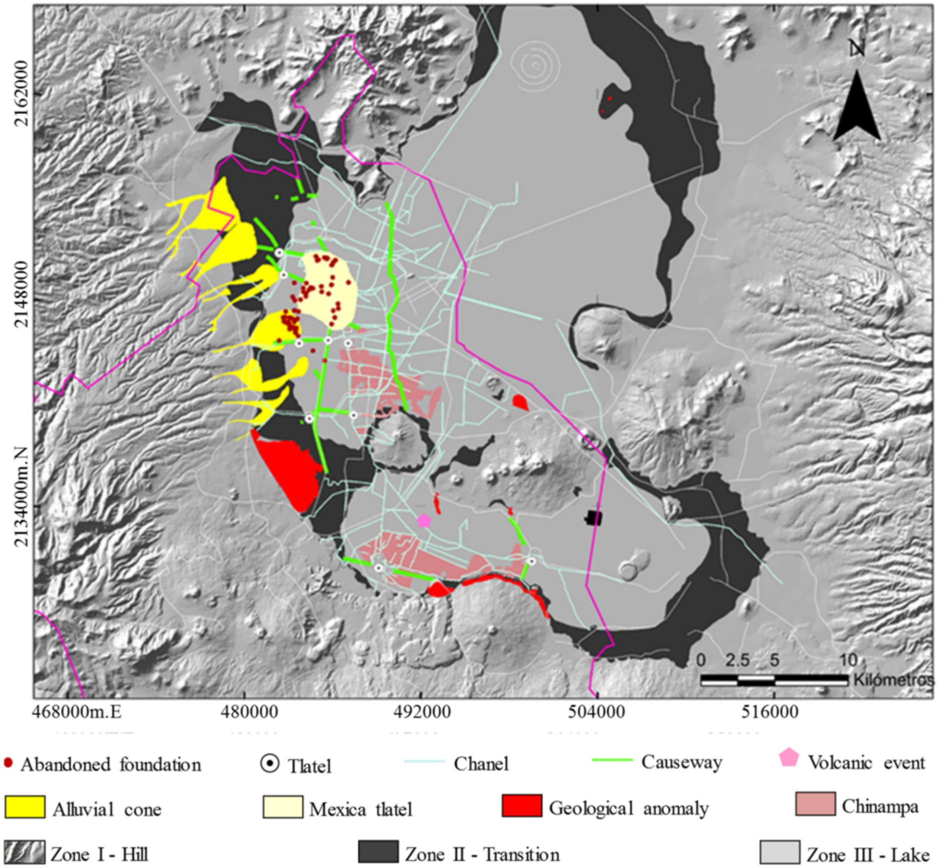


**Figure 10.** Geotechnical anomalies within the lacustrine clays of Mexico City.

Natural anomalies due to interference between the soft soil deposits and other contiguous geological formations are conspicuous, especially in the perimeter of the Lake zone.

Water content in Mexico City clays varies considerably, depending on the location of individual sites. Sites in the built area, having been subjected to external overburdens contain less pore water than the so-called virgin clays that are typical of the less or newly urbanized areas.

In general, soils towards the edges of the former lake are less humid than in the central part, a situation that is favored by the existence of sands and sandy silts interspersed with the upper clays in the so-called transition zone (Ovando, 2011 [36]). On the east side of the former lake, alluvial fans shown in Figure 10 originate very complex and heterogeneous local soil conditions including the presence of coarse granular materials and boulders. In other areas, volcanic materials produced by recent eruptions such as volcanic tuffs or basaltic lava, are occasionally found interspersed within the lacustrine materials, especially in the contact with the Santa Catarina and the Chichinautzin ranges, in the south part of the lacustrine zone.

The shallow lakes of Mexico City basin have been, for many centuries, the site of intense human activity. Artificial islands (*Tlateles*), many of them topped by religious monuments (*Teocalli*), as well as causeways were built with sandy and silty fills brought from the surrounding hills with a thickness varying from a few meters to 15m. Later, as the lakes were recessing as a result of the drainage works, canals were constructed to conduct the water to the still inundated lower part of the valley in Texcoco. These canals were subsequently filled with the surficial material of the dry crust layer or with transported sandy and silty materials. Agriculture techniques adapted to the environment were developed in the south of the lacustrine area since the pre-Columbian era. In the *chinampas* or “floating gardens” a large amount of organic matter was piled upon the soil surface for agricultural purposes. During reconnaissance surveys, geotechnical engineers should thus not be surprised to encounter down to a significant depth some materials with properties quite different from those of the typical lacustrine clays.

The regional subsidence of the Lake and Transition Zones due to pumping of underground water from the deep aquifers also contributes to the subsoil heterogeneity and evolution of its properties with time. Carrillo (1948 [63]) was the first to establish a clear correlation between subsidence and piezometric drawdown induced by pumping. The settlement accumulated since 1862 has reached 14.5m in some areas (Auvinet *et al.*, 2017 [30]). Figure 11 presents an updated evaluation of the subsidence rate. Groundwater pumping from the deep aquifer system underneath the city is now about 52 $m^3/s$, representing 72% of potable water provided to the city dwellers and cannot be stopped without serious social consequences. This phenomenon damages drainage and transport systems as well as other services of the city and generates severe foundation behavior problems (Auvinet *et al*., 2017 [30]).

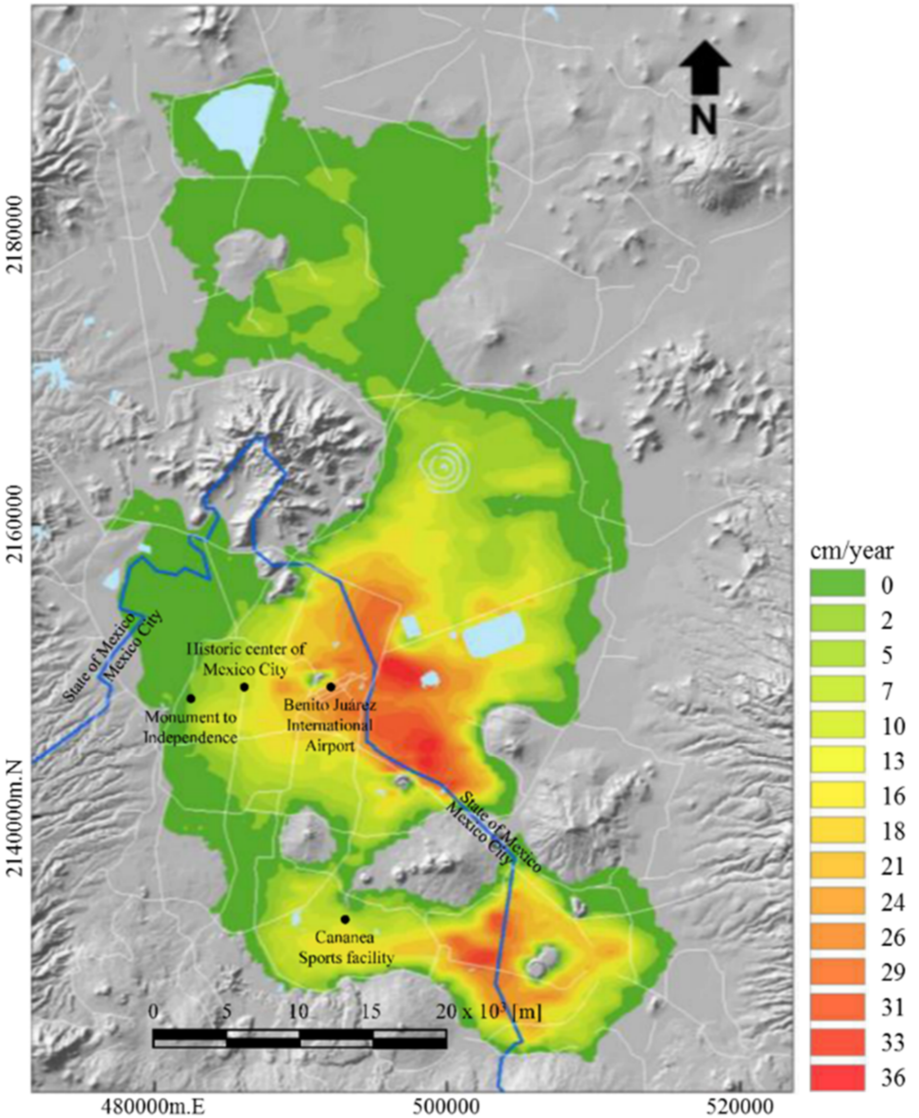


**Figure 11.** Subsidence rate in Mexico City lacustrine area.

Static and dynamic properties of the subsoil are progressively affected by the ongoing regional consolidation process and are expected to present drastic variations in the future (Ovando *et al.,* 2007 [64]; Jaime and Méndez, 2010 [65]); Figure 12 shows the evolution of CPT results obtained at the Secretaría de Comunicaciones y Transportes (SCT) site in 1985, 2000, and 2011 (González, 2012 [66]).

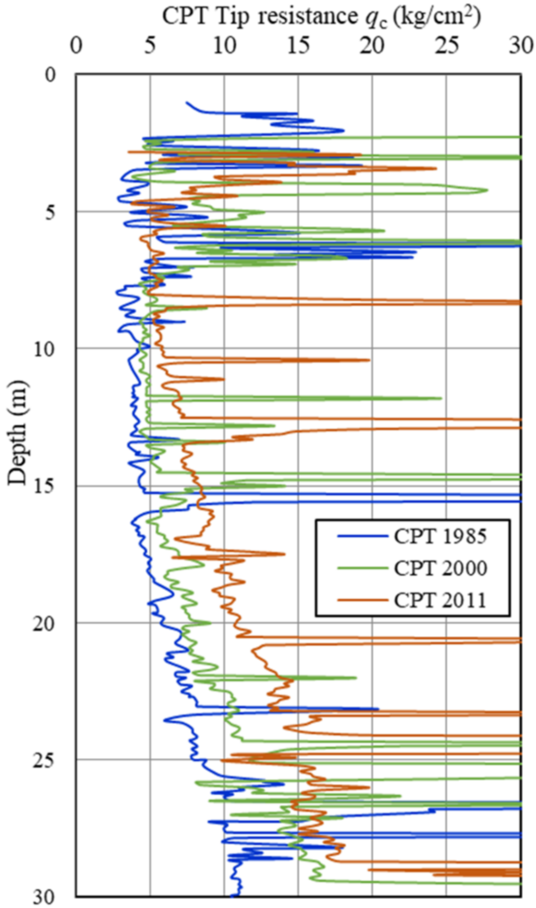


**Figure 12.** Variation of CPT profile with time, SCT site, Lake Zone, 1985, 2000, 2011.

Implications of the evolution of Mexico City subsoil properties due to water pumping and in particular the effects of future regional subsidence on the seismic response have been evaluated and shown to be very significant (Ovando *et al*., 2003 [67]; 2007 [64]). It has been recognized that in the future it will be necessary to adapt the Building code seismic requirements to this evolution.

The subsidence phenomenon also has severe consequences in some abrupt transition zones, especially in the contact of the soft materials of the Lake Zone with the Santa Catarina and Chichinautzin ranges (Figure 13). Large fissures due to differential settlements with steps that can exceed 50cm have developed progressively and created a critical geotechnical environment (Auvinet *et al.*, 2011 [68]; 2017 [30]). These fissures affect street pavement, public services and constructions. They are reactivated during large earthquakes as happened on September 19$^{th}$, 2017 (Figure 14a).

Other fissures are induced in the Lake zone by hydraulic fracturing of the clay formation in flooding areas (Figure 14b).

Special solutions for mitigating the consequences of this phenomenon have been developed (Auvinet *et al*., 2019 [69]).

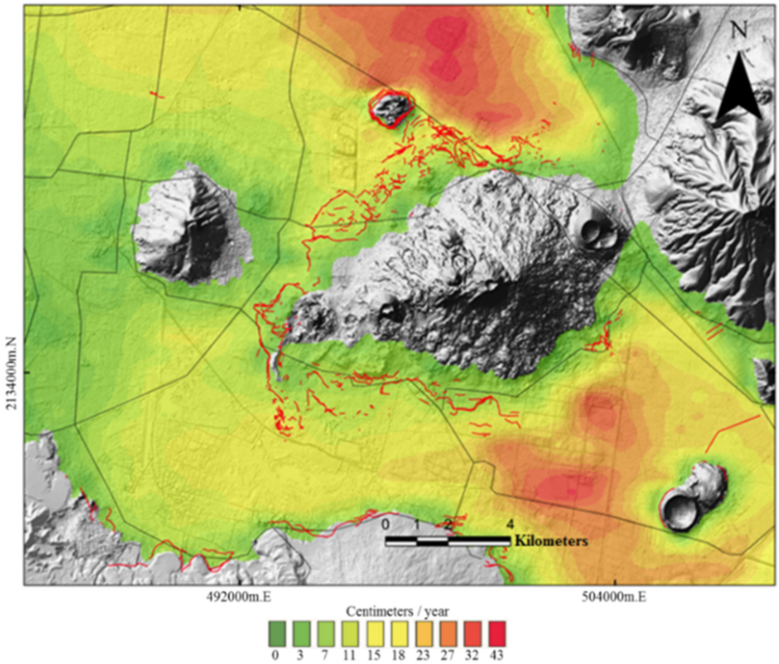


**Figure 13.** Soil fissuring around Santa Catarina range due to regional subsidence.


(a) (b)

**Figure 14.** Soil fractures induced by (a) regional subsidence (b) hydraulic fracturing in flooding zones.

## 5. Modeling spatial variations of soft soils

### *5.1. Deterministic models*

During the early years of Geotechnical Engineering, a soft soil deposit was frequently pictured as a simple half space medium with homogeneous properties. This was equivalent to ignoring spatial soil variability. To take into account the existence of contrasting horizontal layers, approximate methods were considered acceptable (Steinbrenner, 1934 [70]; Button, 1953 [71]). This simple model was also accepted and is in fact still used for dynamic soil-structure interaction analyses based on the half space theory (Richart *et al.*, 1970 [72]).

Subsequently, simple variations models, generally linear, were used to describe spatial variations of properties presenting a tendency to increase with depth.

Ladd and Foote (1974 [73]) formalized a system to present and characterize the variation of undrained shear strength within soft soil masses. This system, known as SHANSEP (Stress History and Normalized Soil Engineering Properties) was based on the observation that the shear strength of many soils can be normalized with respect to the vertical consolidation pressure. When stress strain curves measured in consolidated-undrained (CU) triaxial tests are plotted, a normalized plot can be drawn in which the strain axis is unchanged and the stress axis is normalized by dividing the axial stress difference by the vertical consolidation pressure. For many soft soils, unique curves are obtained for each value of overconsolidation ratio *OCR*. As the overconsolidation ratio increases from 1 to higher values, the strain at peak stress decreases. The general idea behind the SHANSEP method is thus to perform a series of laboratory tests with a careful control of the stress conditions during consolidation and of the stress path during undrained shear. These tests can be performed over a range of stress histories and stress paths. The in situ stress history of the soil is then evaluated, and the stress path to which the soil will be imposed is determined. Then, strengths from the laboratory tests, which most closely replicate the field conditions, are used to predict the field behavior (Bay *et al.*, 2005 [74]). Based on SHANSEP concepts, Ladd and Foote (1974 [73]) empirically developed the following relationship:

$$\frac{s_u}{\sigma_0^{'}} = S(OCR)^m \tag{8}$$

where: $s_u$ = undrained shear strength, $OCR$ = overconsolidation ratio, $\sigma'_0$ = effective vertical stress at the considered elevation, $m$ = exponent that usually falls between 0.75 and 1.0 and is established by curve fitting, and $S$ = normally consolidated ratio $(s_u/\sigma'_{vo})_{\mathrm{nc}}$.

Term $S$ varies as a function of the failure mode (testing method, strain rate). Ladd and De Groot (2003 [1]) recommended $S = 0.25$ with a standard deviation of 0.05 (for simple shear loading) and $m = 0.8$ for most soils (Robertson, 2012 [32]). The above equation is also supported by Critical State Soil Mechanics (CSSM) where $S = (1/2)\sin\varphi'$ in direct simple shear (DSS) loading, and, $m = 1 - C_s/C_c$, where $C_s$ is the swelling index and $C_c$ is the compression index (Robertson, 2012 [32]).

A critical analysis of the SHANSEP methodology was presented by Almeida (2004 [15]). According to this author, destructuration and loss of anisotropy can occur when the method is used in natural clays.

*5.2. Statistical and probabilistic models*

Variations of soft soil properties within a geotechnical medium can be represented resorting to descriptive statistics and tools such as tables or histograms (Figure 9).

Expanding the scope of this approach, it is possible to develop probabilistic models of the spatial variation of the properties of interest by considering them as random variables and fitting a probability density model to histograms obtained from sampling results in order to describe the random behavior of these variables. It becomes then possible to resort to statistical inference, i.e. to the estimation of the general characteristics of the population (a zone within the earth mass) based on a limited number of samples resorting to point estimates or confidence intervals.

Representing spatial variation of soil properties by means of random variables has however, the inconvenience of neither taking into account the specific position of the samples within the medium nor the existing dependence among them. There is no doubt that the properties of two soil samples tend in general to present a closer similarity when they are obtained at contiguous rather than distant locations. A spatial correlation structure, generally strongly anisotropic, exists in most geotechnical media and especially in soft soils.

To take into account spatial correlation, a more advanced formalism based on the concept of spatial random functions or random *field* has been introduced (Vanmarcke, 1983 [75]; 2010 [76]; Auvinet, 2002 [23]). It is then considered that, at each point $X$ of the medium, the property of interest is a random variable $V(X)$. To describe such a field, the following parameters and functions are introduced (Appendix II):

- Expected value:

$$\mu_V(X) = E\{V(X)\} \tag{9}$$

- Variance:

$$\sigma_V^2(X) = \mathrm{Var}\left[V(X)\right] \tag{10}$$

- Autocovariance function:

$$C_V(X_1,X_2) = \mathrm{Cov}\left[V(X_1),V(X_2)\right] = E\left\{\left[V(X_1)-\mu_V(X_1)\right]\left[V(X_2)-\mu_V(X_2)\right]\right\} \tag{11}$$

The function known as *autocovariance*, is used to describe the spatial linear correlation among the variables in two different points. In the simplest models it is accepted that the field is wide-sense stationary (constant expected value and autocovariance depending only on the distance between the two points considered), at least locally, or present wide-sense stationary increments. The field parameters are obtained from experimental data assuming that the field is ergodic and using statistical estimators. Developing random field models has proven particularly useful in geotechnical media of lacustrine or alluvial origin, where a conspicuous horizontal continuity exists.

In some instances, a trend in the data can be observed suggesting a deterministic variation of the property with depth. This trend can be removed from the data in order to define a stationary residual random field. The trend is commonly assumed to be linear and defined by linear regression. Note however that, for some properties such as shear strength, the trend can also be defined using deterministic considerations such as those implicit in the SHANSEP model (5.1).

When a general random field model has been established, it becomes possible to define a conditional field with respect to actually measured values. This field is no longer stationary since it presents a smaller uncertainty close to the sampling points. As exposed in Appendix II, conditional expected values of the properties of interest at points in which no measurements were performed can be obtained (point estimation) using the linear estimation technique (Auvinet, 2002 [23]; Appendix II) or any of its variants such as the *kriging* technique (Krige, 1962 [77]; Matheron, 1965 [78]; Juárez, 2015 [79]).

Note that this type of estimation assumes that the estimated values can be expressed as a linear combination of the contiguous measured values. As explained in Appendix I, this is not rigorously the case for properties such as the water content $w$ defined by Eq. (1). Using the linear estimation technique in this case can then be only considered as a first approximation, especially for high water contents.

By combining a large number of estimation points, according to a regular mesh, virtual borings and cross-sections of the subsoil and maps of the depth and thickness of the different layers can be obtained. These graphs represent the conditional expected value of the physical or geometrical property of interest. This, incidentally, leads to a smoothing effect characteristic of this type of estimation. An important advantage of this method on some other approaches based for example on artificial intelligence is that it is coherent: estimations performed at the points where measurements were made does coincide with the measured values.

It is also possible to estimate the average value of the same properties in a certain domain, for example, a finite element or a potentially unsafe failure surface (global estimation).

In all cases, it is convenient to calculate and represent the estimation variance in complementary graphs (Appendix II), in order to detect the areas where information is scarce and additional exploration is in order. To optimize the location of new sampling sites, the concept of *gain* (Azzouz et Bacconnet, 1988 [80]) is particularly useful. This approach contributes to eliminating part of the subjectivity currently existing in the design and interpretation of reconnaissance surveys.

These techniques provide tools that supplement, but does not substitute, traditional interpolation criteria based on geological evidences and in particular on geomorphology and sedimentology. The technique lends to computer programming and therefore to the simultaneous handling of large amounts of data that could be hardly evaluated with the traditional approach; it requires a careful reviewing and systematic organization of the data. The validity of the results obtained depends on the characteristics of the field. It is more likely to provide useful results in fields with an approximate Gaussian-type behavior (Appendix II). It is also better applied to structured media such as lacustrine or alluvial deposits rather than to chaotic media such as conglomerates, breccia or colluvium deposits.

"Plausible" rather than "expected" configurations of the spatial variation of the properties can be obtained by simulation (Appendix II). These simulations provide "realistic" virtual borings, cross-sections or maps, with no smoothing effect. Generating a large number of these images facilitates the evaluation of the possibility (and if desired, the probability) of reaching or exceeding locally some extreme conditions that could be critical for the project under study. The simulation is called unconditional if it is only compatible with the field parameters and conditional if the location and the characteristics of the available samples are also taken into account.

The estimation techniques can also be used when data from several random fields corresponding to different soil parameters are available. This is of foremost importance in Geotechnical engineering since it allows estimating critical (primary) properties such as mechanical parameters from (secondary) variables more easily determined such as physical or index properties, taking advantage of correlations between both types of properties. This strategy is commonly known as multivariate approach (Wackernagel, 2003 [81]) or "cokriging" (Appendix II). In the context of this lecture, it will be called "multifield" approach.

Note that, alternatively, spatial variability of geotechnical variables can be modeled by means of random functions known as *copulas* (Nelsen, 2006 [82]; Phoon and Ching, 2015 [83]; Vázquez and Auvinet, 2014 [84]). Copulas express spatial dependence without the influence of the first-order distribution functions (Appendix II). Thus, more realistic spatial variability descriptions can be attained.

It should also be observed that in soils submitted to consolidation, the evolution of static and dynamic parameters of the deforming deposit (Figure 12) occurs within a context of pronounced uncertainty. Therefore, introducing a spatio-temporal random field $V(X, \mathrm{t})$ may be helpful to increase the degree of realism of long-term predictions made with geomechanical models and should be considered (Vázquez and Auvinet, 2015 [85]).

### *5.3. Reduction of variance in soils*

When a soil property is represented by a random field, the "scale effect" or "variance reduction" concept acquires an outstanding importance. Consider the average value $V_\Omega$ of a certain property represented by a stationary random field $V(X)$, in a subdomain $\Omega$ (segment, surface or volume) of $R^p$ ($p$ = 1, 2 or 3):

$$V_\Omega = \frac{1}{\Omega}\int_\Omega V(X)dX \tag{12}$$

According to Eqs. (21) and (25) of Appendix II:

$$E\{V_\Omega\} = E\left\{\frac{1}{\Omega}\int_\Omega V(X)dX\right\} = E\{V(X)\} \tag{13}$$

$$\mathrm{Var}[V_\Omega] = \frac{\mathrm{Var}[V(X)]}{\Omega^2}\int_\Omega\int_\Omega \rho_V(X_1, X_2)\, dX_1 dX_2 \tag{14}$$

where $\rho_V(X_1, X_2)$ is the autocorrelation coefficient or normalized autocovariance of the field (Appendix II).

As exposed in Appendix II, since the autocorrelation coefficient is smaller than or equal in absolute value to unity, the variance of the average value of a stationary random property in a subdomain $\Omega$ tends to decrease when the dimensions of such subdomain increase (except in the trivial case of perfect correlation). This is the so-called reduction of variance or scale effect phenomenon, analogous to the well-known law of large numbers. This phenomenon has important consequences in geomechanics:

a) At a small scale, index properties such as porosity, void ratio, unit weight and water content are some sort of average values involving random amount of voids, solids and water. These properties can only be defined unambiguously for samples with a size sufficiently large to guarantee that the associated variance is small. The problem of the convergence of these averages towards stable values was already a concern for the ancient Greeks philosophers who called it the *Soritos* problem ("How many grains are necessary for an assembly of particles to be considered as a sand?"). Auvinet *et al.* (1984 [86]; 1986 [87]) have proposed a probabilistic solution to this problem for granular media.

b) At a larger scale, the above averages are commonly considered in geotechnical engineering as punctual values. These values generally also present random variations due to a complex geological formation process or other factors leading to random fields *V(X)* such as those considered in this lecture (Appendix II). Depending on the volume of soil affected by field tests or geotechnical structures, averages of these punctual values are affected by a significant variance reduction effect.

c) This variance reduction effect makes it strictly necessary clarifying the size of the samples tested in laboratory or the dimensions of the zone affected by a given field test. The scattering of the results is strongly dependent on these geometrical parameters (Eq. (14)).

d) Variance of the average value of punctual soil properties along a vertical axis (for example along a borehole, Appendix III), a surface (for example failure surface) or within a given volume (for example fine element) is generally much smaller than the variance of punctual values. This should be taken into account in any geotechnical reliability analysis.

e) Accuracy of geotechnical engineering predictions owes much to the variance reduction or scale effect, since the safety of most geotechnical structures does not depends on the uncertainty on local shear strength parameters but on the much lower uncertainty on average properties in large subdomains of the geotechnical mass.

### *5.4. Modeling spatial variations of the subsoil of Mexico City.*

Not so long ago, the upper clay formation in Mexico City lake zone used to be idealized as a simple half space medium with homogeneous properties. As an example, immediate displacements due to excavations were successfully modelled assuming the medium to be elastic with a small strain undrained modulus obtained from geophysical measurements (Auvinet, 1969 [88]). Considering the subsoil as a homogeneous or horizontally stratified half space medium is still implicit in the techniques proposed in Mexico City building code for dynamic soil-structure interaction analysis (GCDMX, 2018b [89]).

A statistical approach was used by Marsal and Mazari (2017 [33]) to describe spatial variations of Mexico City clays, from a large number of experiments performed during the late 50's and early 60's of the last century on samples retrieved at different locations in the lacustrine zone in the central part of the city. Assuming that large sub-zones of this part of the city subsoil were "statistically homogeneous", those authors prepared tables and histograms for each sub-zone and established correlations between index and mechanical properties that have been extremely valuable for several generations of geotechnical engineers. To illustrate the above, Figure 15 presents a correlation between coefficient of compressibility, $a_v$, in the preconsolidation interval, and water content, $w$ (Eq. (1)).

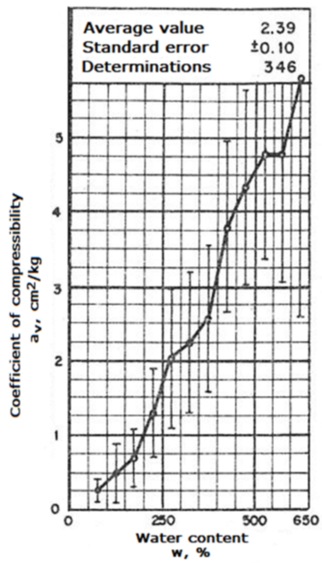


**Figure 15.** Statistical correlation between coefficient of compressibility, $a_v$, in preconsolidation interval, and water content, $w$, (Eq. (1)), Marsal and Mazari (2017 [33]).

Water content has also been related to undrained shear strength from UU tests (Mazari, 1996 [90]). Dispersion is large and only allows for the identification of a general trend with a rather wide range of variability (Figure 16). Similar correlations between undrained shear strength obtained from CPT tests and water contents have been established for the Texcoco Lake (Alanis, 2003 [53]).

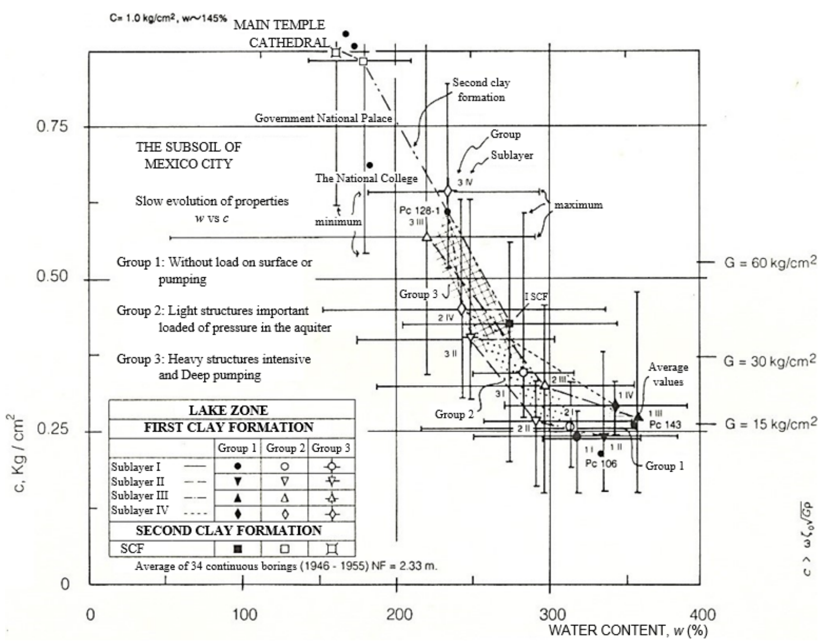


**Figure 16.** Shear strength c ($s_u$) *vs* water content $w$ (Eq. (1)) for Mexico City clays.

The correlations proposed by Marsal and Mazari are strongly affected by the definition of water content that was adopted in the statistical analyses (Eq. (1)). As an example, a correlation between coefficient of volumetric compressibility, $m_v$ , and water content $w$ deduced from Figure 15 is presented in Figure 17 (left hand side). This correlation suggests that, unexpectedly, coefficient $m_v$ remains practically constant for values of $w$ exceeding 400 %. In fact, the non-linear relationship implicit in Eq. (1) causes a distortion of the correlation graph that is no longer observed when $w$ (Eq. (1)) is substituted by $w'$ (Eq. (2)) (Figure 12, right hand side).

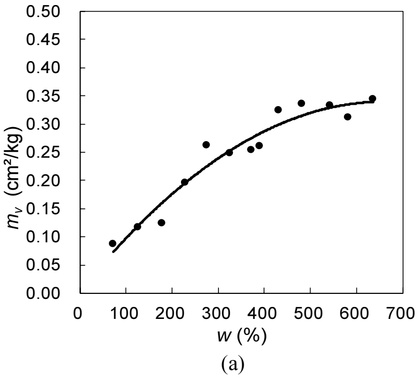


**Figure 17.** Correlation between coefficient of volumetric compressibility $m_v$ and water content defined by (a) Eq. (1) and (b) Eq. (2).

Modifying the definition of water content generally improves the correlation of this parameter with other properties. Figure 18 shows how correlation between shear wave velocity $V_s$ and water content improves when switching from definition of Eq. (1) to definitions of Eq. (2) or Eq. (3). When applied to the correlation of Figure 16, or to the correlations proposed by Alanis (2003, [53]) this transformation has similar consequences.

Figure 17 and 18 suggest that water contents $w'$ (Eq. (2)) and $w''$ (Eq. (3)) provide a better insight into mechanical properties of soft soils than the classical parameter $w$ (Eq. (1)).

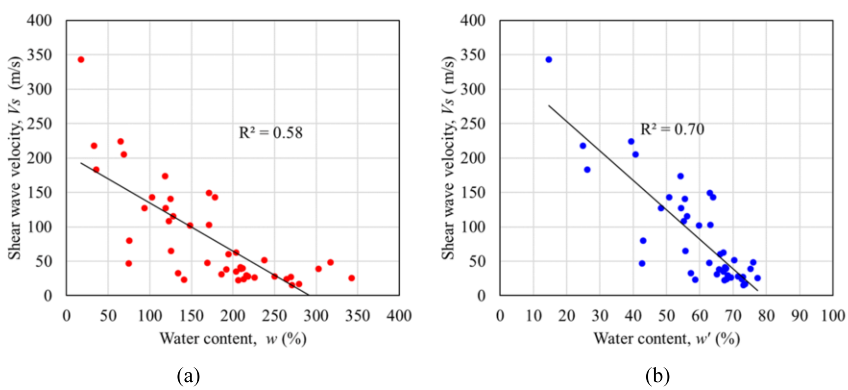


**Figure 18.** Correlations between shear wave velocity, $Vs$, and water content defined by: (a) Eq. (1), (b) Eq. (2), (c) Eq. (3).

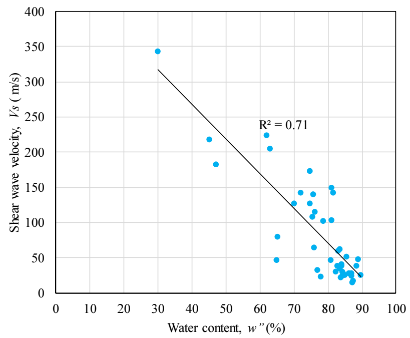


(c)

**Figure 18.** (*continued*) Correlations between shear wave velocity, *Vs*, and water content defined by: (a) Eq. (1), (b) Eq. (2), (c) Eq. (3).

Reséndiz and Herrera (1969 [91]) were probably the first to suggest using random fields to describe the variations of Mexico City clays properties. They assumed that all variations in compressibility occurring in a horizontal direction are random and they showed that, within a given natural soil stratum, coefficient of volume compressibility $m_V$ behaves as a Gaussian 2D random field with Dirac delta correlation coefficient (white noise). Based on these considerations they were able to assess the probability of differential settlements of a rectangular foundation exceeding any given tolerable value.

In the last decades, random field models have become particularly useful to describe the clay deposits of the Valley of Mexico (Auvinet *et al*., 2001 [92]; 2002 [93]; 2005 [94]). They have been used for describing spatial variations at different scales.

a) Small scale

The variations of water content in the horizontal cross-section of a clay sample shown on Figure 7 can be considered as local fluctuations of a 2D random field. Parameters of this field can be roughly estimated using common statistics from the scarce data available. The estimation techniques described in Appendix II, can then provide a dense set of punctual values and contours of estimated water content can be established (Figure 19a). Results obtained in the same way but accepting the definitions of Eq. (2) and Eq. (3) for water content are shown respectively on Figures 19b and 19c.

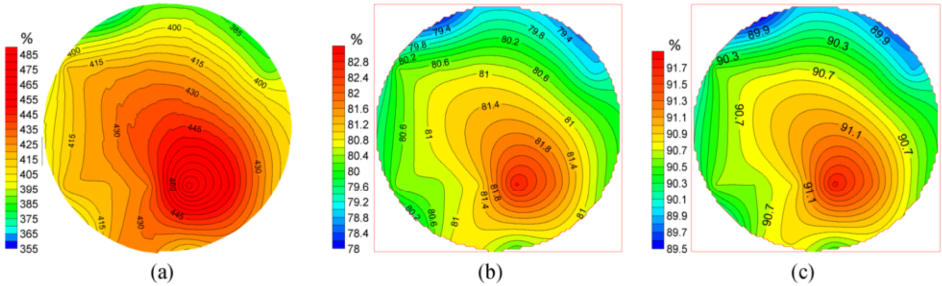


**Figure 19.** Geostatistical estimation of water content contours in a cross-section of a Mexico City clay sample for different definitions of water content; (a) Eq. (1), (b) Eq. (2) and (c) Eq. (3).

The apparent degree of homogeneity of the sample varies significantly depending on the definition of water content adopted. Definition of Eq. (1) tends to exacerbate the differences between the different zones of the sample.

b) Soil profiles 1D geostatistical estimations.

Variations with depth of soil properties of the upper clay formation of the Lake Zone of Mexico City can be described by a 1D random field.

In the case of the water content profile obtained within the upper clay formation shown in Figure 20a, a trend suggesting reduction of water content with depth is observed. This trend can be removed from the data in order to define a stationary residual random field (Figure 20b). Figure 21 shows vertical correlograms for the original (Figure 21a) and residual (Figure 21b) fields.

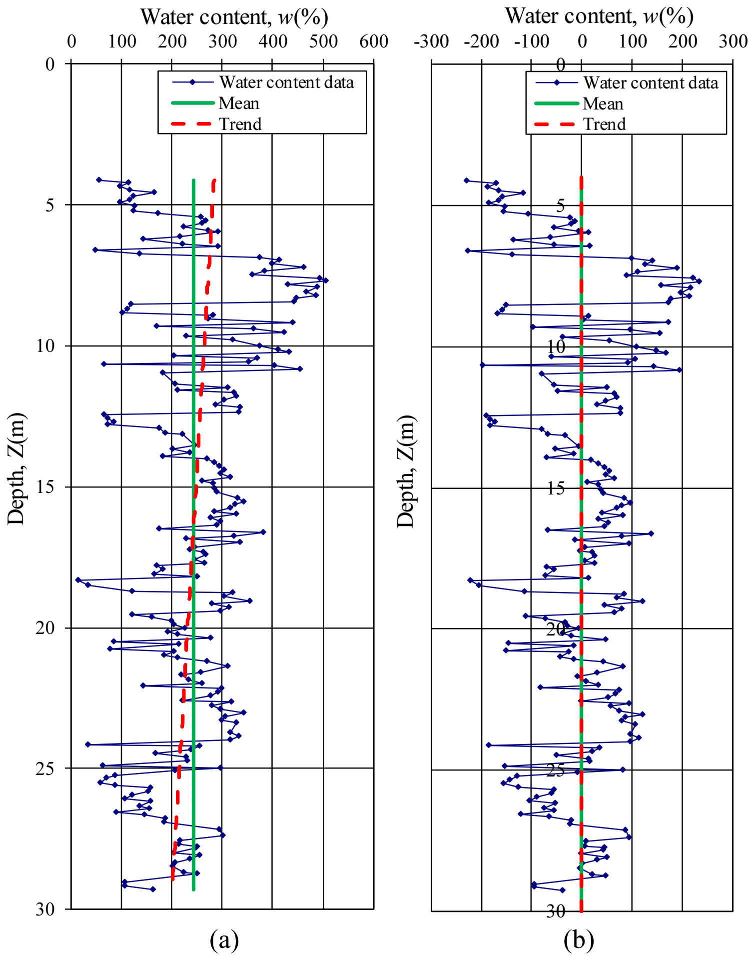


**Figure 20.** Typical water content profile ($w$, Eq. (1)), in the upper clay formation of the Lake Zone. (a) Original field (b) Residual stationary field.

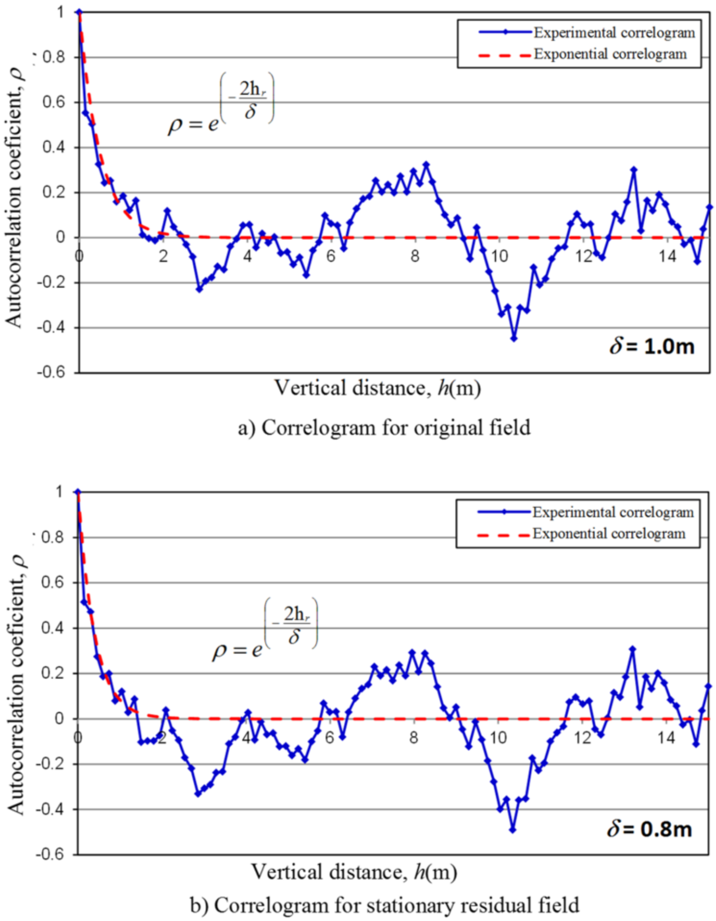


**Figure 21.** Vertical correlograms for water content profiles of Figure 20.

In both cases, the correlograms exhibit a harmonic behaviour suggesting that the variation of the characteristics of the soil with depth present some periodicity. In practice, this is generally ignored ignored and an exponential function is adjusted to the first stretch of the correlogram to take advantage of the higher correlations corresponding to short vertical distances. Note that the correlation distance $\delta$ of the residual field is slightly shorter that the correlation distance of the original field. Both types of correlogramas can be used to obtain more detailed water content profiles, interpolating vertically between measurement points using the estimation techniques presented in Appendix II.

On the other hand, water content profiles can be used as a support for estimating other properties resorting to "multifield" analysis or "cokriging", (Wackernagel, H., 2003 [81]; Delgado Muñiz, 2017 [95]; Appendix II). Figure 22 shows how a shear wave velocity profile (Figure 22a) can be improved (Figure 22c) by cokriging using water content $w$ (Eq. (1)) as a supporting secondary field (Figure 22b).

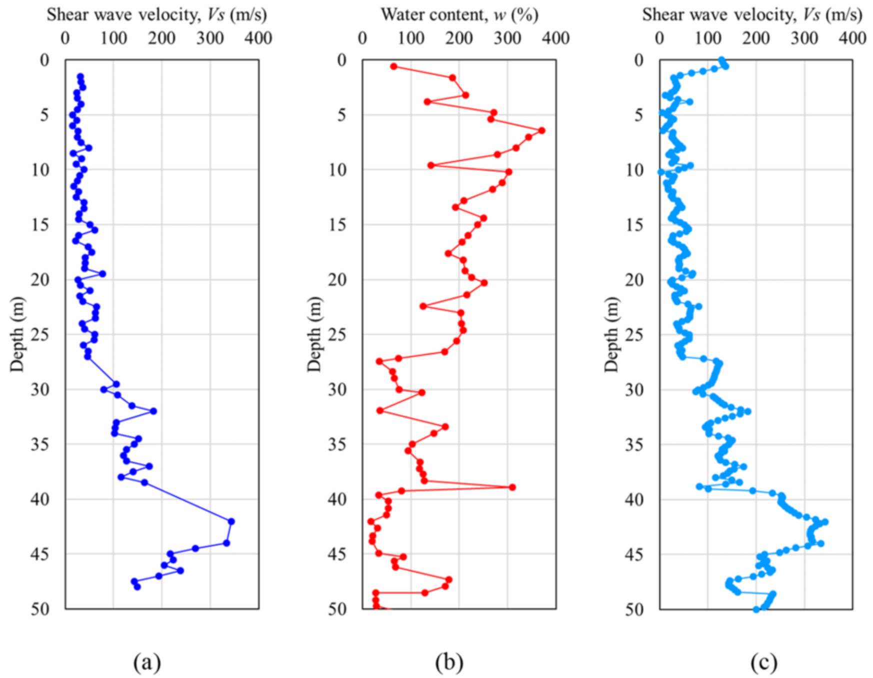


**Figure 22.** Original *Vs* (a) and *w* (Eq. (1)) (b) profiles and improved *Vs* profile (c) obtained by cokriging, using water content as a secondary random field.

The respective auto-correlograms of *Vs* and *w* and the cross-correlogram of *Vs* and *w* deduced from the profiles of Figure 22 and used in the cokriging estimation are shown on Figure 23.

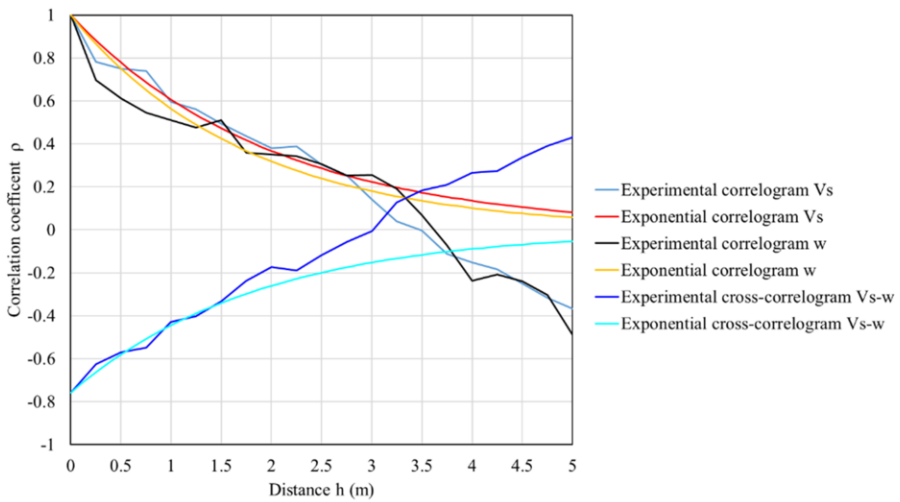


**Figure 23.** Vertical autocorrelograms of *Vs* and *w* and cross-correlogram *Vs-w* obtained from profiles of Figure 22.

Figure 22c shows that the improved shear wave velocity profile reflects some features of the water content profile that were not present in the original $V_s$ profile, especially close to the surface and at depth where shear wave velocity measurements were scarce (i.e. from 27 to 30m, from 38 to 44m and beyond 48m).

The above cokriging estimation was repeated with better behaved variable *w*' (Eq. (2)). Figure 24 shows how the shear wave velocity profile (Figure 24a) was also improved (Figure 24c) by cokriging using water content *w'* (Eq. (2)) as a secondary field (Figure 24b).

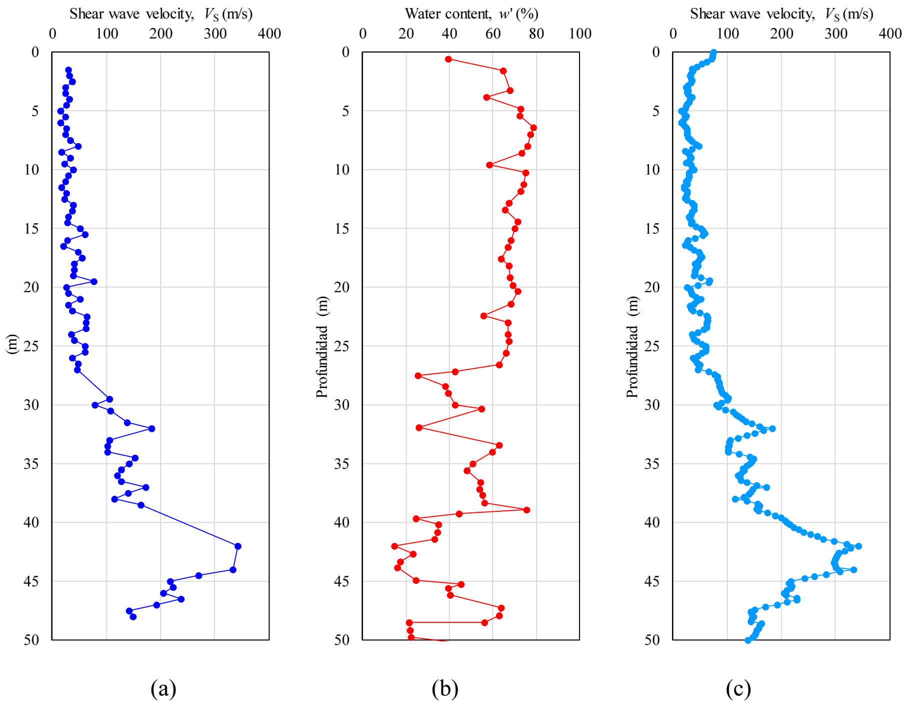


**Figure 24.** Original *Vs* (a) and *w'* (Eq. (2)) (b) profiles and improved *Vs* profile (c) obtained by cokriging, using water content *w*' as a secondary random field.

The auto-correlograms of $V_s$ and *w'* and the cross-correlogram of $V_s$ and *w'* that were deduced from the profiles of Figure 24 and used in the cokriging estimation are shown on Figure 25.

Figure 24c shows again how the improved shear wave velocity profile reflects features of the water content profile that were not present in the original $V_s$ profile. The influence of the secondary field *w*' is however less significant than in the case of Figure 22c, suggesting that using definition of Eq. (1) for water content may exaggerate spatial variations of other variables when used in cokriging estimations.

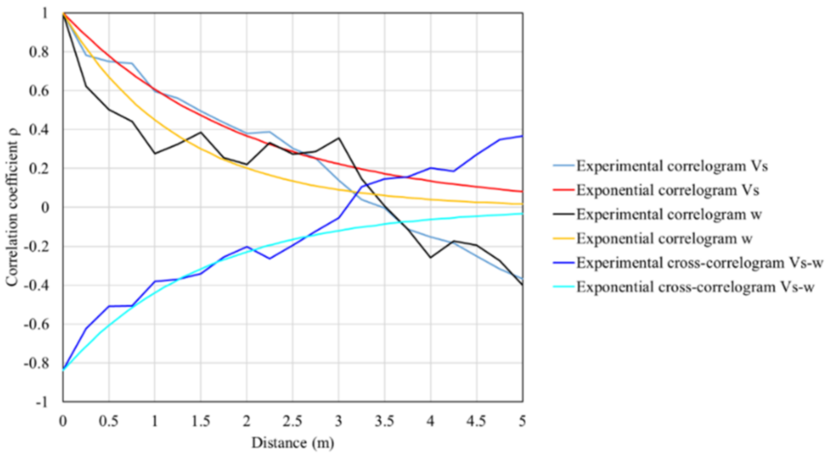


**Figure 25.** Vertical auto-correlograms of $V_s$ and $w'$ (Eq. (2)) and vertical cross-correlogram $V_s$-$w'$ for profiles of Figure 24.

On Figure 26, vertical profiles of shear wave velocity $V_s$ (Figure 26a) and CPT tip resistance $q_c$ (Figure 26b) are presented. The shear wave velocity profile was improved interpolating vertically between measurements using the estimation techniques of Appendix II (kriging, Figure 26c).

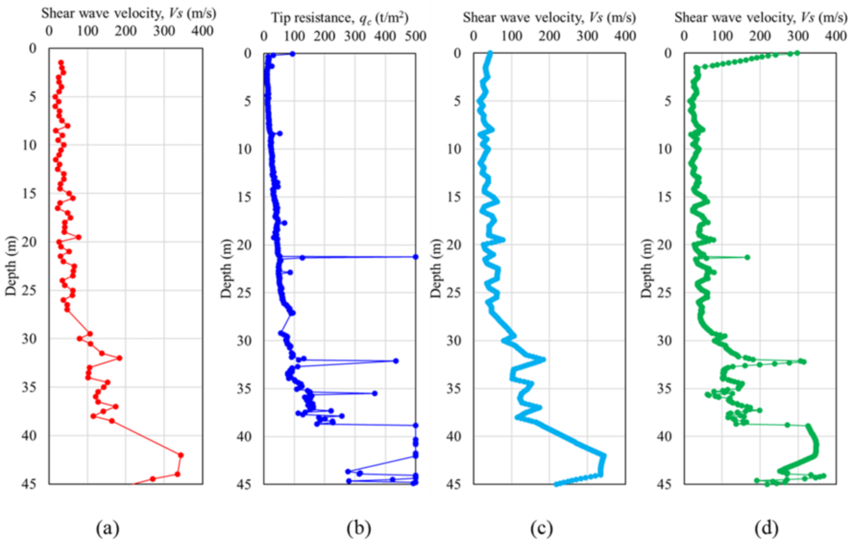


**Figure 26.** Improved $V_s$ profile obtained by kriging (c) and cokriging (d), using CPT tip resistance $q_c$ (b) as a secondary random field.

It was also taken advantage of the correlation between shear wave velocity $V_s$ and CPT tip resistance $q_c$ (Figure 27) to improve further the estimated shear wave velocity profile using $q_c$ as a secondary field for cokriging (Figure 26d). The improved profile reflects some features of the CPT tip resistance profile that were not present in the original $V_s$ profile, especially the effect of sand or silt lenses at different elevations.

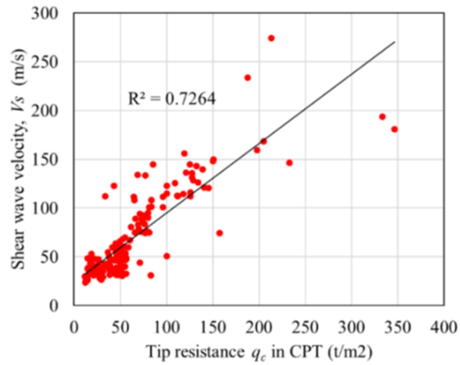


**Figure 27.** Empirical correlation between shear wave velocity $V_s$ and CPT tip resistance, $q_c$. (1t/m$^2$ = 10kPa).

c) 2D geostatistical estimations

Since 1992, approximately 10,000 boring logs obtained in the basin of Mexico City have been collected and a Geographic Information System focused on the geotechnical properties of the subsoil has been developed (Auvinet *et al*., 2017 [30]). This system constitutes a valuable database that can be used to perform geostatistical analyses.

As an example, it has been possible (Juárez *et al*., 2016 [96]) to assess the depth of the *deep deposits* (DP) below the clay formations in the Lake Zone of Mexico City. This depth was represented by a 2D random field defined in the Lake Zone area. Figure 28 shows the location of the main data used in the analysis.

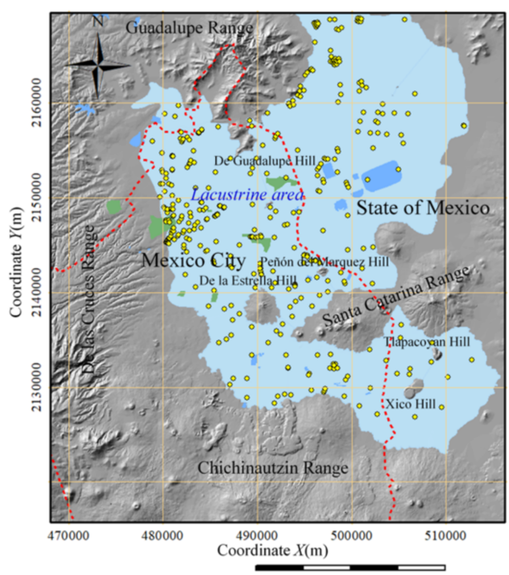


**Figure 28.** Location of *Deep Deposits* depth data.

Using the techniques described in Appendix II and appropriate correlation models; it was possible to establish a contour map of the estimated depth of Deep Deposits (Figure 29). This map is valuable since these deposits constitute the inferior boundary of most analytical or numerical models, including seismic site effects models. It can also be useful for preliminary design of deep foundations.

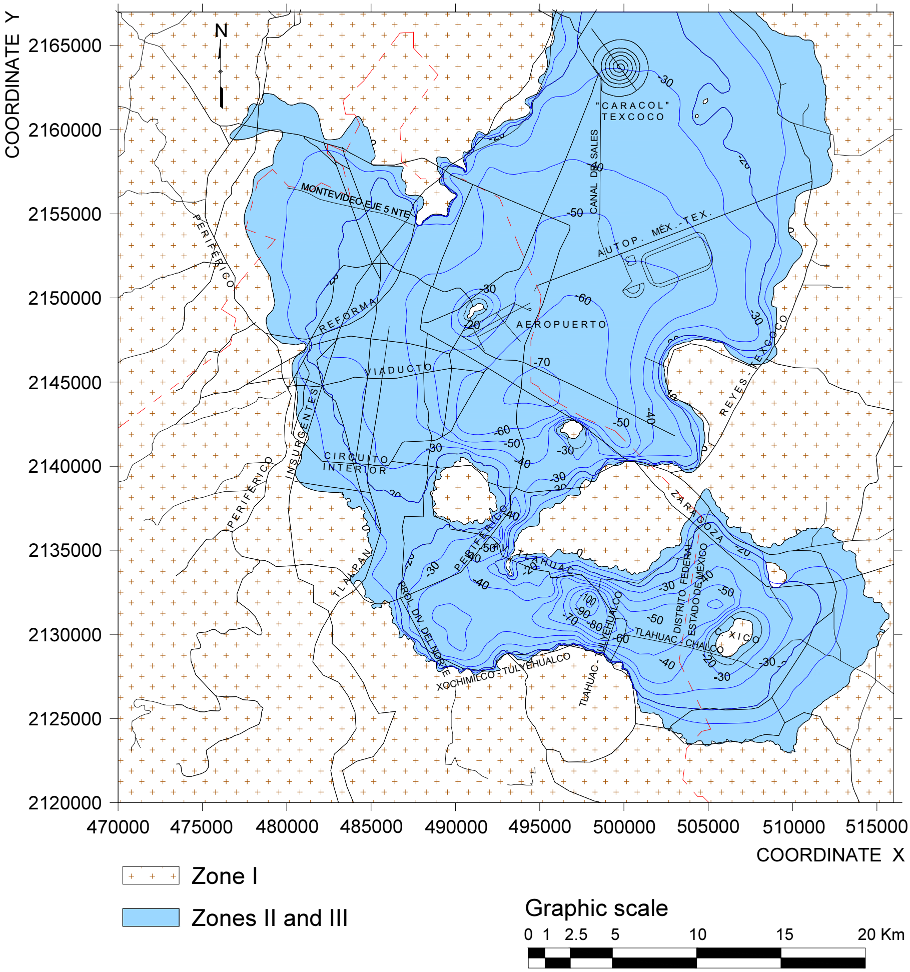


**Figure 29.** Contour map of estimated *Deep Deposits* depth within the Lake Zone in Mexico City.

d) 3D geostatistical estimations

The database on Mexico City subsoil mentioned in the previous section has been useful to improve the current knowledge on the subsoil of different zones of the Valley of Mexico. A large number of theses related to specific zones of the lacustrine area were presented (Flores Tapia, 2000 [97]; Aguilar, 2001 [98]; Pantoja, 2002 [99], Morales, 2004 [100]; Valencia, 2007 [101]; Jiménez, 2007 [102]; Pérez, 2009 [104]; Rodríguez, 2010 [105]; Hinojosa, 2010 [106]; Tenorio, 2013 [103]; Hernández Vizcarra, 2013 [107]; Juárez, 2015 [79]; Barranco Eyssautier, 2016 [108]; Delgado Muñiz, 2017 [95]).

Virtual subsoil cross-sections at different sites of the lacustrine zone have been established. These 2D or 3D models representing the water content or other estimated geotechnical parameters, have provided a valuable overview of the subsoil conditions in Mexico City (Auvinet *et al*., 2017 [30]).

The autocorrelation function commonly used in these models is of the exponential type:

$$\rho_V(r,z) = \exp\left\{-2\left(\frac{r}{\delta_r} + \frac{z}{\delta_z}\right)\right\} \tag{15}$$

where parameters $\delta_r$ and $\delta_z$ are, respectively, the horizontal and vertical correlation distances and $r = \sqrt{(x_i - x_j)^2 + (y_i - y_j)^2}$ and $z = |z_i - z_j|$ are respectively the horizontal and vertical distances between two different points of the soil mass with respective coordinates $(x_i, y_i, z_i)$ and $(x_j, y_j, z_j)$.

The correlation structure of the materials of the lacustrine zone of Mexico City is highly anisotropic. In Figures 21, 23 and 25 it was shown that the vertical correlation distance of the water content is of the order a few meters. Figure 30 shows that the horizontal correlation distance in unlimited domains can attain several kilometres.

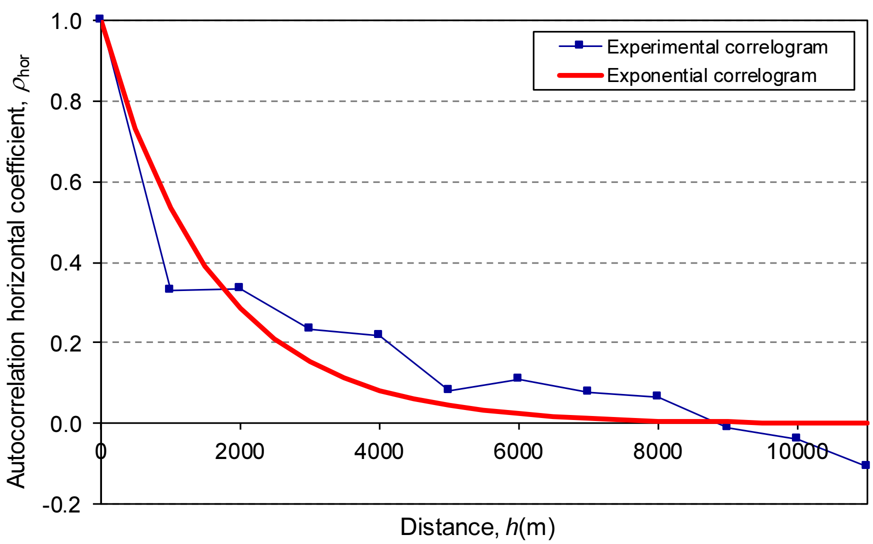


**Figure 30.** Typical horizontal correlogram for water content field in Mexico City Lake Zone.

Figure 31 shows a longitudinal profile of the estimated water content of the subsoil below an embankment used for the preloading of an area where a runway was being built (Mendoza *et al*., 2018 [51]).

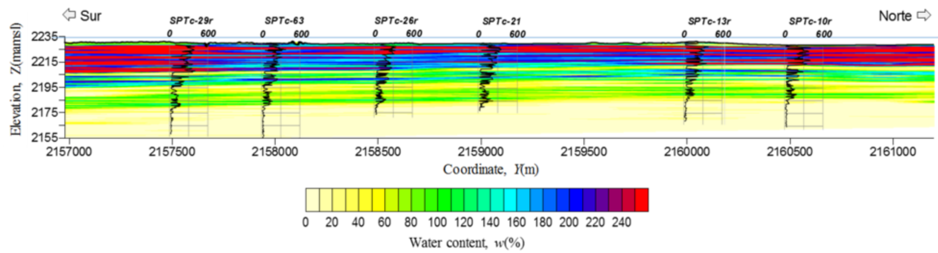


(a)

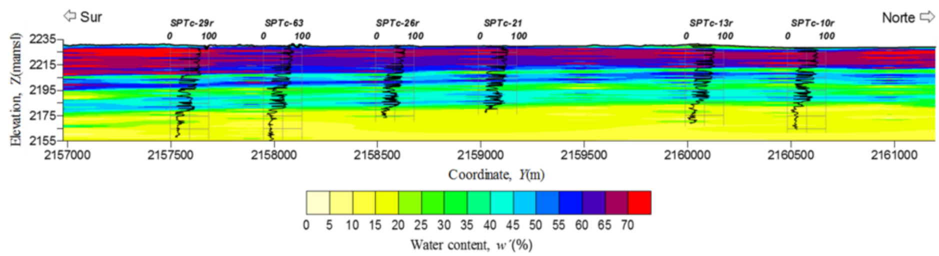


(b)

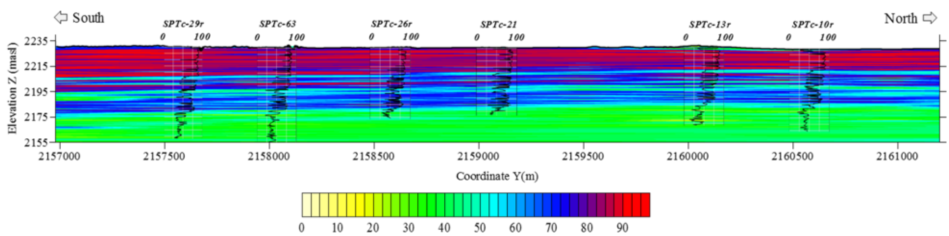


(c)

**Figure 31.** Longitudinal profile of estimated water content defined by (a) Eq. (1), (b) Eq. (2) and (c) Eq. (3) (Runway 6, NAICM).

To dispose of more realistic synthetic pictures of the longitudinal profile of water content in the subsoil, simulated profiles were obtained using the techniques described in Appendix II. Profile presented in Figure 32 corresponds to a simulation performed with the Eq. (1) definition of water content.

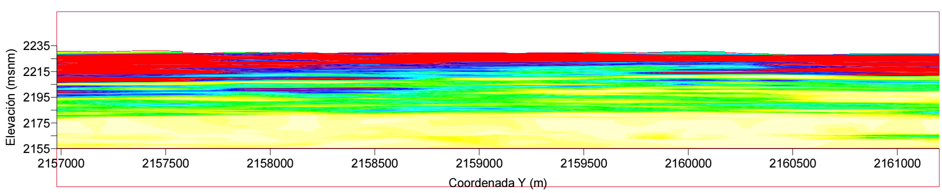


**Figure 32**. Longitudinal profile of simulated water content defined by Eq. (1) (Runway 6, NAICM).

The five profiles of Figure 33 were established with the definition of water content given by Eq. (2). The same differences are observed as in the case of estimations (Figure 31). As could be expected, the simulated profiles are less homogeneous than the estimated profiles.

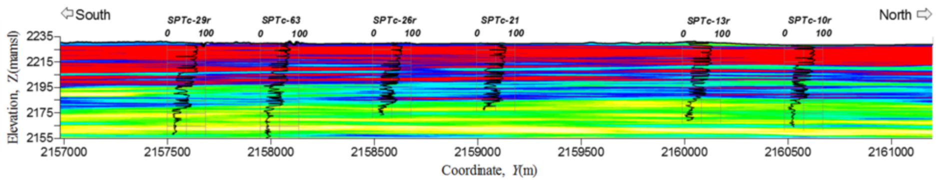


Simulation 1.

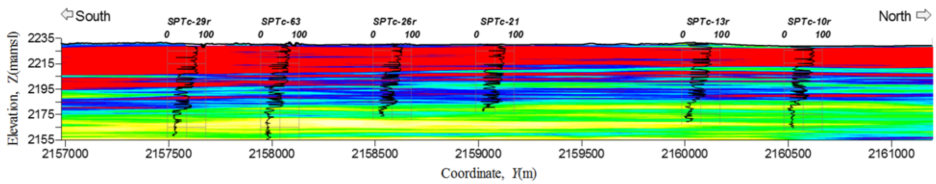


Simulation 2.

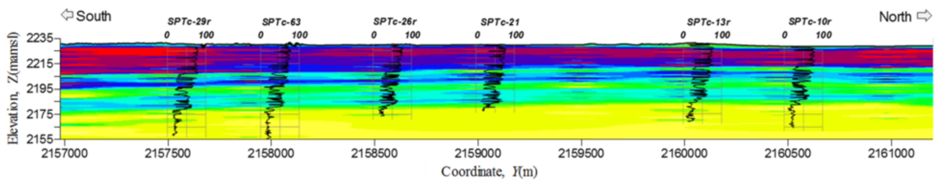


Simulation 3.

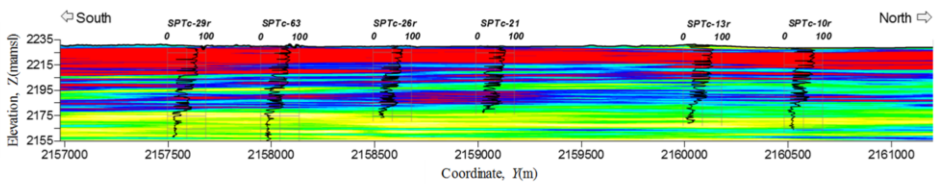


Simulation 4.

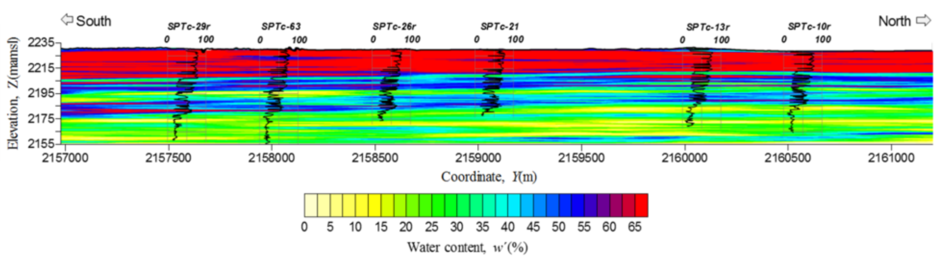


Simulation 5.

**Figure 33.** Longitudinal profiles of simulated water content *w*' defined by Eq. (2) (Runway 6, NAICM).

It can be verified that the average of several simulations such as those presented in Figure 33 tends to coincide with the estimated profile (Figure 31b) as the number of simulations increases.

Figure 34 shows geostatistical 3D models of soil profile (water content *w* (Eq. (1)) and CPT tip resistance $q_c$) for the X shaped Terminal Building of NAICM. These two models provide complementary visions of the subsoil of the area.

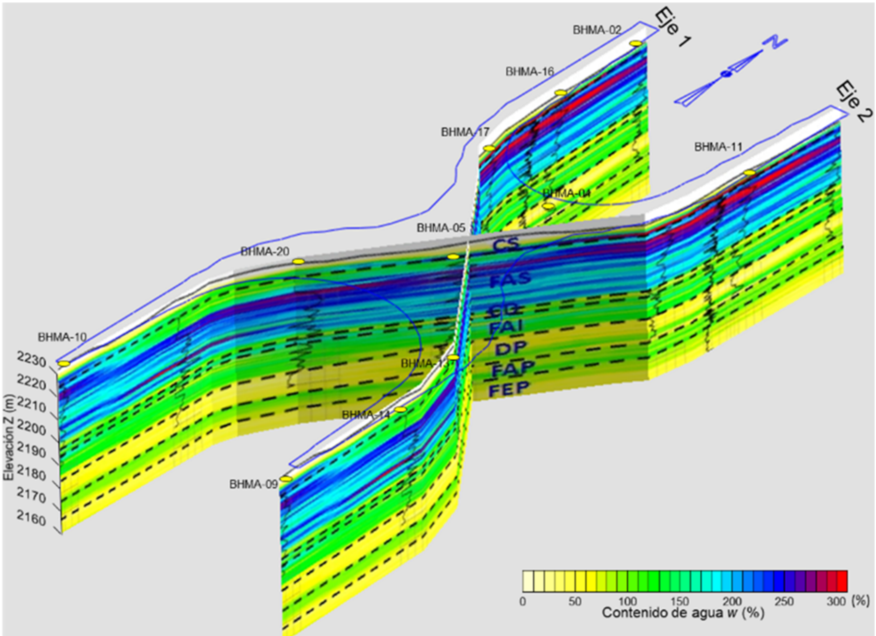


(a)

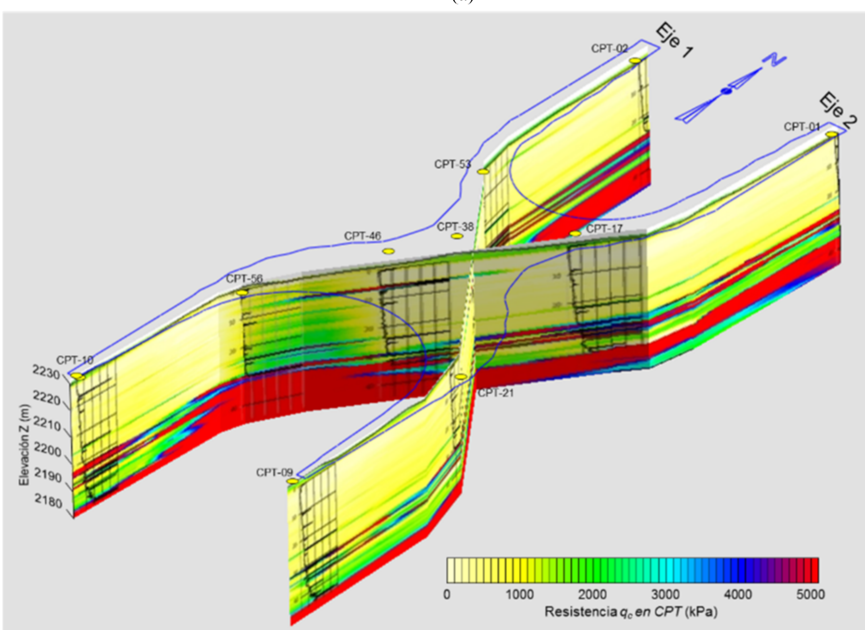


(b)

**Figure 34.** Longitudinal profile of: (a) estimated water content *w* (Eq. (1)) and (b) CPT tip resistance $q_c$. (Terminal building area, NAICM).

Figure 35 shows longitudinal profiles of estimated shear wave velocity *Vs* (kriging), (a) and CPT tip resistance $q_c$ (b) for the east side of the Terminal building of NAICM. A Shear wave velocity *Vs* profile (c) improved by cokriging with $q_c$ is also presented.

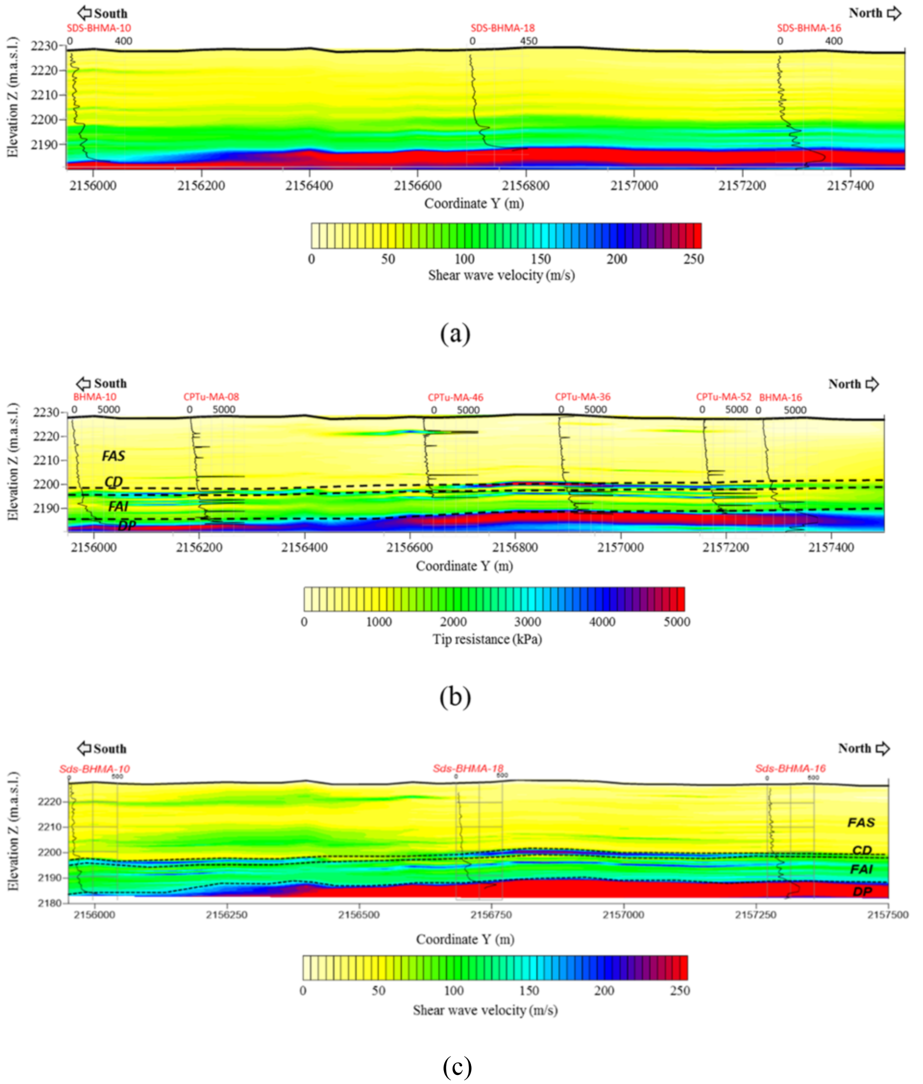


**Figure 35.** Longitudinal profiles of estimated soil properties: (a) Shear wave velocity $Vs$ (kriging), (b) CPT tip resistance $q_c$ (kriging), (c) Shear wave velocity $Vs$ improved by cokriging with $q_c$ (Terminal building, east side).

Figure 36 shows the estimated profiles of water content $w$ (Eq. (1)) along the 12 lines of the subway system of Mexico City (Auvinet *et al*., 2017 [30]). An obvious advantage of this type of representation is that it can be easily updated when new boreholes results become available.

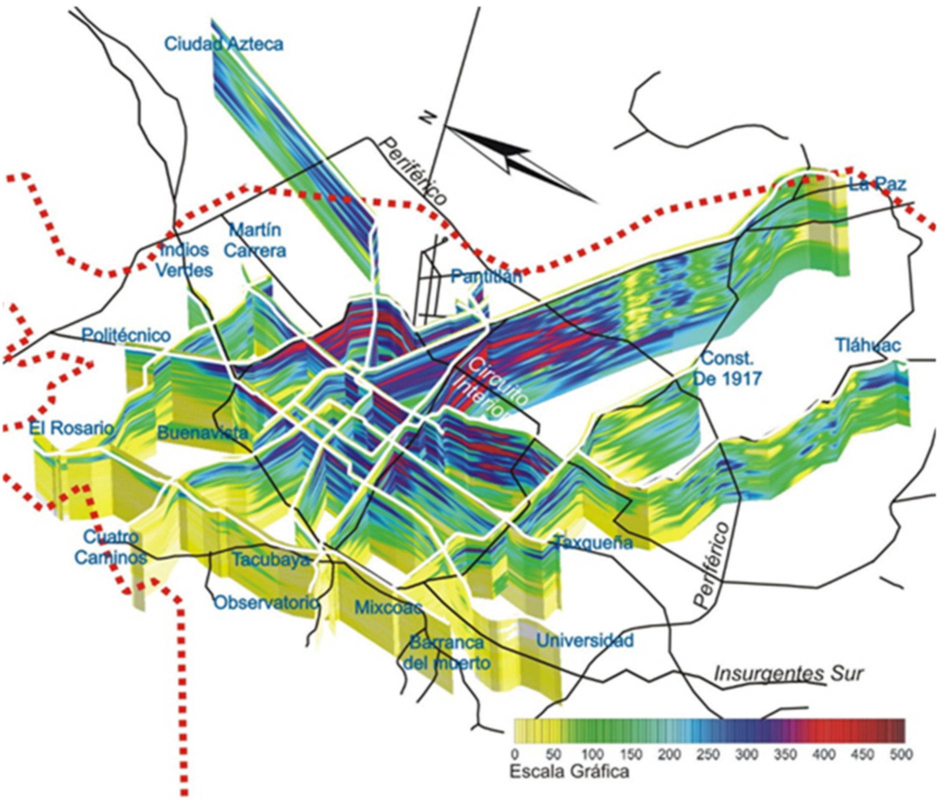


**Figure 36.** Spatial distribution of estimated water content along the 12 lines of Mexico City subway system.

Together with the estimated properties profiles, geostatistical analyses provide profiles of the estimation error (standard deviation of the estimation, Appendix II). These profiles can be used to define an optimum position for additional boreholes in an exploration program.

As seen in Figure 37, for a tunnel exploration program, adding a new borehole (SM1) (b) changes significantly the original estimation error profile (a). One should look *a priori* for the position of new boreholes that bring more “light” to the existing knowledge of subsoil characteristics,

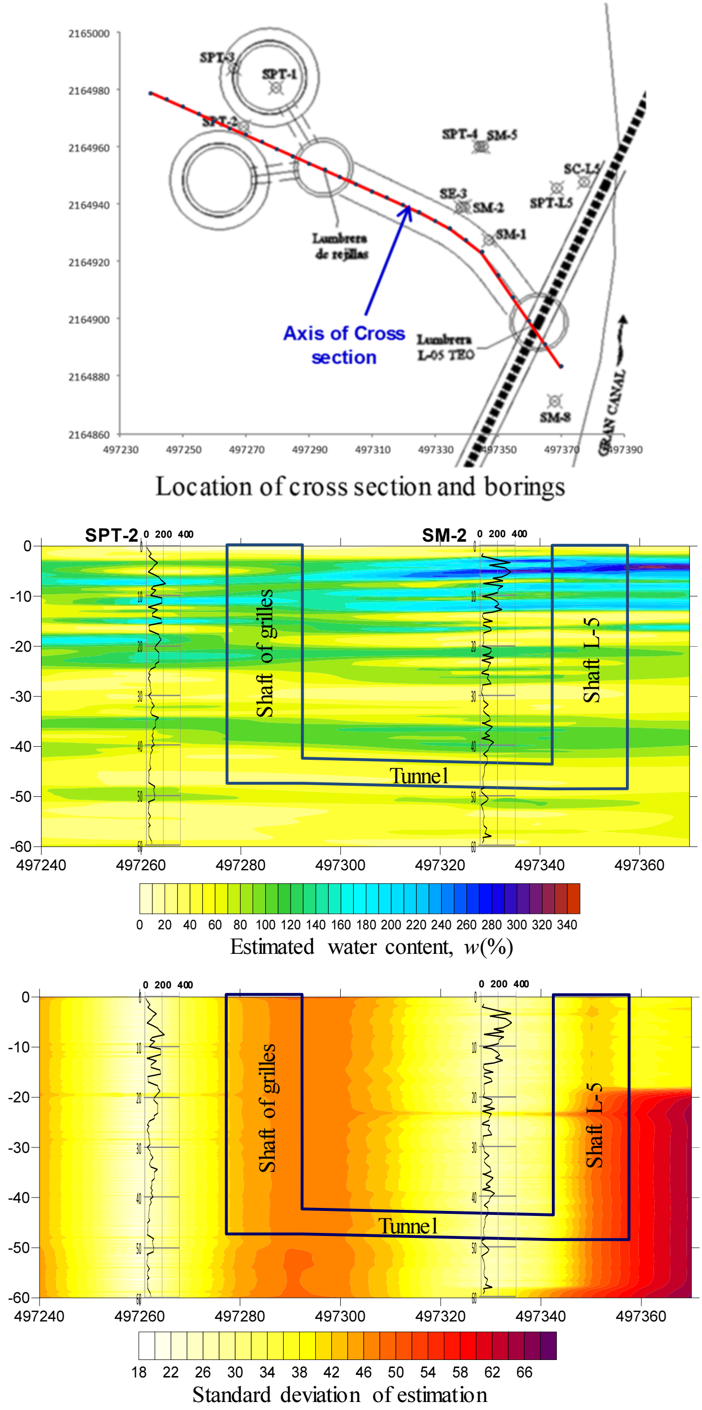


(a)

**Figure 37.** "Light" brought about by boreholes improving knowledge of soil characteristics (a) before borehole SPT1 was performed and (b) after it was performed.

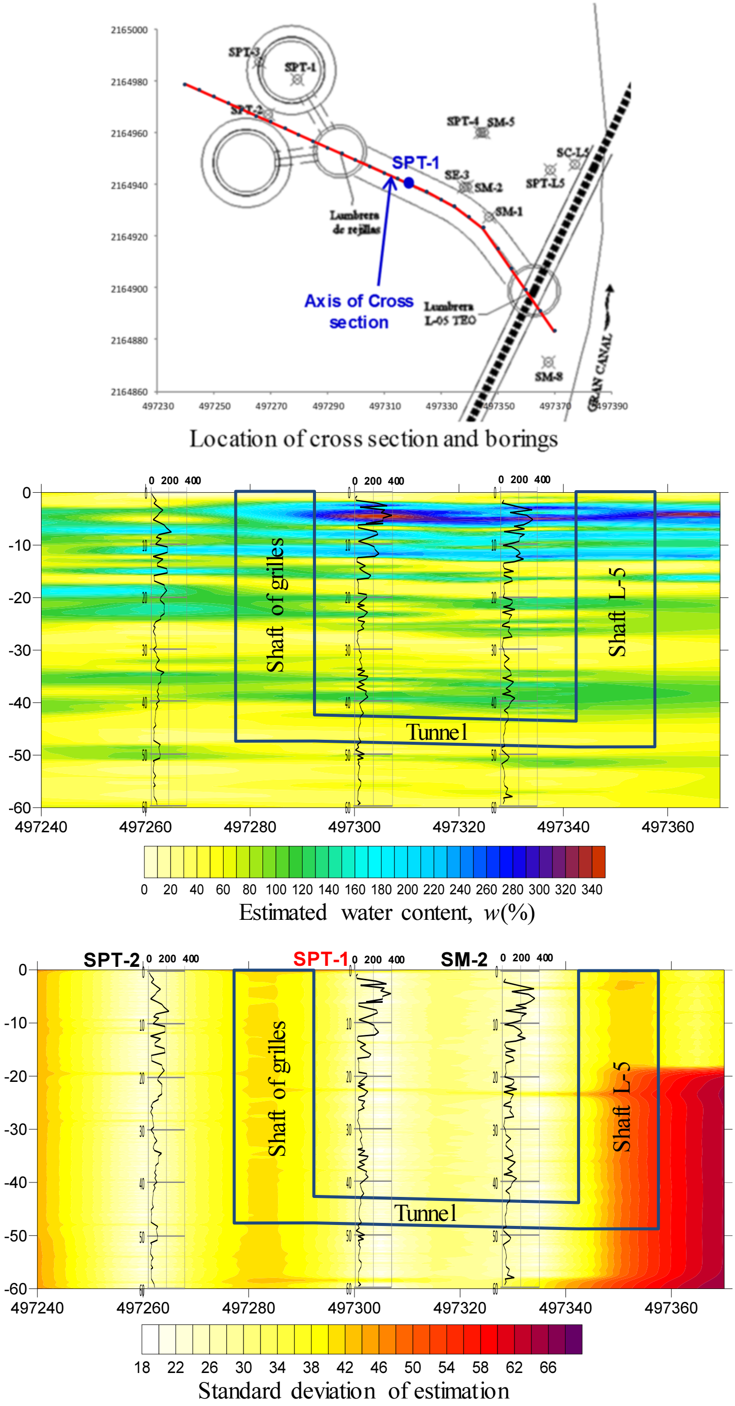


(b)

**Figure 37.** (*continued*) "Light" brought about by boreholes improving knowledge of soil characteristics (a) before borehole SPT1 was performed and (b) after it was performed.

## 6. Geotechnical analysis considering soft soils spatial variations

### *6.1. Available methods*

Geotechnical analyses can take into account spatial variations of soft soils resorting to probabilistic techniques.

Many analyses are found in the literature in which soil properties are considered as random variables (Magnan and Boureahoua, 2001 [109]). Most of these studies attempt to take into account uncertainty due to lack of knowledge of soil parameters but few of them take into account explicitly the spatial variability of these parameters.

The uncertainty on the results of a geotechnical analysis for a structure built on a soil mass represented by a random field can be obtained in some instances by analytical methods. However, in most cases it is necessary to resort to numerical methods. In this context, the stochastic finite element method (SFEM) is a particularly useful technique. Auvinet *et al.* (1996 [110]; 2000 [111]; 2002 [23]) exposed the theoretical bases of this method. SFEM generally resorts to the method of perturbations (Mathews and Walker, 1964 [112]), to a punctual approximation (Rosenblueth, 1975 [113]) or to the Monte Carlo technique based on a series of simulations of the random field. Another SFEM technique: the “Spectral approach” (Ghanem and Spanos, 1991 [114]; Pineda, 2015 [115]) has also proven to be useful for application in geotechnical engineering.

Stochastic geotechnical analyses can be brought a step forward and be used for evaluating the probability of failure (or of exceedance of a critical limit) or its complement to unity, reliability. This ambitious objective can seldom be reached but, frequently, it is at least possible to obtain a representative value of the so-called “index of reliability”. The precepts of modern risk and reliability theory first appeared in fundamental papers by Freudenthal (Freudenthal *et al.*, 1964 [116]). This work was followed by contributions of a generation of researchers in structural engineering, including Ang, Cornell, Ditlevsen, Hasofer, Lind, Rackwitz. Rosenblueth and Esteva. Auvinet (2002 [23]) presented a summary of the main concepts of the reliability theory.

### *6.2. Dealing with spatial variability in Mexico City clays*

To show how the stochastic approach can be used in geotechnical analyses performed in soft soils such as those of Mexico City, some very simple examples will be presented.

#### *6.2.1. Friction pile*

Friction piles are commonly used in the lacustrine clays of Mexico City in order to reduce the settlements of superficial or compensated foundations (design in terms or settlements) or as the main foundation system (design in terms of bearing capacity). These are generally prefabricated piles with tip located about three meters above the first hard layer.

The bearing capacity of a friction pile installed in a soft soil medium modelled as a 1D stationary (vertical) random field can be estimated together with the corresponding uncertainty.

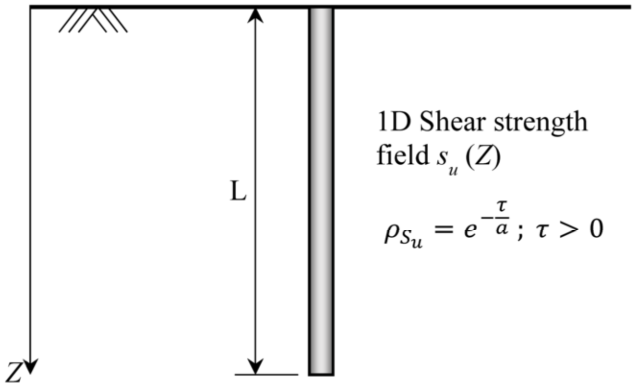


**Figure 38.** Friction pile in soft soil with undrained shear strength considered as a 1D random field.

Considering a typical case in Mexico City (Figure 38) where shear strength $s_u(Z)$ is assumed to be a stationary 1D random field with expected value $E\{s_u\}$, variance Var$[s_u]$ and coefficient of autocorrelation function of the exponential type:

$$\rho_{s_u} = e^{-\frac{\tau}{a}}; \tau > 0 \tag{16}$$

where $\delta = 2a$ is the correlation distance and $\tau = Z_1 - Z_2$.

The friction bearing capacity $Q$ along a pile of length $L$ and perimeter $P$ can be estimated as:

$$Q = s_{uL} PL \tag{17}$$

where $S_{uL}$ is the average shear strength:

$$s_{uL} = \frac{1}{L}\int_0^L s_u(Z)\, dZ \tag{18}$$

Then (Appendix III):

$$E\{Q\} = E\{s_{uL}\}PL = E\{s_u\}PL \tag{19}$$

and:

$$\mathrm{Var}[Q] = \mathrm{Var}[s_{uL}]\left(P^2L^2\right) = \frac{2a^2}{L^2}\mathrm{Var}[s_u]\left[\frac{L}{a} + e^{\frac{-L}{a}} - 1\right]\left(P^2L^2\right) \tag{20}$$

The coefficient of variation of random variable $Q$ is:

$$CV[Q] = \frac{\sqrt{\mathrm{Var}[Q]}}{E\{Q\}} \tag{21}$$

When the $L/\delta$ ratio increases, this coefficient decreases by a factor $R$ represented in Figure 39. For a typical 30m long friction pile in Mexico City clays where vertical correlation distance $\delta$ is of the order of 2.5m, this factor presents a value of 35%.

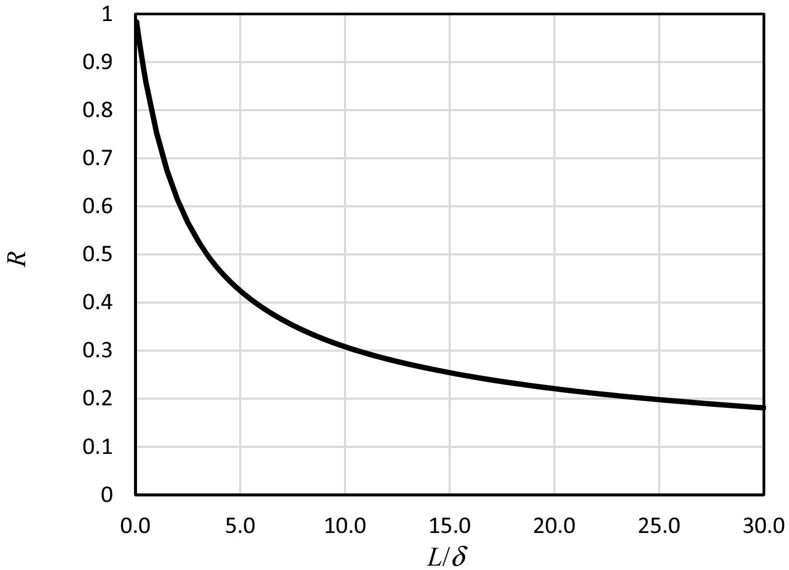


**Figure 39.** Reduction of coefficient of variation of friction pile bearing capacity, $Q$, as a function of ratio between pile length $L$ and vertical correlation distance $\delta = 2a$.

This illustrates the fact, already mentioned in this lecture, that in most cases, the stability of geotechnical structures does not depend on the uncertainty on local shear strength parameters but on the much lower uncertainty prevailing on average properties in large subdomains within the geotechnical medium (in this case along the pile shaft).

The same example could have been developed for a passive horizontal anchor of the type sometimes used in excavations as part of retaining systems. In this case, the correlation distance would be much longer (Figure 30) and the reduction of the variance of the limit capacity of this anchor as a function of length would be hardly significant. Reliability of this type of reinforcement elements within anisotropic random fields is thus strongly dependent on their orientation in space.

### *6.2.2. Footing*

As an illustration of the application of the spectral approach in stochastic analyses, the uncertainty (standard deviation) on the vertical settlement of a flexible superficial footing is evaluated. The footing is 6m wide and transmits a uniform pressure $p$ = 50 kPa to a

20m thick clay layer that could correspond to the transition zone of Mexico City (Figure 38). To assess the uncertainty on the settlements of points A and B indicated in the figure due to soil spatial variations, a simplified 2D stochastic finite element analysis was carried out although a 3D analysis would in fact be more realistic. The soil is considered to be an elastic medium with a drained Young modulus represented by a stationary isotropic random field $E'(X)$ with expected value 4,000 kPa and coefficient of variation of 25%. Poisson´s ratio $\nu'$ is considered as deterministic and equal to 0.3. The expected vertical settlement evaluated by a deterministic analysis is of the order of 25cm at the centre of the footing.

The uncertainty on the vertical settlements of points A and B, respectively $\delta_A$ and $\delta_B$, is highly dependent on the horizontal correlation distance of the random field. For a very short correlation distance (white noise material), the medium is an extremely heterogeneous medium that behaves as a deterministic material due to the reduction of variance effect. For very large correlation distances, the material behaves as a strictly homogeneous but random material. This can be appreciated in Figure 40 where the standard deviation of vertical displacements $\delta_A$ and $\delta_B$ is represented as a function of the correlation distance.

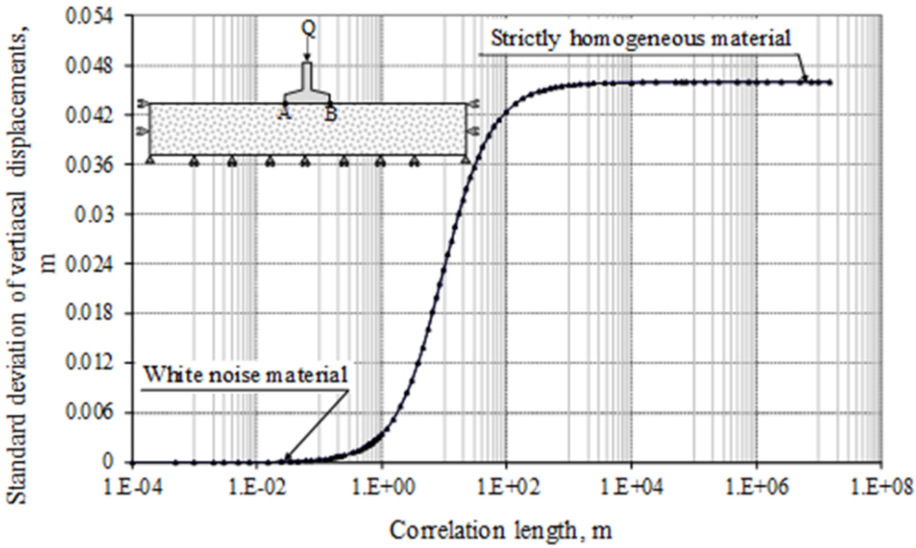


**Figure 40.** Uncertainty on displacements of a footing on a random material as a function of correlation distance.

The variance of the differential settlement between points A and B can be expressed as:

$$\mathrm{Var}[\delta_A - \delta_B] = \mathrm{Var}[\delta_A] + \mathrm{Var}[\delta_B] - 2\mathrm{Cov}[\delta_A, \delta_B] \tag{22}$$

The corresponding standard deviation of this differential settlement between points A and B is presented on Figure 41.

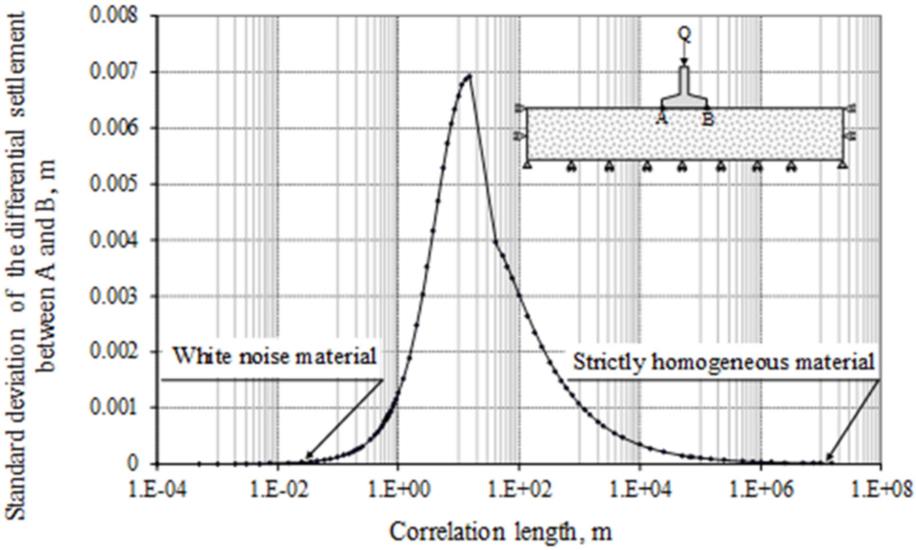


**Figure 41.** Uncertainty on differential displacements between points A and B for a footing built on a random material as a function of correlation distance.

It can be seen that the standard deviation of the differential settlement between points A and B is nil for the white noise material, then reaches a maximum value when the correlation length is about twice the horizontal dimension of the footing and finally decreases again towards zero for the strictly homogeneous material.

This example illustrates the paramount influence on the behavior of a geotechnical structure of the relation between the dimensions of this structure and the correlation length of the soil (stochastic field) on which it is built.

### *6.2.3. Slope stability*

When assessing the stability of slopes such as those created when constructing unsupported excavations, spatial variations of the soil can be taken into account (Auvinet and González, 2000 [117]).

Contrary to what is commonly found in the technical literature, this type of problem can only be addressed resorting to a 3D analysis. Assuming that a plain strain condition prevails, as assumed in standard 2D equilibrium analyses, is equivalent to accepting that no spatial variation of the soil properties exists along the direction normal to the slope cross-section considered, an obviously unacceptable consideration when assessing the influence of soil properties spatial variations.

A 3D limit equilibrium analysis may thus be performed. Among the available 3D stability analysis methods, the algorithm proposed by Hungr (1987 [118]) presents, among other advantages, some flexibility regarding the type of slip surface that can be considered. In this model, based on a generalization of simplified Bishop's method, the potential sliding mass is divided into an orthogonal assembly of vertical columns. For rotational surfaces, the safety factor, *SF*, is derived iteratively from the sum of moments around a common horizontal axis. For cohesive soils:

$$SF = \frac{MR}{MM} = \frac{\sum_{i=1}^{n} s_{ui} a_i R_i}{\sum_{i=1}^{n} W_i x_i + Ed} \tag{23}$$

where *MR* and *MM* are respectively the moments of resisting and driving forces; $s_{ui}$ is the shear strength at base of column *I*; $a_i$ is the area of base of column *i*, $R_i$ is the moment arm of resisting force *I* ; $W_i$ is the total weight of the column and $x_i$ is the distance from the reference axis to the center of the column. *E* is the resultant of all horizontal components of applied point loads, if any, with a moment arm *d*, and *n* is the total number of active columns (Figure 42).

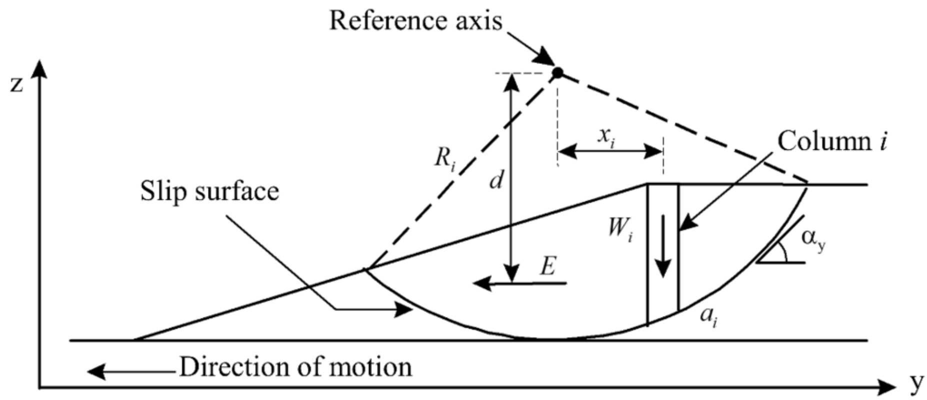


**Figure 42.** Cross-section of slope and potential slip surface.

In the case of non-rotational surfaces, it is possible to derive the factor of safety from the horizontal forces equilibrium in the direction of the motion (Figure 42):

$$SF = \frac{FR}{FM} = \frac{\sum_{i=1}^{n} s_{ui} a_i \cos\alpha_y}{\sum_{i=1}^{n} N_i \cos\gamma_z \tan\alpha_y + E} \tag{24}$$

where *FR* and *FM* are respectively the resisting and driving forces and $\gamma_z$ and $\alpha_y$ are defined on Figure 43. $N_i$ is the total normal force acting on the column base derived from the vertical force equilibrium.

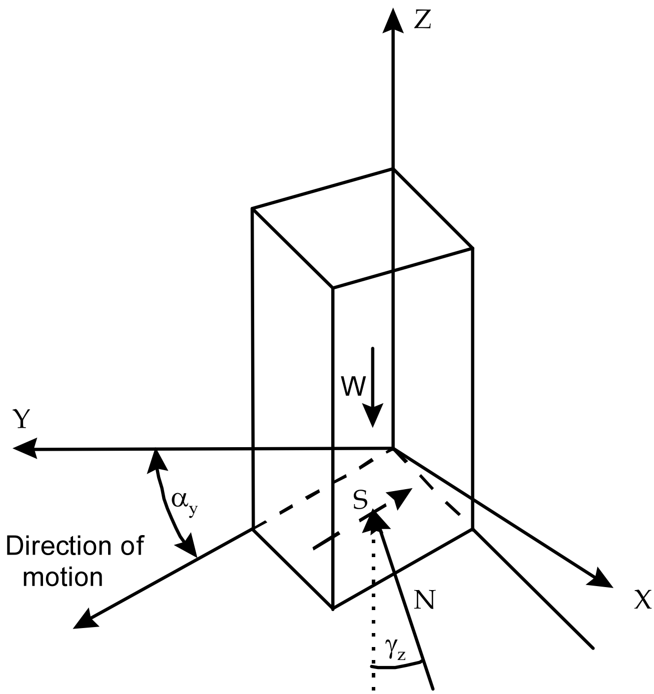


**Figure 43.** Forces acting on base of a single column.

When the mechanical properties of a soil mass are affected by uncertainty due to spatial variations, variables *MR* and *MM* of Eq. (23) (respectively *FR* and *FM* in the case of non-rotational mechanisms) must be considered as random variables. The probability of failure associated to a particular slip surface can then be defined as $P_f = P[SF<1]$ where *SF* is the safety factor. Reliability is the complement to unity of probability of failure. An equivalent formulation can be introduced defining safety margin, *SM* = *MR*-*MM* (respectively, *FR*-*FM*). Probability of failure is then defined as $P_f = P[SM < 0]$. Reliability can be expressed in term of a reliability index $\beta$ defined as:

$$\beta = \frac{E\{SM\}}{\sigma_{SM}} \tag{25}$$

where:

$$\sigma_{SM} = \sqrt{\sigma_{MR}^2 + \sigma_{MM}^2 - 2\mathrm{Cov}\left[MR, MM\right]} \tag{26}$$

The short-term resisting forces along the potential slip surface depend on the undrained shear strength $s_u$ along this surface. On the other hand, the driving forces depend on the specific weight of the soil. In most cases, uncertainty on specific weight can be neglected and $\sigma_{SM} = \sigma_{MR}$. Eq. (25) can then be written:

$$\beta = \frac{E\{SM\}}{\sigma_{MR}} \tag{27}$$

A first order approximation of the expected value of the safety margin can be evaluated performing a deterministic stability analysis with the expected value of the shear strength:

$$E\{SM\} \cong E\{MR\}\left(1 - \frac{1}{E\{SF\}}\right) \tag{28}$$

On the other hand, as shown below, standard deviation $\sigma_{MR}$ of the resisting moment can be defined in terms of the parameters of the shear strength random field $s_u(X)$. For sliding mass divided in vertical columns as in Hungr's model, variance of the moment of resisting forces can be calculated as:

$$\mathrm{Var}\left[MR\right] = \mathrm{Var}\left[s_u\right]\left[\sum_{i=1}^{n}\left(a_i R_i\right)^2 + 2\sum_{i=1}^{n}\sum_{j=i+1}^{n} a_i R_i a_j R_j \rho_{s_u}\left(X_i, X_j\right)\right] \tag{29}$$

where $n$ is the number of columns.

In this expression, the variance of average shear strength at the base of each column is considered to coincide with the point variance of the field (mid-point method). In the same way, the correlation between the average shear strength at the base of different columns is considered equal to the correlation between point values of this property in $X_i$ and $X_j$, at base of columns $i$ and $j$. This approximation can be considered as acceptable when the number of columns considered in the analysis is large.

In the case of non-rotational slip surfaces, a similar procedure can be used substituting $MR$ by $FR$ in Eq. (28), and writing:

$$\mathrm{Var}\left[FR\right] = \mathrm{Var}\left[s_u\right]\left[\sum_{i=1}^{n} a_i^2 \cos^2 \alpha_{y_i} + 2\sum_{i=1}^{n}\sum_{j=i+1}^{n} a_i \cos\alpha_{y_i} a_j \cos\alpha_{y_j} \rho_{s_u}(X_i, X_j)\right] \tag{30}$$

These expressions make it possible to estimate the reliability index associated to three-dimensional failure mechanisms.

Algorithms to perform the corresponding computations have been developed (Auvinet and González, 2000 [117]). In these algorithms, autocorrelations functions of the type indicated in Eq. (15) are used.

If the shear strength random field can be considered as Gaussian, $SM$ is also Gaussian and the probability of failure can be expressed as:

$$P\left[SM \le 0\right] = \Phi\left(\frac{0 - E\{SM\}}{\sigma_{SM}}\right) = \Phi(-\beta) \tag{31}$$

where $\Phi$ is the normalized Gaussian probability distribution function.

The above considerations refer to the reliability associated to a particular slip surface. It must be emphasized that the global failure probability of a slope is the probability that one of the many possible failure mechanisms develops. This probability is difficult to assess; however, taking into account that a significant correlation generally exists between soil properties along close critical slip surfaces, the highest probability of failure found for particular critical surfaces can generally be considered as a useful lower limit of the global probability of failure.

For soils with highly anisotropic autocorrelation function like Mexico City clays, the reliability associated to specific slope failure surfaces is strongly dependent on their shape. Mechanisms with long horizontal planar sections (Figure 44) may present a higher deterministic safety factor than cylindrical or spherical surfaces but they are generally associated to a higher probability of failure and lower reliability. This is because along horizontal planar surfaces, the autocorrelation coefficient function remains close to unity and the variance reduction effect implicit in Eq. (30) is much less pronounced that in the case of a rotational mechanism (Eq. (29)) (Auvinet and González, 2000 [117]).

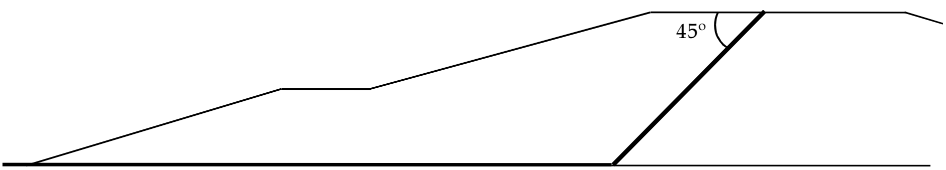


**Figure 44.** Semi planar failure mechanism.

Figures 45 and 46 present the case of a slope failure in a trial excavation in the former Texcoco Lake area in Mexico City soft clays.

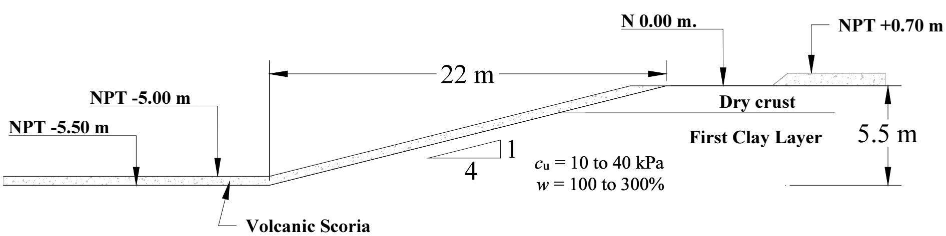


**Figure 45.** Slope of a trial excavation in Mexico City clay.

The failure occurred along a practically horizontal planar surface similar to the one presented in Figure 44, when the excavation with a 4:1 slope reached a depth of 5.5m (Figure 46) (Mendoza *et al*., 2018 [119]; Schmitter *et al*., 2018 [120]).

**Figure 46.** Semi planar failure mechanism of a trial excavation slope (Courtesy, W.I. Paniagua).

As far as stability of geotechnical structures is concerned, the anisotropy of the correlation structure of the soil mass is thus probably more relevant than the mechanical anisotropy observed in the laboratory at the sample level.

## 7. Geotechnical solutions for mitigating the effects of spatial variations of soft soils

### *7.1. Available techniques*

When constructing on spatially variable soft soils, geotechnical engineers may consider two options. The first one consists of adapting the geotechnical solution to the varying characteristics of the soil. This will lead to complex designs with varying dimensions of footings, number of piles, etc. When possible, he may however consider a second option aiming at erasing to some degree the mechanical differences between distinct zones of the soil mass. This will make it necessary to use some sort of soil improvement technique (Mitchell, 1981 [121]; Pilot *et al.*, 1985 [122]).

Improvement techniques have been developing considerably in the last decades (Schaefer, 2012 [123]). They may consist of grouting, soil stabilization using admixtures, thermal stabilization, or soil reinforcement. The most common method is probably consolidation by gravitational or vacuum preloading, generally with the help of vertical drains (Mesri and Khan, 2012 [124])

### *7.2. Mitigating the effects of soil spatial variations in Mexico City clays by preloading.*

The gravitational preloading method has been implemented for different geotechnical structures built on Mexico City clay, including industrial embankments (Auvinet, 1979 [125]) and runways (Mendoza *et al.*, 2018 [51]). This well-known technique consists of placing on the ground a preload (embankment) equal to the final load that will be transmitted to the soil by the geotechnical structure. This preload is applied during a time sufficient for the total settlement to occur before the end of construction.

To accelerate the settlements and reduce the preloading period, a surcharge may be added and vertical drains be installed (Figure 47).

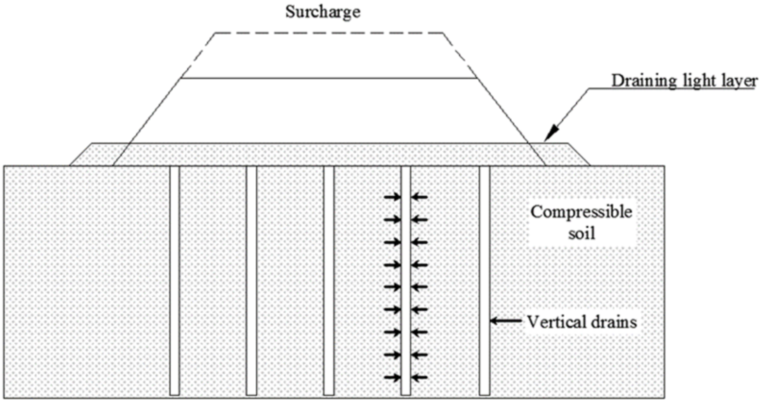


**Figure 47.** Preloading system.

The surcharge and the temporal part of the preload are removed when the induced vertical displacement reaches a target settlement that guarantees an acceptable behavior of the geotechnical structure during operation and future maintenance works.

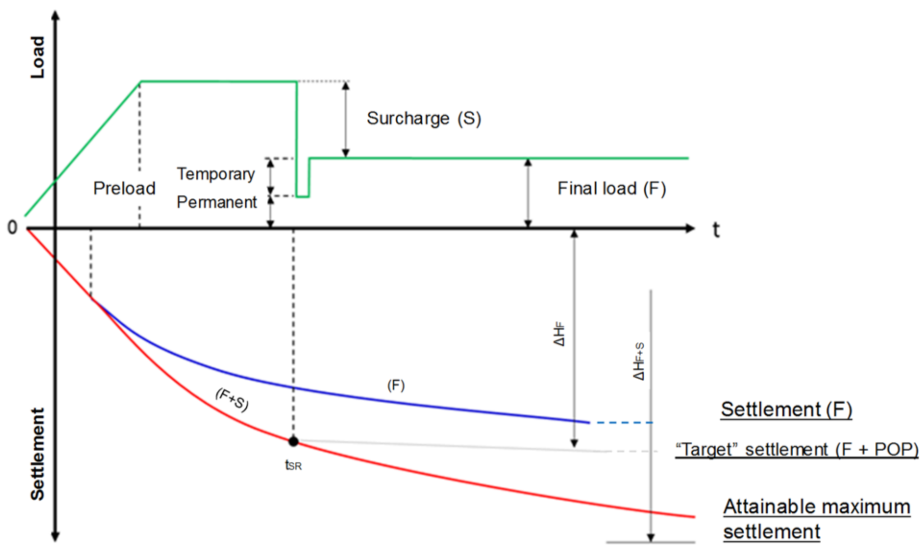


**Figure 48.** Principle of preloading with surcharge.

As shown on Figure 48, the objective of this technique is to induce with the permanent and temporary preload and the surcharge (red curve) a settlement equal to at least 100% the total settlement $\Delta H_f$ (primary plus secondary consolidation) that would be expected for the final structure without preloading (asymptotic value reached by blue curve). In fact, a settlement clearly larger than $\Delta H_f$ should be reached for the soil to attain an overconsolidated state, allowing safe future maintenance works during the lifetime of the geotechnical structure, including those that could require some additional loading of the soil, without inducing significant settlements. Reaching a clearly overconsolidated state also contributes to mitigating the effects of the secondary consolidation of the soil on the final structure (Ladd and De Groot, 2003 [1]).

When applying this technique, it is necessary to take into account that the soil parameters commonly present strong spatial variations due to different factors, including the loading history of the site.

Special attention must be lent to the initial Over Consolidation Ratio (*OCR*):

$$OCR = \frac{\sigma'_p}{\sigma'_0} \tag{32}$$

where $\sigma'_p$ = yield stress at the considered elevation, and $\sigma'_0$ = current effective vertical stress at the considered elevation.

Disposing of an accurate value of *OCR* is essential since consolidation settlement of a soil layer submitted to a stress increment $\Delta\sigma$ is commonly calculated from odometer tests results as:

$$\Delta H = H\left[\frac{C_d}{1+e_0}\log OCR + \frac{C_c}{1+e_0}\log\frac{\sigma'_0 + \Delta\sigma}{\sigma'_p}\right] \tag{33}$$

$$\text{when } \sigma'_{0_z} \le \sigma'_p \text{ and } \sigma'_{0_z} + \Delta\sigma \ge \sigma'_p$$

where $C_c$ = compression index, $C_d$ = swelling index, $e_0$ = initial void ratio, and $H$=layer thickness.

*OCR* is a parameter difficult to define with accuracy. The actual value of yield stress $\sigma'_p$ is not easily derived from laboratory tests due to disturbance of samples and differences between competing methods that have been proposed for estimating this stress from the compressibility curve (Note that, as suggested in Appendix 1 for Mexico City clays, the yield stress may be easier to obtain from $n - \log \sigma'$ curve rather than from the classical compressibility curve $e - \log \sigma'$).

On the other hand, for soil close to the surface, the effective stress in the denominator of Eq. (32) is small and very sensitive to the seasonally changing elevation of the water table.

These uncertainties further increase the natural randomness of *OCR* due to spatial variations within the soil mass.

A more stable parameter defining the position of the current effective vertical stress with respect to the yield stress is the pre-consolidation overburden pressure or *POP*:

$$POP = \sigma'_p - \sigma'_0 \tag{34}$$

To avoid future differential settlements associated to spatial variability of the soil and initial conditions, the objective of preloading should then be inducing in the subsoil along the future geotechnical structure a final pre-consolidation overburden pressure (*POP*), such that:

$$\mathrm{Min}\left(POP\right) > \Delta p \tag{35}$$

where $\Delta p$ is a stress margin allowing safe future maintenance works during the lifetime of the geotechnical structure, without inducing significant settlements. Stress margin $\Delta p$ must be taken into account when assessing the target settlement (Figure 48).

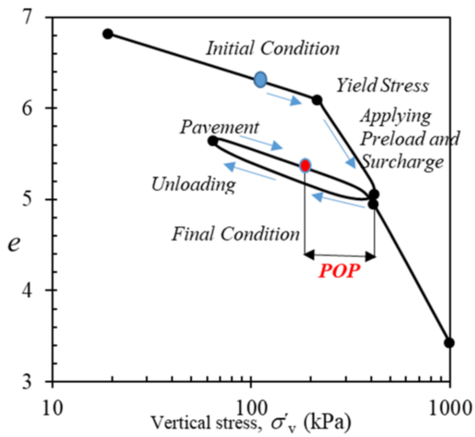


**Figure 49.** Target final condition.

Following the above rule will guarantee that all future volume changes of the soil will take place along the recompression branch of the compressibility curve, minimizing differential settlements (Figure 49),

This requires a thorough assessment of the spatial variations of current and final effective vertical stress $\sigma'_0$, yield stress $\sigma'_p$ and/or *OCR* within the soil.

Figure 50 shows the variation of the estimated initial yield stress $\sigma'_p$ in the subsoil along an embankment longitudinal axis (runway in former Texcoco Lake) obtained by the estimation techniques of Appendix II.

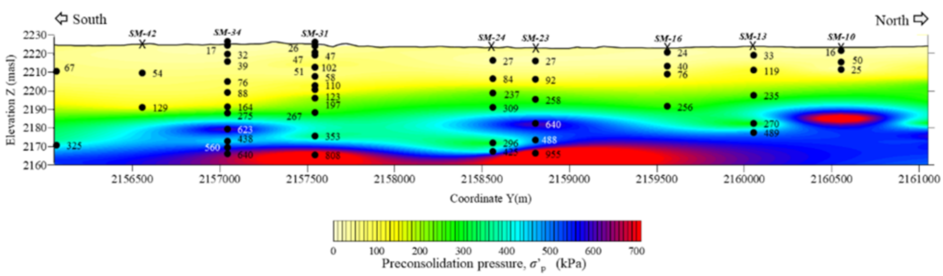


**Figure 50.** Variations of yield stress $\sigma'_p$ along embankment longitudinal axis. (Runway 2, NAICM).

A strict evaluation of compliance of condition (35) should in fact be based on simulations of the above field (Figure 51), in order to take into account possible local soft points.

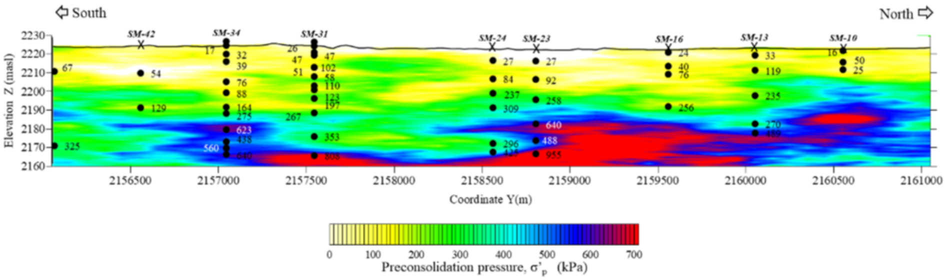


**Figure 51**. Conditional simulation of the $\sigma'_p$ field along embankment longitudinal axis (Runway 2, NAICM).

Note that condition (35) can be difficult to attain uniformly in the soil when vacuum preloading is applied on contiguous panels due to the peculiar conditions prevailing in the joints between the panels.

Furthermore, when implementing the preloading technique, the following issues must also be addressed:

- Final load

To reduce the load transmitted to the soil by the final geotechnical structure (and the target settlement), it can be convenient to install in the basis of the preloading embankment a layer of light material whose function will be mainly to absorb settlements and will only contribute marginally to the final weight of the structure. A light granular material (for example volcanic scoria, known locally in Mexico as *Tezontle*) divided by sieving into several uniform size fractions can be installed in successive thin layers separated by geotextile sheets. Uniform size fractions present a higher porosity than the original granular material (Auvinet, 1986 [87]). The wall effect between the granular material and the geotextile sheets also increases porosity. Dry unit weight as low as 9kN/m$^3$ can be attained.

- Water table

When the water table is close to the surface, during preloading, the superficial natural soil and the preloading materials become partially submerged. This new condition reduces the efficiency of preloading since the original unit weight $\gamma_m$ of these materials becomes:

$$\gamma_{sub} = \gamma_{sat} - \gamma_w \tag{36}$$

where $\gamma_{sub}$ = buoyant unit weight of soil, $\gamma_{sat}$ = unit weight of saturated soil, and $\gamma_w$ = water unit weight.

For such situations, a pumping installation aimed at maintaining the materials above the water table can be implemented. This system increases the efficiency of preloading and can, in some cases, make the surcharge unnecessary (Auvinet, 2016 [126]; 2016 [127]).

- Vertical drains

Vertical drains are useful for reducing the time required for the consolidation of a soft soil layer submitted to preloading, especially when the thickness of the layer exceeds about 5m. The designer must then choose between vertical sand drains and Prefabricated Vertical Drains (PVD). Installation time of PVD is generally much shorter. However, it must be taken into account that sand drains can contribute to reduce significantly the target settlement when designed to act as a reinforcement of the soil. They can also contribute to a better homogenization of the soil, eliminating at least part of the effects of spatial variations of soil compressibility and reducing differential settlements.

It must also be taken into account that any kind of vertical drain can modify the hydraulic conditions prevailing in the subsoil. In the case of Mexico City, a drawdown condition generally exists due to deep pumping (Figure 52).

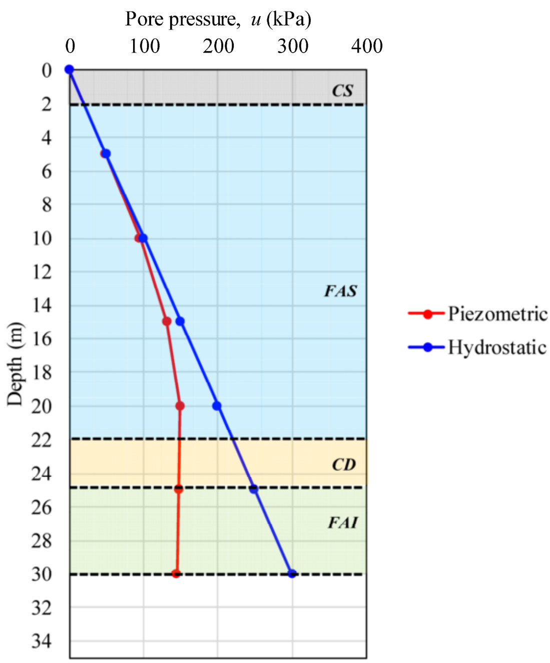


**Figure 52.** Typical pore pressure depletion within Mexico City subsoil.

When vertical drains are installed, the hydrostatic condition is reestablished down to the tip of the drains. A strong hydraulic gradient then develops between this level and the first hard permeable layer where pore pressure is depleted. This induces a vertical strain concentration in the soil by consolidation at this elevation as shown by extensometers measurements (Figure 53).

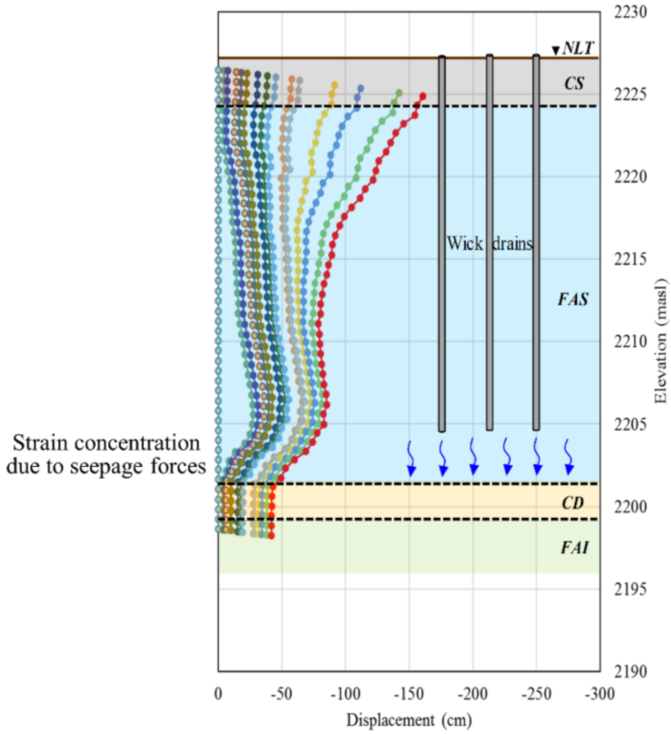


**Figure 53.** Settlement induced by seepage forces between the tip of PVD drains and first hard permeable layer (CD).

This phenomenon must be taken into account when assessing the target settlement.

## 8. Conclusions

Among the sources of uncertainty prevailing in the geotechnical characterization of soft soils, spatial variability was singled out as one of the most difficult to deal with. For an accurate evaluation of the subsoil conditions, spatial variations of the soil profile and mechanical properties as well as the groundwater conditions must be assessed by performing a sufficient number of soil explorations and field tests, processing a generally large amount of data and developing either deterministic or probabilistic models representing these variations.

The techniques available to develop such models and some difficulties encountered to implement them in practice were examined in this lecture. Emphasis was placed on geostatistical methods for estimation and simulation of spatial variations of soft soils represented by single or multiple random fields. A discussion showing the limitations of the concepts of void ratio and gravimetric water content commonly used in Geotechnical engineering, in the context of statistical analyses of spatial variations of soft soils was presented.

Geotechnical analysis and design methods that take into account soft soils spatial variations were also reviewed together with some construction techniques aimed at mitigating consequences of soil variability. The above considerations were illustrated by applications to the Mexico City highly compressible volcanic lacustrine clays. Models of the spatial variability of Mexico City subsoil developed over the years for different projects using traditional and geostatistical techniques were presented. Simple examples of the geotechnical analysis and construction methods that can be used by geotechnical engineers to deal with soil spatial variability were discussed.

During the preparation of this lecture, the author kept constantly in mind the great influence of Professor Arthur Casagrande in the formation of what in time became a buoyant Mexican School of Geotechnical Engineering that, year after year, has faced competently the extremely difficult conditions of Mexico City subsoil as well as other challenging geotechnical problems in the rest of the country.

## Acknowledgments

This lecture is a tribute to researchers and practitioners, many of them directly or indirectly former students of Professor Arthur Casagrande, who contributed during the last century to a better knowledge of the subsoil of Mexico City.

The author also wants to acknowledge the most valuable comments and contributions of Moisés Juárez Camarena, Edgar Méndez Sánchez, Marco Pérez Ángeles, Marcos Delgado Muñiz, Felipe Vázquez Guillen, Alma Rosa Pineda and Francisco Hernández Vizcarra and the help of Eduardo Martínez Hernández during the preparation of this lecture.

## List of Symbols

| Symbol | Nomenclature |
|---|---|
| $a$ | area |
| $a_v$ | coefficient of compressibility |
| $c$ | salt concentration in % |
| $C(u_1,\ldots,u_n)$ | n-dimensional copula |
| $c(u_1,\ldots,u_n)$ | copula density |
| $C_c$ | compression index |
| $C_{cn}$ | compression index in terms of porosity |
| CD | first hard layer in Mexico City Lake Zone. |
| *CL* | low compressibility clay |
| *CH* | high compressibility clay |
| Cov[ ] | covariance |
| CPT | Cone Penetration Test |
| CPTu | Cone Penetration Test with pore pressure measurement |
| CU | consolidated undrained triaxial test |
| $C_s$ | swelling index |
| $C_{sn}$ | swelling index, in terms of porosity |
| $C_S$ | spatial copula |
| $C_V(X_1, X_2) = \mathrm{Cov}[V(X_1), V(X_2)]$ | random field autocovariance function |
| $C_V(X_1, X_2) = C_V(X_2 - X_1) = C_V(h)$ | stationary random field autocovariance function |
| CV[ ] | coefficient of variation |
| $d$ | moment arm |

| | |
|---|---|
| DMT | Marchetti dilatometer test |
| $e$ | void ratio |
| $F_V(v; X)$ | probability distribution function of field $V(X)$ |
| $\underline{E\{\ \}}$ | mathematical expectation operator |
| $exp\ \{\ \}$ | exponential operator |
| $E$ | resultant of all horizontal components of forces |
| $E'$ | drained modulus |
| FAI | lower clay formation in Mexico City Lake zone |
| FAS | upper clay formation in Mexico City Lake zone |
| $G_0$ | small strain shear modulus |
| $G_s$ | specific density of solids |
| $H$ | layer thickness |
| $I_V(v, X)$ | indicator function |
| $\mathbf{K}$ | covariance matrix |
| $m$ | exponent |
| $m_v$ | coefficient of volume compressibility |
| ML | low compressibility silt |
| MH | high compressibility silt. |
| $Min\ (\ )$ | minimum |
| $MM$ | moment of driving forces |
| $MR$ | moment of resisting forces |
| $n$ | porosity |
| n | number |
| $Ni$ | total normal force acting on the column base |
| $N_k$ | cone factor |
| $OCR$ | Over Consolidation Ratio |
| OH | high compressibility organic soil |
| OL | low compressibility organic soil |
| $p$ | pressure |
| PCA | test pit |
| $P_f$ | probability of failure |
| PI | plasticity index |
| PND | dynamic cone penetrometer |
| $POP$ | preconsolidation overburden pressure |
| $q_c$ | tip resistance in CPT test |
| $q_u$ | unconfined compressive strength |
| $Q$ | friction bearing capacity of pile |
| $R_i$ | moment arm of resisting force i |
| $R_V\left(X_1, X_2\right) = E\left\{V(X_1)V(X_2)\right\}$ | autocorrelation function |
| $s_u$ | undrained shear strength |
| $s_{ui}$ | shear strength at base of column $i$ |
| $s_{uL}$ | average undrained shear strength along a segment with length $L$ |
| $s_u$ (Z) | 1D undrained shear strength random field |
| $S$ | normally consolidated ratio $\left(s_u / \sigma'_{v0}\right)_{nc}$ |
| SC | continuous sampling |
| SDMT | seismic dilatometer test |
| S$ds$ | suspended logging |

| | |
|---|---|
| *SF* | safety factor |
| SM | mixed boring (SPT + undisturbed sampling) |
| *SM* | safety margin |
| SPT | Standard Penetration Test |
| SS | selective sampling |
| $s_u$ | undrained shear strength |
| USCS | Unified Soil Classification System |
| UU | undrained triaxial test |
| $V$ | random variable |
| $V(X)$ | random field |
| $V(X.t)$ | spatio-temporal random field |
| Var[ ] | variance |
| $V_S$ | shear wave velocity |
| $V_{\mathrm{S}}$ | volume of solids in sample |
| VST | vane shear test |
| $V_{\mathrm{T}}$ | total volume of sample. |
| $V_{\Omega}$ | average value of field $V(X)$ on subdomain $\Omega$ |
| $\mathbf{V}$ | vector of random variables |
| $w$, | gravimetric water content (Eq. (1)) |
| $w'$ | gravimetric water content (Eq. (2)) |
| $w''$ | volumetric water content (Eq. (3)) |
| $w_{ap}$ | apparent water content (including salt in solids, Eq. (1)). |
| $W_i$ | weight of column $i$ |
| $w_L$ | liquidity limit |
| $w_P$ | plasticity limit |
| $W_{\mathrm{W}}$ | weight of water in sample |
| $W_{\mathrm{S}}$ | weight of solids in sample |
| $W_{\mathrm{T}}$ | total weight of sample ($=W_{\mathrm{W}}+W_{\mathrm{S}}$) |
| $\alpha_y$ | angle |
| $\beta$ | reliability index |
| $\delta$ | correlation distance |
| $\delta_{\mathrm{A}}$ | settlement of point A |
| $\delta_{\mathrm{B}}$ | settlement of point B |
| $\lambda$ | coefficient |
| $\phi'$ | internal friction angle |
| $\Phi$ | normalized Gaussian probability distribution function |
| $\gamma_z$ | angle |
| $\gamma_{sub}$ | buoyant unit weight of soil |
| $\gamma_{sat}$ | unit weight of saturated soil |
| $\gamma_w$ | unit weight of water |

$2\gamma_V(h) = E\left\{\left[V(X+h) - V(X)\right]^2\right\}$ variogram

$\mu_V\left(X\right) = E\left\{V(X)\right\}$ expected value of random field $V(X)$

| | |
|---|---|
| $\nu$ | Lagrange multiplier |
| $\nu'$ | Poisson's ratio |

$\sigma_V^2(X) = \mathrm{Var}\left[V(X)\right]$ variance of random field $V(X)$

$\rho_V(X_1, X_2) = \rho_V(h)$ autocorrelation coefficient (normalized autocovariance) of stationary random field.

$\sigma'_{vo}$ *in situ* effective vertical stress

$\sigma_0$ total vertical stress at the level of the measurement

$\sigma'_p$ yield stress

Other symbols:

1D uni-dimensional

2D bi-dimensional

3D three-dimensional

## References


[1] Ladd, C.C., and De Groot, Don J., (2003). "Recommended Practice for Soft Ground Site Characterization", Arthur Casagrande Lecture, 12th Pan-American Conference on Soil Mechanics and Geotechnical Engineering, Massachusetts Institute of Technology, Cambridge, MA, USA

[2] Casagrande, A., (1948). "Classification and identification of soils". Transactions, American Society of Civil Engineers, Vol. 113, 901-930.

[3] Spangler M.G. and Handy, R., (1982). "Soil Engineering", p. 177, 4th edition, Harper & Row.

[4] Gutiérrez García, A., (2006). "Determination of Atterberg limits: uncertainty and implications", Journal of the Geotechnical and Geoenvironmental Engineering, March.

[5] Moreno-Maroto J.M. and Alonso-Azcárate (2018). "What is a clay? A new definition of "clay" based on plasticity and its impact on the most widespread soil classification systems", Applied Clay Science, 161, 57-63.

[6] ASTM (1989) D2487-85, D2488-84.

[7] Perrin, J., (1974). "Classifications des sols organiques", Bulletin de Liaison des LPC, France, No 69, 39-47.

[8] Magnan, J.P.; (1980). "Classification géotechnique des sols", Bulletin de Liaison des LPC, France, No 105, 49-52.

[9] Akagi, H., (2004). "3D F.E. Analysis of the deformation of underground structure constructed in a soft subsiding reclaimed area", Proceedings, ISSMGE TC36 workshop on "Foundation engineering in difficult soft soil conditions", SMIG-I de I, UNAM, Mexico, 211-216.

[10] Phien-wej, N., Thepparak, S. and Giao, P.H., (2009). "Prediction of differential settlement of structures in sinking Bangkok ground", Proceedings, ISSMGE TC36 workshop, "Geotechnical Engineering in urban areas affected by land subsidence", SMIG, Mexico City.

[11] Kempfert, H.G. and Raithel, M., (2005). "Experiences on Dike Foundations and landfills on very soft soils", Proceedings, ISSMGE TC36 workshop on "Foundation engineering in difficult soft soil conditions", SMIG-I de I, UNAM, Mexico, 211-216.

[12] Kempfert, H.G., (2006). "Excavations and Foundations in Soft Soils", Springer Verlag, Berlin-Heidelberg-NY, 576 Seiten.

[13] Mitchell, J.K. and Coutinho, R.Q., (1991). "Occurrence, geotechnical properties and special problems of some soils in America", Proceedings, IX Pan-American Conference on Soil Mechanics and Foundation Engineering, Viña del Mar, Chile, Vol. IV, 1651-1735.

[14] Coutinho, R.Q. and Oliveira, J.T.R., (2005). "Behavior of Recife soft clays", Proceedings, ISSMGE TC36 workshop on "Foundation engineering in difficult soft soil conditions", SMIG-I de I, UNAM, Mexico, 57-86

[15] Almeida, M.S.S., Futai, M.M. and Marques, M.E.S., (2004). "Theoretical and practical concepts to assess the behaviour of Río de Janeiro clays", Proceedings, ISSMGE TC36 workshop on "Foundation engineering in difficult soft soil conditions", SMIG-Ide I, UNAM, Mexico, 43-56.

[16] Martínez, J.M., (1991). "Propiedades geotécnicas del subsuelo de Bogotá", Proceedings, IX Pan-American Conference on Soil Mechanics and Foundation Engineering, Viña del Mar, Chile, Vol. 1, 143-154.

[17] Caicedo, B., Mendoza, C., López, F. and Lizcano, A., (2018). "Behavior of diatomaceous soil in lacustrine deposits of Bogotá, Colombia", Journal of Rock Mechanics and Geotechnical Engineering, 10, 367-379.

[18] Whitman, R., (1996). "Organization and Evaluating Uncertainty in Geotechnical Engineering". Proceedings "Uncertainty 96", ASCE, New York, 1-28.
[19] Lacasse, S., and Nadim, F., (1996). "Uncertainty in characterizing soil properties", *Uncertainty in he Geologic Environment*, GSP No 58, ASCE, 49-75.
[20] Fenton, G., (1997). "Probabilistic methods in Geotechnical Engineering", ASCE GeoLogan´97 Conference Logan, Utah, 1-95.
[21] Phoon, K., and Kulhawy, F., (1999). "Characterization of Geotechnical Variability", Canadian Geotechnical Journal, 612-624.
[22] Auvinet, G., (2001), "La gestion de l'incertitude en géomécanique", key-note lecture, Proceedings, First Albert Caquot Conference, Paris, France.
[23] Auvinet, G., (2002). "Uncertainty in Geotechnical Engineering/Incertidumbre en Geotecnia", Sixteenth Nabor Carrillo Lecture/Decimosexta Conferencia Nabor Carrillo. (English/Español), Sociedad Mexicana de Mecánica de Suelos, Mexico, 131p., ISBN: 968-5350 10-8.
[24] Baecher, G.B. and Christian, J.T., (2003). "Reliability and Statistics in Geotechnical Engineering", John Wiley & Sons, Ltd ISBN: 0-471-49833-5
[25] Huber, M., (2013). "Soil variability and its consequences in geotechnical engineering", Doctoral Thesis, Institut fur Geotechnik der Universitat Stuttgart, Germany
[26] Del Castillo and Ordoñez, (1893). "Plano geológico y petrográfico de la ciudad de México", Comisión Geológica Mexicana, México.
[27] Mooser, F., (1978). "Geología del relleno cuaternario de la cuenca de México", Memoria, Simposio "El subsuelo y la ingeniería de cimentaciones en el área urbana del valle de México", SMMS, Ciudad de México, México.
[28] Mooser, F., Montiel, A. y Zuñiga, A. (1996). "Nuevo mapa geológico de las Cuencas de México, Toluca y Puebla: estratigrafía, tectónica regional y aspectos geotérmicos", Comisión Federal de Electricidad, Ciudad de México, México.
[29] Mooser, F., (2018). "Geología del Valle de México y otras regiones del país", Colegio de Ingenieros Civiles de México, Volumen 1, Ciudad de México, México.
[30] Auvinet, G., Méndez, E. and Juárez, M., (2017). "El subsuelo de la Ciudad de México/The Subsoil of Mexico City, Vol. 3", Third edition of 1959 book by Marsal and Mazari, UNAM, Mexico, ISBN 978-607-02-8198-3.
[31] Robertson, P.K., (2009). "Interpretation of cone penetration tests - a unified approach". Canadian Geotechnical Journal 46 (11): 1337-1345, 2009.
[32] Robertson, P.K., (2012). "The James K. Mitchell Lecture: Interpretation of in-situ tests-some insights", Geotechnical and geophysical Site Characterization, Porto de Galinhas, Brazil.
[33] Marsal R.J., and Mazari, M., (2017). "El subsuelo de la Ciudad de México/The subsoil of Mexico City, Vol. 1 and 2", Third edition (first edition: 1959), UNAM, Mexico, ISBN 978-607-02-8198-3.
[34] Zeevaert, L., (1972). Foundation Engineering for Difficult Subsoil Conditions. Van Nostrand Reinhold Company, New York.
[35] Santoyo, E. Ovando, E., Mooser, F. y León, E., (2005). "Síntesis geotécnica de la Cuenca del Valle de México", TGC Geotecnia, México. ISBN: 968-5571-06-6.
[36] Ovando Shelley, E., (2011). "Some geotechnical properties to characterize Mexico City clay", Proceedings, XIVth Pan-American Conference on Soil Mechanics and Geotechnical Engineering, paper 889, Canadian Geotechnical Society, Toronto, Canada.
[37] Zeevaert, L., (1952). "Estratigrafía y problemas de ingeniería en los depósitos de arcillas lacustre de la Ciudad de México", Congreso Científico del IV Centenario de la Universidad Nacional Autónoma de México, México, pp. 155-176, Mexico.
[38] Leonards, G. and Girault, P. (1961). "A study on the one dimensional consolidation test", Proceedings, Fifth International Conference on Soil Mechanics and Foundation Engineering, Vol. 1, 213-218.
[39] Girault, P. (1964). "Mineralogía de las arcillas del Valle de México". Revista Ingeniería, Facultad de Ingeniería, UNAM, México.
[40] Lo, K.Y., (1962). "Shear strength properties of a sample of volcanic material of the Valley of Mexico, Geotechnique, Vol. XII, 4, U.K., 303-310.
[41] Mesri, G., Rokhsar, A. and Bohor, B.F., (1975). "Composition and compressibility of typical samples of Mexico City clay", Geotechnique 25 (3): 527-554.
[42] Peralta y Fabi, R., (1973). Aspectos Micro estructurales del Subsuelo de la Ciudad de México; Informe a la Fundación "Ricardo J. Zevada", Instituto de Ingeniería, UNAM.
[43] Diaz-Rodriguez, J.A., (2003). "Characterization and engineering properties of Mexico City lacustrine soils". Characterization and Engineering Properties of Natural Soils, Vol. 1, Balkema, Rotterdam: 725-755.
[44] Cruz, I.R. and Mayne, P. (2006). "Interpretation of CPTU tests carried out in lacustrine Mexico City clay", Site & Geomaterial Characterization (GSP 149, Proc. GeoShanghai), ASCE, Reston/VA: 24-31.

[45] Mayne, P., (2017), "Yield stress profile in soft clays by piezocone", TC214 Session, 19th ICSMGE, Seoul, South Korea.
[46] Rangel-Nuñez, J.L., Almanza-Hernández, F. e Ibarra-Razo, E., (2019). "Caracterización de las series arcillosas del Valle de México con el microscopio electrónico y pruebas convencionales de mecánica de suelos. Pan-American Conference on Soil Mechanics and Geotechnical Engineering, Cancún, Mexico.
[47] Walkley, A. and Black, A., (1934). "An examination of the Degtjareff method for determining of soil organic matter, and proposed modification of the chromic acid titration method", Soil Science. 37:29-38.
[48] Díaz-Rodríguez, J.A., Leroueil, S., and Aleman, J.D., (1992). "Yielding of Mexico City clay and other natural clays", Journal of the Geotechnical Engineering Division, ASCE, 118 (7), pp. 981-995.
[49] Wheeler, S.J., (2003). "An anisotropic elastoplastic model for soft clays", Canadian Geotechnical Journal, 40, Canada, 403-418.
[50] Santoyo, E., (2010). "Exploración de suelos/Soil exploration", XXa Conferencia Nabor Carrillo/XXth Nabor Carrillo Lecture, Sociedad Mexicana de Ingeniería Geotécnica, México.
[51] Mendoza, M., Ovando E., Auvinet, G., López-Acosta N., Botero, E., Ossa, A., Flores, O. y Juárez, M. (2018). "Investigaciones y Estudios Especiales Relacionados con Aspectos Geotécnicos del Diseño y la Construcción del Nuevo Aeropuerto Internacional de la Ciudad de México (NAICM)", Convenio GACM-IIUNAM, Informe final, México.
[52] Santoyo E., Lin R. y Ovando E. (1989). "El cono en la exploración geotécnica", TGC Geotecnia, México.
[53] Alanis, R., (2003), "Caracterización geotécnica del ex lago de Texcoco", Tesis de maestría, Programa de Maestría y Doctorado en Ingeniería, Ingeniería Civil, Geotecnia, UNAM, Mexico.
[54] Montañez, L., (1983). "Exploración con cono eléctrico en la Ciudad de México", Tesis de maestría, División de Posgrado de la Facultad de Ingeniería, UNAM, México.
[55] Rodríguez, J.F., (2011), "Modelado del comportamiento de pilotes e inclusiones sometidos a consolidación regional en la zona lacustre de la Ciudad de México", Tesis doctoral, Programa de Maestría y Doctorado en Ingeniería, Ingeniería Civil, UNAM, Mexico.
[56] Ossa, A., (2004). "Modelo elasto-visco-plástico (EVP) para el estudio de la consolidación unidimensional de los suelos", Tesis de maestría, Programa de Maestría y Doctorado en Ingeniería, UNAM, Ciudad de México, México.
[57] Romo, M.P. and Auvinet, G. (1992). "Seismic behavior of foundations on cohesive softs soils" in *Recent advances in Earthquake Engineering and Structural Dynam*ics, edited by V. Davidovici, Ouest-Editions, pp. 311-328, Paris, France.
[58] Marsal, R.J. (1975). "The lacustrine clays of the valley of Mexico", Contribution of Instituto de Ingeniería, UNAM to the 1975 International clay conference, Publication E16, Instituto de Ingeniería, Universidad Nacional Autónoma de México, Mexico.
[59] GDCDMX, Gobierno de la Ciudad de México (2017a). "Normas Técnicas Complementarias para diseño y construcción de cimentaciones", Gaceta de la Ciudad de México, diciembre, Mexico.
[60] Murillo, R. y Morales, R., (1991). "El subsuelo del ex Lago de Texcoco", Proceedings, IXth Pan-American Conference on Soil Mechanics and Foundation Engineering, 213-225, Viña del mar, Chile.
[61] Marsal, R. J. y Graue, R, (1969). "El subsuelo del Lago de Texcoco", Volumen Nabor Carrillo; Ciudad de México, México, 167-202.
[62] Méndez, E., Auvinet, G., Matus, U. and Juárez, M., (2010). "Caracterización de anomalías geotécnicas en las zonas lacustre y de transición de la ciudad de México", XXVa Reunión Nacional de Mecánica de Suelos e Ingeniería Geotécnica, SMIG, Acapulco, México, Vol. 1, 311-321.
[63] Carrillo, N., (1948). "Influence of Artesian wells on the sinking of Mexico City", Proceedings, Second international Conference on Soil Mechanics and Foundation Engineering, Vol.7, 156-159, Rotterdam, Netherlands.
[64] Ovando-Shelley E., Romo, M. P. and Ossa, A. (2007). "The sinking of Mexico city: Its effects on soil properties and seismic response". Soil Dynamics and Earthquake Engineering, 27, No. 4, 333-343.
[65] Jaime, A. and Méndez, S., (2010), "Evolution of Mexico clay properties affected by land subsidence", International Association of Hydrological Sciences, Publication 339, 232-234, Mexico.
[66] González Rodríguez, R., (2012), "Estado actual y perspectivas a futuro de las condiciones del Centro Nacional de la SCT desde el punto de vistas geotécnico", Tesis de maestría, Programa de estudios de maestría y doctorado en Ingeniería, UNAM.
[67] Ovando-Shelley, E., Romo, M.P., Contreras, N. and Giralt, A., (2003), "Effects of regional subsidence on the seismic response of Mexico City clay deposits", Elsevier Science Ltd, 12th European Conference on Earthquake Engineering, paper reference 248, 8p.
[68] Auvinet, G., (2011). "Soil fracturing induced by land subsidence" in "Land subsidence, Associated Hazards and the Role of Natural Resources Development", 339, 0-26
[69] Auvinet, G., Sánchez-Guzmán, J. y Pineda, A.R, (2019). "Mitigación de daños ocasionados por grietas en el suelo", Revista Ingeniería Investigación y Tecnología, Facultad de Ingeniería, UNAM, Mexico. (publication pending)

[70] Steinbrenner, (1934). Tafeln zur setzungberechnung, Die Strasse.
[71] Button, S.J., (1953). "The bearing capacity of footings on a two layer cohesive subsoil", Third International Conference on Soil Mechanics and Foundation Engineering, Zurich, Switzerland.
[72] Richardt, F.E., Hall, J.R. and Woods, R.D., (1970). "Vibrations of soils foundations", Prentice Hall.
[73] Ladd, C.C. and Foote, R., (1974), "A new design procedure for stability of soft clays", Journal of the Geotechnical Engineering Division. ASCE, Vol. 100, No GT7, pp. 763-786.
[74] Bay, J.A., Anderson, R., Colocino, T.M. and Budge, A.S., (2005). "Evaluation of Shansep parameters for soft Bonneville clays", Report No UT-03.13, Utah State University, Dept. of Civil and Environmental Engineering.
[75] Vanmarcke, E.H., (1983). "Random fields: Analysis and Synthesis", MIT Press, Cambridge, Ma.
[76] Vanmarcke, E.H., (2010). "Random fields: Analysis and Synthesis", World Scientific, Princeton University.
[77] Krige, D. G., (1962). "Statistical application in mine valuation", J. Institute Mine Survey, South Africa
[78] Matheron, G., (1965). "Les variables généralisées et leur estimation", Masson et Cie, France.
[79] Juárez, M., (2015). "Análisis geoestadístico del subsuelo de la zona lacustre de la Cuenca de México", Tesis doctoral, Programa de Maestría y Doctorado en Ingeniería, Ingeniería Civil, Geotecnia, UNAM, Ciudad de México, México
[80] Azzouz, M. et Bacconnet, C., (1988). "Optimisation d'une campagne de reconnaissance par géostatistique", Symposium on Reliability–based design in Civil Engineering, Lausanne, Switzerland, 269-276.
[81] Wackernagel, H., (2003). Multivariate Geostatistics. An Introduction with Applications. Springer, 3rd Edition, Berlin, Germany, 387p.
[82] Nelsen, R.B. (2006). "An introduction to copulas", Springer-Verlag, New York, 2nd Edition, pp. 269.
[83] Phoon, K., and Ching, J., (2015) "Risk and reliability in geotechnical engineering", CRC Press, New York.
[84] Vázquez, F. y Auvinet, G., (2014). "Simulación de campos aleatorios con dependencia no multigaussiana empleando cópulas", Ingeniería, Investigación y Tecnología, FI-UNAM, Vol. XV, Núm 4, Mexico.
[85] Vásquez-Guillén, F. y Auvinet, G., (2015). "Simulación de campos aleatorios espacio-temporales utilizando un filtro de Kalman modificado", Ingeniería, Investigación y Tecnología, FI-UNAM, Vol. XVI, Núm 1, 1-12, Mexico.
[86] Auvinet, G. and Bouvard, D., (1984). "Effet d'échelle géométrique dans les milieux granulaires", Revue Française de Géotechnique, N° 25, 63-69, avril, Paris, France.
[87] Auvinet, G., (1986) "Estructura de medios granulares", Tesis doctoral, División de Estudios de Posgrado de la Facultad de Ingeniería, UNAM, (2 vol.), México.
[88] Auvinet, G., (1969), "Desplazamientos horizontales producidos en un subsuelo arcilloso por cargas superficiales y por hinca de pilotes", Tesis para obtener el grado de Maestro en Ingeniería, División de Estudios de Posgrado, Facultad de Ingeniería, UNAM, México.
[89] GDCDMX, Gobierno de la Ciudad de México (2017b). "Normas Técnicas Complementarias para diseño por sismo", Gaceta de la Ciudad de México, diciembre, México.
[90] Mazari, M., (1996). "La isla de los perros". El Colegio Nacional, CDMX, México.
[91] Reséndiz, D. and Herrera, I., (1969). "A probabilistic formulation of settlement-controlled Design", Proceedings, 7th International Conference on Soil Mechanics and Foundation Engineering, Mexico, Vol 2, pp 217-225.
[92] Auvinet, G., Juárez, M. and Medina, Z., (2001), "Geostatistical interpretation of soil exploration" Proceedings, International Conference on Soil Mechanics and Geotechnical Engineering, Istanbul, Turkey, Vol.1, pp. 373-376.
[93] Auvinet, G., and Juárez, M., (2002). "Geostatistical characterization and simulation of Mexico Valley subsoil", Proceedings, IASTED International Conference, Modelling and Simulation 2002, Marina del Rey, California, USA. pp. 208-212
[94] Auvinet, G., Juárez. M. and Valdez P., (2005), "Caractérisation géostatistique du sol de la ville de Mexico", Revue Française de Géotechnique, No 110, Paris, France.
[95] Delgado Muñiz, M., (2017). "Análisis geoestadístico multivariable de las propiedades geotécnicas del subsuelo lacustre del valle de México", Tesis de maestría, Programa de Maestría y Doctorado en Ingeniería, Ingeniería Civil, Geotecnia, UNAM, Ciudad de México, Mexico.
[96] Juárez, M., Auvinet, G. and Méndez, E., (2016) "Geotechnical zoning of Mexico valley subsoil", Ingeniería Investigación y Tecnología, Volume XVII (issue 3), July-September, Art. 1036, ISSN 1405-7743 FI-UNAM, Ciudad de México, México.
[97] Flores Tapia, L.I., (2000). "Contribución a la zonificación geotécnica de la zona sur de la cuenca de México", Tesis profesional, Facultad de Ingeniería, UNAM, Ciudad de México. México.

[98] Aguilar, R., (2001), “Zonificación geotécnica del Cerro de la Estrella y sus alrededores”, Tesis Profesional, Escuela Superior de Ingeniería y Arquitectura, Unidad Zacatenco, Instituto Politécnica nacional, México.
[99] Pantoja, A., (2002). “Análisis Geoestadístico del subsuelo en el norte de la zona lacustre del Valle de México”. Tesis de Maestría, Universidad Nacional Autónoma de México, Ciudad de México, México.
[100] Morales, A., (2004). “Aplicación de la geoestadística a la descripción estratigráfica del subsuelo de la zona de los ex-lagos de Xochimilco y Chalco”, Tesis de Maestría ESIA-UZ, IPN, Ciudad de México, México.
[101] Valencia, D., (2007). “Contribución a la zonificación geotécnica de la zona norte del Valle de México”, Tesis de Maestría, ESIA-UZ, IPN, Ciudad de México, México.
[102] Jiménez, O., (2007). “Caracterización geoestadística del subsuelo de la zona poniente del Valle de México”, Tesis de Maestría, ESIA-UZ-IPN, Ciudad de México, México.
[103] Tenorio, A., (2013). “Aplicación de la Geoestadística a la Caracterización Geotécnica del Subsuelo de la Zona Central de la Ciudad de México”, Tesis de Maestría, Universidad Nacional Autónoma de México, Ciudad de México, México.
[104] Pérez, D., (2009). “Modelado del hundimiento de la zona lacustre del valle de México. Aspectos estratigráficos y piezométricos”, Tesis de maestría, SEPI, ESIA-IPN, México.
[105] Rodríguez, M.E., (2010). “Caracterización geoestadística del subsuelo del ex lago de Texcoco”, Tesis de Maestría, ESIA, Unidad Zacatenco, Instituto Politécnico Nacional, Ciudad de México, México
[106] Hinojosa, J., (2010). “Comportamiento del suelo en la zona próxima al cerro del marqués y sus efectos en obras de infraestructura”, Tesis de Maestría SEPI, ESIA-IPN, Ciudad de México, Mexico.
[107] Hernández Vizcarra, F., (2013). “Caracterización geotécnica del subsuelo de la zona norte de la Cuenca de México”, Tesis de maestría SEPI, ESIA-IPN, Ciudad de México, México.
[108] Barranco-Eyssautier, A., (2016). “Caracterización geotécnica del subsuelo de la zona sur del valle de México con aplicación a una obra de infraestructura”, Tesis de licenciatura, UNAM, México.
[109] Magnan, J.P., et Bourehaoua, A., (2001). “Analyse probabiliste de la consolidation unidimensionnelle des sols”, Revue Française de Géotechnique, 2ème trimestre, pp 10-25, France.
[110] Auvinet, G., Bouayed, A., Orlandi, S. and López A., (1996). "Stochastic Finite Element Method in Geomechanics", Proceedings, Geotechnical Engineering Congress, "Uncertainty 96", University of Wisconsin, Geotechnical Engineering Division, ASCE Geotechnical Special Publication N° 58, Vol. 2, 1239-1253, ISBN: 0-7844-0188-8, USA.
[111] Auvinet, G., Mellah R., Masrouri F. and Rodríguez, J.F., (2000). "La méthode des éléments finis stochastiques en Géotechnique", Revue Française de Géotechnique N° 93, Paris, France, 67-79.
[112] Mathews, J. and Walker, R.L., (1964). Mathematical methods of Physics, 2nd edition, Benjamin Publishers, 286-298.
[113] Rosenblueth, E., (1975). “Point estimates for probability moments”, Proceedings of National Academy of Science of the U.S.A., 72(10), 3812-3814.
[114] Ghanem, R.G. and Spanos, P.D., (1991). “Stochastic finite elements, A spectral approach”, Springer-Verlag, New York.
[115] Pineda A.R., (2015). “Análisis estocástico de estructuras térreas: enfoque espectral”, Tesis doctoral, Programa de Maestría y Doctorado en Ingeniería, Ingeniería Civil, Geotecnia, UNAM, Ciudad de México, México.
[116] Freudenthal, A.M., Garrelts, J.M. and Shinozuka, M. (1964). “The analysis of structural safety”, Belvoir Defense Technical Information Center.
[117] Auvinet, G. and González, J.L., (2000). "Three dimensional reliability analysis of earth slopes", Computers and Geotechnics 26, 247-261, Elsevier.
[118] Hungr, O., (1987). “An extension of Bishop’s simplified method of slope stability to three dimensions”, Géotechnique 38, No 1, 155-156, London.
[119] Mendoza, M.J., Mendoza, S., Rufiar, M. and González, D., (2018). “Slope stability of a slope excavation in the soft clayey soil of the ancient Texcoco lake”, Proceedings, XXIX Reunion de Nacional de Ingeniería Geotécnica, León, Guanajuato, Mexico.
[120] Schmitter, J.J., Pérez, A. and Romero, W. (2018). “Thought about the behavior of the Texcoco former Lake subsoil, while being excavated”, Proceedings, XXIX Reunion de Nacional de Ingeniería Geotécnica, León, Guanajuato, Mexico.
[121] Mitchell, J.K., (1981). “Soil Improvement: State-of-the-Art Report”, Proceedings of the 10th International Conference on Soil Mechanics and Foundation Engineering, Stockholm, Sweden, 509-565.
[122] Pilot, G., Queyroi, D. et Chaput, D., (1985), “Amélioration des sols de foundation. Choix des méthodes d´exécution”, LCPC, Ministère de l´urbanime, du logement et des transports, Paris, France.
[123] Schaefer, V. (2012). “Ground improvement in the 21st Century. A comprehensive Web-based Information System”, ASCE GSP, May, Conference GeoCongress 2012.

[124] Mesri, G. and Khan, A.Q., (2012) “Ground improvement using vacuum loading together with vertical drains”, Journal of Geotechnical and Geoenvironmental Engineering, ASCE, June.
[125] Auvinet, G., (1979). "Precarga en arcillas del Valle de México", Memoria, Simposio sobre "Mejoramiento masivo de suelos", Sociedad Mexicana de Mecánica de Suelos, 100-102, CDMX, México.
[126] Auvinet, G., (2016), “Técnica de precarga alternativa para las pistas del NAICM”, Nota Técnica del II-UNAM No. GEO-35. Elaborada para: Grupo Aeroportuario de la Ciudad de México (GACM), Mexico.
[127] Auvinet, G. y Pérez Ángeles M., (2016), “Terraplenes y bordos sobre suelos blandos”, Memoria de la XXVIII Reunión Nacional de Ingeniería Geotécnica, SMIG, Conferencia magistral, 23-26 de noviembre, Mérida, Yucatán, México.

## Appendix I. Considerations about some physical properties of soft soils

a) Void ratio

In geotechnical engineering, the widely used physical property known as *void ratio e* is defined as:

$$e = \frac{V_V}{V_S} \tag{1}$$

where $V_V$ = volume of voids (including water) in sample, and $V_S$ = volume of solids in sample.

This parameter is extremely unstable for small samples (Auvinet, 1986 [1]) and for soft soils with high water content. When applied to the microstructure of soils, according to Eq. (1) $e$ tends towards extreme values:

$$e = \infty \text{ for } V_S = 0$$
$$e = 0 \text{ for } V_V = 0$$

It is also easy to verify that if a heterogeneous sample is divided into $k$ parts of the same size, the void ratio of the sample as a whole is not the average of the $k$ void ratios of the different subsamples. This is of course a consequence of the high non-linearity of Eq. (1) with respect to $V_S$. Averaging local void ratios introduces a bias and overestimates the actual void ratio of the whole sample. Void ratio is thus an ill-fitted parameter for statistical analyses of soft soils spatial variations. Note that Compression index $C_c$ and Swelling index $C_s$ are incremental void ratios.

These inconveniences can of course be avoided by sticking to another common physical property, porosity, $n$, defined as:

$$n = \frac{V_V}{V_T} \tag{2}$$

where $V_V$ = volume of voids in sample, and $V_T$ = total volume of sample.

Porosity is a stable parameter ranging between 0 and unity (100%) that can be averaged over a volume.

Note that, as it is well known:

$$n = \frac{e}{(1+e)} \quad \text{and} \quad e = \frac{n}{(1-n)} \tag{3}$$

However, if porosity $n$ is considered as a random variable with expected value $E\{n\}$ and standard deviation $\sigma_n$ within an heterogeneous random medium, the corresponding expected value of void ratio $E\{e\}$ will present a biased value that can be estimated using a second order approximation (Papoulis, 1985 [2]) :

$$E\{e\} \cong \frac{E\{n\}}{1-E\{n\}} + \frac{1}{2}\left[\frac{d^2e}{dn^2}\right]_m \sigma_n^2 = \frac{E\{n\}}{1-E\{n\}} + \frac{\sigma_n^2}{(1-E\{n\})^3} \tag{4}$$

and reciprocally:

$$E\{n\} \cong \frac{E\{e\}}{1+E\{e\}} + \frac{1}{2}\left[\frac{d^2n}{de^2}\right]_m \sigma_e^2 = \frac{E\{e\}}{1+E\{e\}} - \frac{\sigma_e^2}{(1+E\{e\})^3} \tag{5}$$

Most expressions in terms of void ratio can also be readily expressed in terms of porosity.

As an example, Figure 1 shows a typical $e - \log \sigma'$ compressibility curve for Mexico City clays and the corresponding $n - \log \sigma'$ curve. Comparing these graphs it can be observed that, at least in this case, the second representation looks, as a matter of fact, better-suited than the first one for determining the preconsolidation pressure $\sigma'_p$ and the slope of the virgin and recompression branches.

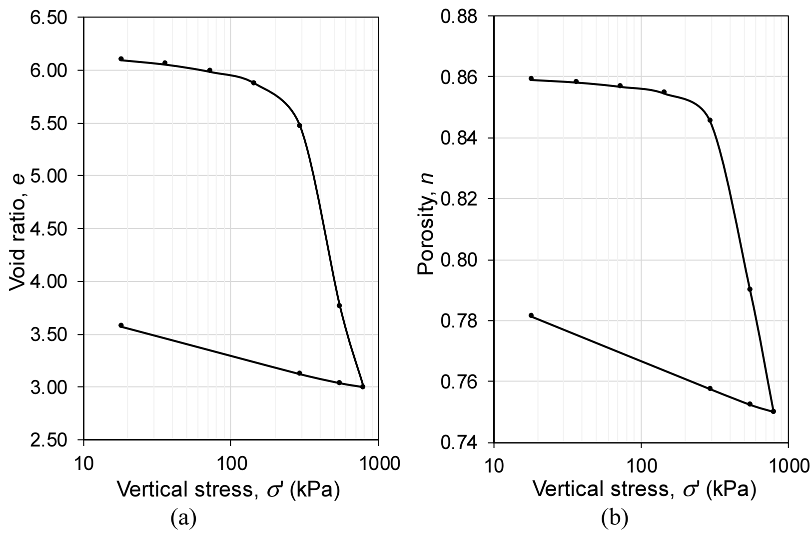


**Figure 1.** Compressibility curves expressed in term of (a) void ratio $e$ and (b) porosity $n$.

The settlement $\Delta H$ of a layer with thickness $H$, usually calculated as:

$$\Delta H = \frac{e_0 - e}{1 + e_0} H \tag{6}$$

where $e_0$ is the initial void ratio and $e$ is the void ratio after the settlement has occurred.
Can also be calculated as:

$$\Delta H = \frac{n_0 - n}{1 - n} H \tag{7}$$

Where $n_0$ is the initial porosity and $n$ is the porosity after the settlement has occurred.

In a more general form, the settlement of a soil layer submitted to a stress increment $\Delta\sigma$ can be calculated from compressibility curve in terms of porosity as:

$$\Delta H = H\left[\frac{C_{dn}}{1-n}\log\frac{\sigma'_p}{\sigma'_0} + \frac{C_{cn}}{1-n}\log\frac{\sigma'_0 + \Delta\sigma}{\sigma'_p}\right] \tag{8}$$

when $\sigma'_{0_z} \leq \sigma'_p$ and $\sigma'_{0_z} + \Delta\sigma \geq \sigma'_p$

where $C_{cn}$ = compression index (from $n$-log$\sigma'$ curve), $C_{dn}$ = swelling index (from $n$-log$\sigma'$ curve), $n$ = final porosity, and $H$ = layer thickness.

Void ratio thus appears as an unnecessary parameter, redundant with porosity, and with the inconveniences mentioned above in the context of statistical analyses of soft soils spatial variations.

b) Water content

In the same way, in geotechnical engineering, the physical property known as *gravimetric water content* $w$ is defined as:

$$w = \frac{W_W}{W_S} \tag{9}$$

where $W_w$ = weight of water in sample, and $W_S$ = weight of solids in sample.

This is also a very unstable parameter for small samples and for soft soils with high water content. When applied to the microstructure of soils, according to Eq. (9), $w$ tends towards extreme values:

$$w = \infty \text{ for } W_S = 0$$
$$w = 0 \text{ for } W_W = 0$$

It is also easy to verify that if a sample is divided into $k$ parts of the same size, the water content $w$ of the sample as a whole is <u>not</u> the average of the water contents of the $k$ different subsamples. This is again a consequence of the non-linearity of Eq. (9) with respect to $W_s$. Averaging local water contents introduces a bias and overestimates the actual water content of the whole sample. Note that Atterberg's limits are also gravimetric water contents.

Taylor (1948 [3]) underlined that definition of Eq. (9) is not standard in all branches of science, the water content being defined in geology, for example, as a percentage of total weight:

$$w' = \frac{W_W}{W_T} \tag{10}$$

where $W_T$ = total weight of sample (=$W_S$+$W_W$)

This parameter is much more stable than the previous one since it can only vary between 0 and 100%. However, it is also easy to verify that if a sample is divided in *k* parts of the same size, water content *w*' of the sample as a whole is not the average of the water content of the *k* different subsamples. Averaging local water contents introduces a small bias and overestimates the actual water content of the whole sample. Strictly speaking, parameter *w*' cannot be averaged either over a volume but the error incurred in using this parameter in statistical analyses is generally small.

Note that:

$$w' = \frac{w}{w+1} \text{ and } w = \frac{w'}{1-w'} \tag{11}$$

A volumetric definition of water content is also commonly used:

$$w'' = \frac{V_W}{V_T} \tag{12}$$

where $V_W$ = volume of water in sample, and $V_T$ = total volume of sample (=$V_W$ + $V_S$ for saturated materials).

This stable parameter varies between 0 and 100 % and can be averaged on a volume. In the case of saturated materials, it is equal to porosity. Note that, also for saturated materials:

$$\begin{gathered} w'' = \frac{G_s w}{1+G_s w} \text{ and } w = \frac{w''}{G_s(1-w'')} \text{ , while:} \\ w'' = \frac{G_S w'}{1+w'(G_S-1)} \text{ and } w' = \frac{w''}{w''+G_S(1-w'')} \end{gathered} \tag{13}$$

where $G_S$ = specific density of solids.

Figure 2 shows how, for saturated materials with high water content, small increases in volumetric water content *w*''(Eq. (12)) correspond to very large increases in gravimetric water content *w* (Eq. (9)) that do not correspond to really significant changes in the composition of the soil sample. Water content *w*' (Eq. (10)) presents a much more stable behavior.

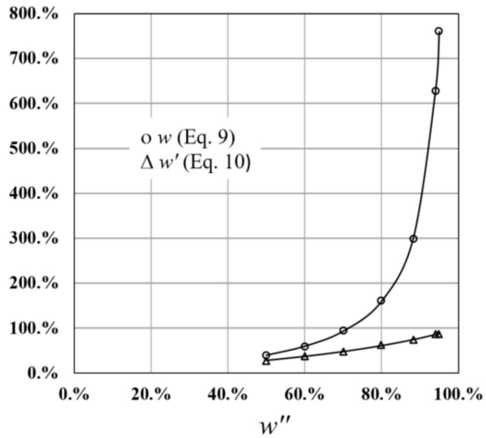


**Figure 2.** Variations of water contents *w* (Eq. (9)) and *w*´ (Eq. (10)) as a function of *w*'' (Eq. (12)).

If the volumetric water content *w''* is considered as a random variable with expected value $E\{w''\}$ and standard deviation $\sigma_{w''}$ within an heterogeneous random medium, the corresponding expected value of water content *w*, $E\{w\}$, can be estimated using a second order approximation as :

$$E\{w\} \cong \frac{E\{w''\}}{G_s(1-E\{w''\})} + \frac{1}{2}\left[\frac{d^2w}{dw''^2}\right]_m \sigma^2_{w''} = \frac{E\{w''\}}{G_s(1-E\{w''\})} + \frac{\sigma^2_{w''}}{G_s(1-E\{w''\})^3} \quad (14)$$

and reciprocally:

$$E\{w''\} \cong \frac{G_sE\{w\}}{1+G_sE\{w\}} + \frac{1}{2}\left[\frac{d^2w''}{dw^2}\right]_m \sigma^2_{w} = \frac{G_sE\{w\}}{1+G_sE\{w\}} - \frac{G_s^2\sigma^2_w}{(1+G_sE\{w\})^3} \quad (15)$$

Similarly,

$$\begin{aligned} E\{w'\} &\cong \frac{E\{w''\}}{E\{w''\}+G_s(1-E\{w''\})} + \frac{1}{2}\left[\frac{d^2w}{dw''^2}\right]_m \sigma^2_{w''} \\ &= \frac{E\{w''\}}{E\{w''\}+G_s(1-E\{w''\})} + \frac{G_s(G_s-1)\sigma^2_{w''}}{[E\{w''\}+G_s(1-E\{w''\})]^3} \end{aligned} \quad (16)$$

and reciprocally:

$$\begin{aligned} E\{w''\} &\cong \frac{G_sE\{w'\}}{1+E\{w'\}(G_s-1)} + \frac{1}{2}\left[\frac{d^2w''}{dw'^2}\right]_m \sigma^2_{w'} \\ &= \frac{G_sE\{w'\}}{1+E\{w'\}(G_s-1)} - \frac{G_s(G_s-1)\sigma^2_{w'}}{[1+E\{w'\}(G_s-1)]^3} \end{aligned} \quad (17)$$

Most existing geotechnical engineering analytical developments have been expressed in terms of parameters defined by Eqs. (1) and (9). These parameters should however be considered as inadequate in a context of statistical analyses of soft soils spatial variability. To illustrate the above, in Table 1, a hypothetical heterogeneous saturated sample was divided into five equal parts with assumed unitary volumes. The specific density of solid was considered to be $G_s = 2.5$.

**Table 1.** Comparison of average and true values of void ratio and water content.

| | | | | | | | Gravimetric 1 | Gravimetric 2 | Volumetric | Void ratio | Porosity |
|---|---|---|---|---|---|---|---|---|---|---|---|
| | | | | | | | $w = W_W/W_S$ | $w' = W_W/W_T$ | $w'' = V_W/V_T$ | $e = V_W/V_S$ | $n = V_W/V_T$ |
| Subsample | $W_W$ | $W_S$ | $W_T$ | $V_W$ | $V_S$ | $V_T$ | $w$,% | $w'$,% | $w''$,% | $e$ | $n$ |
| 1 | 0.88 | 0.29 | 1.18 | 0.88 | 0.12 | 1.00 | 300 | 75 | 88 | 7.50 | 0.88 |
| 2 | 0.80 | 0.50 | 1.30 | 0.80 | 0.20 | 1.00 | 160 | 62 | 80 | 4.00 | 0.80 |
| 3 | 0.70 | 0.75 | 1.45 | 0.70 | 0.30 | 1.00 | 93 | 48 | 70 | 2.33 | 0.70 |
| 4 | 0.60 | 1.00 | 1.60 | 0.60 | 0.40 | 1.00 | 60 | 38 | 60 | 1.50 | 0.60 |
| 5 | 0.50 | 1.25 | 1.75 | 0.50 | 0.50 | 1.00 | 40 | 29 | 50 | 1.00 | 0.50 |
| | | | | | | Average | 131 | 50 | 70 | 3.27 | 0.70 |
| | | | | | | True value | 92 | 48 | 70 | 2.29 | 0.70 |
| | | | | | | Bias | 39 | 2 | 0 | 0.98 | 0 |

A strong bias is observed between the average of the local values of void ratio $e$ and the true value of this same parameter for the whole sample.

Similarly, a bias exists between the average of local values and the true values of the gravimetric water contents (Eqs. (9) and (10)) for the whole sample. The bias of the average value of $w'$ is however much smaller than the bias of the average value of $w$. Volumetric water content $w''$ is clearly the best behaved parameter from a physical and mathematical point of view.

Note that the true value of void ratio $e$ for the whole sample can be calculated directly applying the second relation of Eq. (3) to the unbiased average value of porosity. This true value corresponds to the first term of the development of Eq. (7) while the bias is approximately equal to the second term of this development.

Similarly, the true values of gravimetric water contents $w$ and $w'$ for the whole sample can be calculated directly applying the second and fourth relations of Eq. (13) to the unbiased average value of volumetric water content $w''$. These true values correspond to the first terms of the developments of Eqs, (14) and (16) while the biases are approximately equal to the second terms of these developments.

*References for Appendix I*

[1] Auvinet, G., (1986). "Estructura de medios granulares", Tesis doctoral, División de Estudios de Posgrado de la Facultad de Ingeniería, UNAM, (2 vol.), México.
[2] Papoulis, A., (1985). Probability, Random variables and Stochastic Processes, McGraw-Hill, USA.
[3] Taylor, D.W., (1948). Fundamentals of Soil Mechanics, John Wiley & Sons, New York, USA.

## Appendix II. Random fields and Geotechnical engineering

### *II.1. Definitions*

Let $V(X)$ be a geotechnical variable of either physical (e.g. water content), mechanical (e.g. undrained shear strength), or geometric type (e.g. thickness of a certain stratum), defined at points $X$ of a certain domain $R^P$ ($p = 1, 2,$ or 3). If at each point of the domain this variable is regarded as random, the set of these random variables constitutes a random field (Auvinet, 2002 [1])

To describe such a field, the following parameters and functions are introduced:

- Expected value:

$$\mu_V(X) = E\{V(X)\} \tag{1}$$

- Variance:

$$\sigma_V^2(X) = Var[V(X)] \tag{2}$$

The square root $\sigma_V(X)$ of the variance is known as *standard deviation* whereas the ratio $CV(X) = \sigma_V(X) / E\{V(X)\}$ is defined as the *coefficient of variation*.

- Autocorrelation function:

$$R_V(X_1, X_2) = E\{V(X_1)V(X_2)\} \tag{3}$$

This function, defined in the $R^P$ x $R^P$ space is a mixed second order moment that can be centered introducing the concept of autocovariance function:

- Autocovariance function:

$$\begin{aligned} C_V(X_1, X_2) &= \mathrm{Cov}[V(X_1), V(X_2)] = \\ &E\{[V(X_1) - \mu_V(X_1)][V(X_2) - \mu_V(X_2)]\} \end{aligned} \tag{4}$$

The autocovariance function represents the degree of linear dependence existing between the values of the property of interest in two different points of the medium. It can be written in terms of a dimensionless autocorrelation coefficient (normalized autocovariance function), the value of which always ranges between -1 and +1:

- Autocorrelation coefficient function (normalized autocovariance):

$$\rho_V(X_1, X_2) = \frac{C_V(X_1, X_2)}{\sigma_V(X_1)\sigma_V(X_2)} \tag{5}$$

It should be emphasized that functions (3) to (5) are not intrinsic properties of points $X_1$ and $X_2$ since they also depend on the dominion in which the field has been defined. Actually, if a soil deposit is considered as a whole, it may be possible to find a high correlation between the properties corresponding to two points that belongs to the same substratum; however, this correlation is likely to vanish if the study is limited to analyzing the spatial variations within this particular substratum. Tables providing "typical autocorrelation coefficient functions" found in the literature are thus generally meaningless.

- Probability distribution functions:

$$F_{V_1,\ldots,V_n}\left(v_1,\ \ldots,v_n;\ X_1,\ \ldots,X_n\right)=P\left[V(X_1)\le v_1,\ldots,V(X_n)\le v_n\right] \tag{6}$$

among which special mention should be made of the first-order probability distribution function:

$$F_V(v;X)=P\left[V(X)\le v\right] \tag{7}$$

as well as of its derivatives, namely the joint probability densities:

$$f_{V_1,\ldots,V_n}\left(v_1,\ \ldots,v_n;\ X_1,\ \ldots,X_n\right)\ \text{and}\ f_V(v;X) \tag{8}$$

If these functions (and the associated moments) are invariant by translation in space for any value of $n$ and for any set of points: $X_1,\ldots,X_n$, the random field is said to be *strictly stationary*.

If, in the domain considered, the expected value and other parameters are constant, the medium is called *statistically homogeneous*. If parameters such as the expected value and variance of the field are not constant, it is said that they present a certain *trend* or *drift*.

When it is possible to accept the hypothesis that the expected value of the variable of interest is constant throughout the whole dominion and that the spatial autocovariance only depends on the distance between points $X_1$ and $X_2$, it is said that the field is *wide-sense stationary*; then:

$$C_V\left(X_1,X_2\right)=C_V\left(X_2-X_1\right)=C_V\left(h\right) \tag{9}$$

where $h$ = scalar equal to the distance between points $X_1$ and $X_2$.

Eq. (9) implies that variance of $V(X)$ is also a constant in the whole dominion.

Similarly, in this case, the autocorrelation coefficient can be expressed as:

$$\rho_V\left(X_1,X_2\right)=\rho_V\left(h\right) \tag{10}$$

In many applications, however, it will be more realistic to admit that the previous relationship is only valid along a specified direction, i.e. that the structure of correlation of the medium is anisotropic. In this case, the notations $C_V(h\mathbf{u})$ and $\rho_V(h\mathbf{u})$ can be used, where $\mathbf{u}$ is a unit vector in the direction being considered.

In media with linear drift, the field is not stationary but increments $V(X+h)$ - $V(X)$ can still be stationary. Accordingly, some authors, especially in mining applications, have opted for using the concept of variogram instead of autocovariance. The variogram $2\gamma(h)$ is the second order moment of increment $V(X+h)$ - $V(X)$:

$$2\gamma(h) = E\left\{\left[V(X+h) - V(X)\right]^2\right\} \tag{11}$$

For a wide-sense stationary field:

$$2\gamma(h) = \mathrm{Var}\left[V(X+h) - V(X)\right] \tag{12}$$

$$\gamma(h) = C_V(0) - C_V(h) \tag{13}$$

In most engineering applications, using the concept of variogram fails to present any advantage and therefore autocovariance function is commonly employed instead. As a matter of fact, some of the most common geostatistical softwares systematically convert variograms into autocovariance functions to provide better stability to numerical algorithms (Deutsch and Journel, 1992 [2]).

Note that, alternatively, spatial variability of geotechnical variables can be modeled by means of copulas (Vázquez-Guillén, 2014 [3]). Copulas are of interest as random functions because they express dependence without the influence of the first-order distribution functions. Thus, more realistic spatial variability descriptions can be attained. For a random field constituted by continuous random variables, the $n$-dimensional copula is written as (Nelsen, 2006 [4]):

$$C(u_1 = F_{V_1}(v_1), \ldots, u_n = F_{V_1}(v_n)) = F_{V_1,\ldots,V_n}\left(F_{V_1}^{-1}(u_1), \ldots, F_{Vn}^{-1}(u_n)\right) \tag{14}$$

and the corresponding copula density by:

$$c(u_1,\ldots,u_n) = f_{V_1,\ldots,V_n}(F_{V_1}^{-1}(u_1),\ldots,F_{V_n}^{-1}(u_n)) / \prod_{i=1}^{n} f_{V_i}\left(F_{V_i}^{-1}(u_i)\right) \tag{14a}$$

For example, the multivariate Gaussian copula can be formulated as:

$$C_\Gamma^{\mathrm{G}}\left(u_1,\ldots,u_n\right) = \mathbf{\Phi}_\Gamma\left(\Phi^{-1}(u_1),\ldots,\Phi^{-1}(u_n)\right) \tag{15}$$

where $\mathbf{\Phi}_\Gamma(\cdot)$ is the multivariate Gaussian distribution (see 4.4) with zero mean and correlation matrix $\Gamma$ and $\Phi^{-1}(\ )$ is the inverse of the first-order standard Gaussian distribution.

The corresponding Gaussian copula density is written as:

$$c(u_1,\ldots,u_n) = f_{V_1,\ldots,V_n}(\Phi^{-1}(u_1),\ldots,\Phi^{-1}(u_n)) / \prod_{i=1}^{n} f_{V_i}\left(\Phi^{-1}(u_i)\right) \tag{15a}$$

where $f_{V_1,\dots,V_n}()$ is the multivariate Gaussian density function and $f_{V_i}()$ is the first-order Gaussian density function.

As an example, Figure 1 displays copula density plots of the bivariate Gaussian copula for different correlation coefficients ($\rho$=0.95, 0.85 and 0.45).

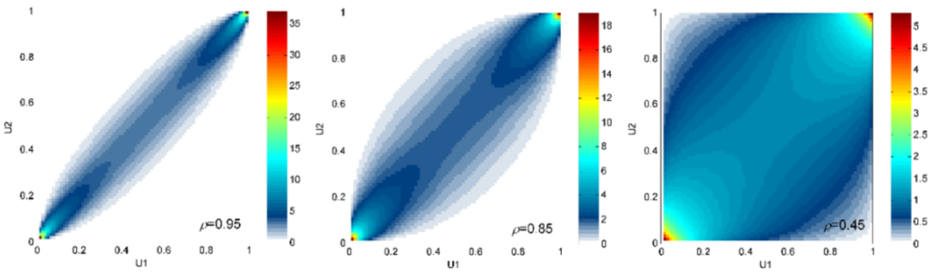


**Figure 1.** Bivariate Gaussian copula density plots for different correlation coefficients.

Similar to a description with autocovariance functions, bivariate spatial copulas are used to describe spatial variability. For any two locations separated by the vector $h\mathbf{u}$, a spatial copula is defined via Sklar`s theorem as (Bárdossy, 2006 [5]):

$$C_S\left(h\mathbf{u};u_1,u_2\right)=C\left(F_V(V(X),F_V(V(X+h\mathbf{u})\right) \tag{16}$$

Hence, the copula becomes a function of the separating vector $h\mathbf{u}$. Note that $u_1$ and $u_2$ are the quantiles of $V(X)$ and $V(X+h\mathbf{u})$, respectively. For a given $h\mathbf{u}$, the spatial copula $C_S(\,)$ describe thus the spatial dependence between the quantiles $u_1,u_2$ of pairs of random variables.

Note also that in soils suffering consolidation, the evolution of static and dynamic parameters of the deforming deposit occurs within a context of pronounced uncertainty. Therefore, the use of a spatio-temporal random field may be helpful to increase the degree of realism of long-term predictions made with geomechanical models. Vázquez and Auvinet (2015 [6]) described this type of random fields and proposed a stochastic simulation technique of such random fields. In the work by Vázquez and Auvinet (2017 [7]), such technique is applied to identify hydraulic conductivities from temporal observations of the hydraulic head field.

*II.2. Statistical estimation of random field parameters*

The descriptive parameters of a random field can be estimated from "discrete" (isolated samples) or "continuous" (boring logs) obtained in an exploratory program. In the latter case, and assuming that the field is statistically homogeneous and ergodic (i.e. its parameters can be estimated from a single sample function or realization), the expected value can be assessed (Auvinet, 2002 [1]) using the following approximation:

$$\mu_V \cong \mu^* = \frac{1}{L}\int_0^L V(x)dx \tag{17}$$

where $L$ = depth of the boring.

Similarly, it is possible to estimate the autocovariance function along the **u** direction as:

$$C_V(h\mathbf{u}) \cong \frac{1}{L}\int_0^L V(x)V(x+h\mathbf{u})dx - \mu^{*2} \tag{18}$$

where **u** is the unit vector in the direction along which the covariance is evaluated and $h$ is a scalar.

Estimating the autocovariance by means of Eq. (18) introduces a small bias, as can be verified by evaluating the expected value of the second member.

On the other hand, if the following indicator function is introduced:

$$I_V(v, X) = \begin{cases} 1 & \text{if} \quad V(X) \le v \\ 0 & \text{if} \quad V(X) > v \end{cases} \tag{19}$$

The field's first-order probability distribution function can be estimated from continuous records based on the relationship:

$$F_V(v, X) = P\left[V(X) \le v\right] \cong \frac{1}{L}\int_0^L I_V(v, x)\,dx \tag{20}$$

Estimation of field parameters in terms of the available data is generally known as *structural analysis*.

In the case of isolated samples, estimations can performed using discrete expressions equivalent to the previous equations (Deutsch and Journel, 1992 [2]). This situation is the most common whenever the variable of interest is of the geometric type (thickness of a given stratum, as an example).

*II.3. Scale effect*

Knowing the major parameters of a random field representing the variations of the properties makes it possible to evaluate the expected value and dispersion of the average values of such properties in subdomains (lines, areas or volumes) contained within the medium. In a stationary field, the mathematical expectation of the average value of the property of interest in a subdomain ω is (Papoulis, 1985 [8]):

$$E\{V_\Omega\} = E\left\{\frac{1}{\Omega}\int_\Omega V(X)\,dX\right\} = E\{V(X)\} \tag{21}$$

and its variance is:

$$\mathrm{Var}\left[V_\Omega\right] = E\left\{V_\Omega^2\right\} - E^2\left\{V_\Omega\right\} \tag{22}$$

that is to say:

$$\mathrm{Var}\left[V_\Omega\right] = \frac{1}{\Omega^2}\left[E\left\{\int_\Omega V(X)\,dX\int_\Omega V(X)\,dX\right\} - E\left\{\int_\Omega V(X)\,dX\right\}^2\right] \tag{23}$$

that can be expressed as:

$$\begin{aligned}\mathrm{Var}\left[V_\Omega\right] = \frac{1}{\Omega^2}\Bigg[&\int_\Omega\int_\Omega E\left\{V(X_1)V(X_2)\right\}dX_1 dX_2 \\ &-\int_\Omega\int_\Omega E\left\{V(X_1)\right\}E\left\{V(X_2)\right\}dX_1 dX_2\Bigg]\end{aligned} \tag{24}$$

or:

$$\mathrm{Var}\left[V_\Omega\right] = \frac{1}{\Omega^2}\int_\Omega\int_\Omega C_V\left(X_1, X_2\right)dX_1 dX_2 \tag{25}$$

Similarly, it can be shown that the covariance between the average values of a given property in two subdomains $\Omega_1$ and $\Omega_2$, with or without overlapping, is:

$$\mathrm{Cov}\left[V_{\Omega_1}, V_{\Omega_2}\right] = \frac{1}{\Omega_1\Omega_2}\int_{\Omega_1}\int_{\Omega_2} C_V\left(X_1, X_2\right)dX_1 dX_2 \tag{26}$$

Eq. (25) can be also written as:

$$\mathrm{Var}\left[V_\Omega\right] = \frac{\mathrm{Var}\left[V(X)\right]}{\Omega^2}\int_\Omega\int_\Omega \rho_V\left(X_1, X_2\right)\, dX_1 dX_2 \tag{27}$$

Since the correlation coefficient is smaller than or equal in absolute value to unity, the variance of the average value of a stationary random property in a given subdomain $\Omega$ tends to decrease when the dimensions of such domain increase (except in the trivial case of perfect correlation).

The above consideration applies to any property that can be averaged on a volume. As seen in Appendix I, strictly speaking, this is not the case of soil gravimetric water content.

*II.4. Conditional estimation*

A problem of utmost interest in geotechnical engineering is the estimation of the value of a property of interest at a point of the medium where no measurement exists (point estimation). A solution to this problem allows interpolating between available data and even defining virtual boring logs and cross-sections of the medium. The problem can be generalized to that of estimating the average value of the same property in any subdomain studied, for instance in a given volume or along a certain potentially critical surface (global estimation).

A technique available to reach this objective is the *unbiased linear conditional estimation with minimal variance*, also known as Wiener's filter. A similar technique used in mining engineering, is known as *kriging* (Krige, 1962 [9]; Matheron, 1965 [10]).

### *II.4.1. Bivariate linear conditional estimation*

Modeling by means of a random field a property defined in a domain, Ω, makes it possible to evaluate the conditional expected value and variance of $V_\Omega$, punctual or average value of this property in a subdomain, $\Omega_1$, in terms of the value $V_{\Omega_2}$, also punctual or average, obtained through direct measurement in another subdomain $\Omega_2$.

A linear estimator $V^*_{\Omega_1}$ is used such that:

$$V^*_{\Omega_1} = aV_{\Omega_2} + b \tag{28}$$

that should be unbiased:

$$E\left\{V^*_{\Omega_1} - V_{\Omega_1}\right\} = 0 \tag{29}$$

It is possible to obtain an expression for the values of $a$ and $b$, so that Eqs. (28) and (29) are simultaneously satisfied, and the expectation of the square of the error or *estimation variance* is minimized:

$$E\left\{(V^*_{\Omega_1} - V_{\Omega_1})^2\right\} = \mathrm{Var}\left[aV_{\Omega_2} + b - V_{\Omega_1}\right] \tag{30}$$

From (29) it can be inferred that the value of $b$ is:

$$b = E\left\{V_{\Omega_1}\right\} - aE\left\{V_{\Omega_2}\right\} \tag{31}$$

On the other hand, it is easy to verify that by making equal to zero the derivative of Eq. (27) with respect to variable $a$, in order to minimize the estimation error, the following result is obtained:

$$a = \frac{\mathrm{Cov}\left[V_{\Omega_1}, V_{\Omega_2}\right]}{\sigma^2_{V_{\Omega_2}}} \tag{32}$$

Eq. (28) providing the estimation becomes:

$$V^*_{\Omega_1} = E\left\{V_{\Omega_1}\right\} + \rho_V\left(V_{\Omega_1}, V_{\Omega_2}\right)\frac{\sigma_{V_{\Omega_1}}}{\sigma_{V_{\Omega_2}}}\left[V_{\Omega_2} - E\left\{V_{\Omega_2}\right\}\right] \tag{33}$$

where $\rho_V\left(V_{\Omega_1}, V_{\Omega_2}\right)$ is the correlation coefficient between $V_{\Omega_1}$ and $V_{\Omega_2}$:

$$\rho_V\left(V_{\Omega_1},\ V_{\Omega_2}\right) = \frac{\operatorname{Cov}\left[V_{\Omega_1},\ V_{\Omega_2}\right]}{\sigma_{V_{\Omega_1}}\ \sigma_{V_{\Omega_2}}} \tag{34}$$

The corresponding minimized estimation variance is equal to:

$$E\left\{(V^*_{\Omega_1} - V_{\Omega_1})^2\right\} = \operatorname{Var}\left[V_{\Omega_1}\right]\ \left(1\text{-}\rho_V^2\right) \tag{35}$$

If the two variables have the same expected value and variance, two extreme situations can prevail regarding the correlation coefficient:

- If $V_{\Omega_1}$ and $V_{\Omega_2}$ are perfectly correlated, then: $\rho_V\left(V_{\Omega_1}, V_{\Omega_2}\right)=1$ and $V^*_{\Omega_1} = V_{\Omega_2}$.
- If $V_{\Omega_1}$ and $V_{\Omega_2}$ are not correlated, the information regarding $\Omega_2$ is useless for reducing uncertainty on $\Omega_1$.

It can be observed that, in the general case, the knowledge of the field in a given subdomain leads to a correction of the expected value and to a reduction of variance of the field or of its average value in other subdomains.

*II.4.2. Multivariate linear estimation*

The previous method can be extended to the estimation of conditional expectations, variances and covariances of punctual or average values taken respectively by a random field in different points or subdomains of the medium studied, based on a certain number of results of measurements also carried out in different points or subdomains.

Let **V** be a vector of dimension $p$ containing the $k$ variables to be estimated and the $p$-$k$ known variables, defined as:

$$\mathbf{V} = \begin{pmatrix} \mathbf{V}_1 \\ \mathbf{V}_2 \end{pmatrix} \text{ with } \mathbf{V}_1 = \begin{pmatrix} V_1 \\ . \\ . \\ . \\ V_k \end{pmatrix} \text{ and } \mathbf{V}_2 = \begin{pmatrix} V_{k+1} \\ . \\ . \\ . \\ V_p \end{pmatrix} \tag{36}$$

$\mathbf{V}_1$ is the vector of the variables to be estimated and $\mathbf{V}_2$ is the vector of the known variables.

Let **U** be the vector, also with a dimension $p$, of the expected values of the variables to be estimated and of the known variables, defined as:

$$\mathbf{U} = \begin{pmatrix} \mathbf{U}_1 \\ \mathbf{U}_2 \end{pmatrix} \text{ with } \mathbf{U}_1 = \begin{pmatrix} \mu_1 \\ \cdot \\ \cdot \\ \cdot \\ \mu_k \end{pmatrix} \text{ and } \mathbf{U}_2 = \begin{pmatrix} \mu_{k+1} \\ \cdot \\ \cdot \\ \cdot \\ \mu_p \end{pmatrix} \quad (37)$$

On the other hand, let **K** be the covariance matrix for the set of variables known and to be estimated:

$$\mathbf{K} = \begin{pmatrix} \mathbf{K}_{11} & \mathbf{K}_{12} \\ \mathbf{K}_{21} & \mathbf{K}_{22} \end{pmatrix} \quad (38)$$

where:

$\mathbf{K}_{11}$ submatrix of covariances between the variables associated to the different estimation points or domains, of order *k*.

$\mathbf{K}_{22}$ submatrix of covariances between the variables associated to the different known points or subdomains, of order *p-k*.

$\mathbf{K}_{12}$ and $\mathbf{K}_{21}$ submatrices of covariances between the different data and the variables associated to the various estimation points or subdomains, respectively of order *k* and *p-k*. It should be observed that $\mathbf{K}_{21} = \mathbf{K}_{12}^{\mathrm{T}}$.

It is possible to obtain a vector $\mathbf{V}_1^*$, an estimate of vector $\mathbf{V}_1$ given that $\mathbf{V}_2$ is known, the elements of which are linear, unbiased and leading to a minimum estimation variance.

The elements of this vector will be linear combinations of the elements of $\mathbf{V}_2$:

$$\mathbf{V}_1^* = \mathbf{A}\mathbf{V}_2 + \mathbf{b} \quad (39)$$

The estimation will be unbiased if:

$$E\left\{\mathbf{V}_1^* - \mathbf{V}_1\right\} = \mathbf{A}\mathbf{U}_2 + \mathbf{b} - \mathbf{U}_1 = 0 \quad (40)$$

The submatrix of the estimation variances will be written as:

$$\mathbf{K}_{11.2} = E\left\{\left(\mathbf{V}_1^* - \mathbf{V}_1\right)\left(\mathbf{V}_1^* - \mathbf{V}_1\right)^{\mathrm{T}}\right\} \quad (41)$$

that is to say:

$$\mathbf{K}_{11.2} = \mathbf{A}\mathbf{K}_{22}\mathbf{A}^{\mathrm{T}} + \mathbf{K}_{11} - \mathbf{A}\mathbf{K}_{12}^{T} - \mathbf{K}_{12}\mathbf{A}^{\mathrm{T}} \quad (42)$$

Proceeding again by derivation in order to minimize the elements of this matrix, it can be shown that the optimum coefficients matrix is:

$$\mathbf{A} = \mathbf{K}_{12}\mathbf{K}_{22}^{-1} \quad (43)$$

Combining the previous equations, the vector of the estimated values is obtained as:

$$\mathbf{V}_1^* = \mathbf{U}_1 + \mathbf{K}_{12}\mathbf{K}_{22}^{-1}(\mathbf{V}_2 - \mathbf{U}_2) \tag{44}$$

and the submatrix of minimized estimation variances is equal to:

$$\mathbf{K}_{11.2} = \mathbf{K}_{11} - \mathbf{K}_{12}\ \mathbf{K}_{22}^{-1}\ \mathbf{K}_{21} \tag{45}$$

This method is useful to estimate punctual or average values of the random field in subdomains of the medium (for instance, finite elements or sets of these elements) taking into account results obtained through sampling.

*II.4.3. Multifield linear estimation*

The same technique can be used when data from different random fields corresponding to different properties of interest are available. This is of foremost importance in Geomechanics since it allows estimating critical (primary) properties such as mechanical parameters from (secondary) variables more easily determined such as index properties. In this case, two fields *V(X)* (primary) and *S(X)* (secondary) will be defined. Their respective expected value, variance and autocovariance will be estimated from the data together with their *cross-covariance* function understood as:

$$\begin{aligned} C_{VS}(X_1, X_2) &= \mathrm{Cov}[V(X_1), S(X_2)] \\ &= E\{[V(X_1) - \mu_V(X_1)][S(X_2) - \mu_S(X_2)]\} \end{aligned} \tag{46}$$

This function represents the linear correlation that may exist between the primary and secondary fields. It can be obtained from the data but also from correlations established in similar geotechnical conditions.

As in 4.2, $\mathbf{V}_1$ will be the vector of the (primary) variables to be estimated but $\mathbf{V}_2$ the vector of the known variables will include some values corresponding to secondary field *S(X)*. Where necessary, the expected values of field *S(X)* will be introduced and auto-covariance will be substituted by cross-covariance in covariance submatrices.

This approach improves considerably the results of the one-field approach whenever the different fields present a good spatial cross-correlation. To avoid numerical problems, cross-covariance coefficient must satisfy the Cauchy-Schwartz inequality; $|\rho_{VS}(h)| \le \sqrt{\rho_{VV}(h)\rho_{SS}(h)}$ for all $h$ ; (Chiles and Delfiner, 1999 [11]).

*II.4.4. Gaussian fields*

A particular case of utmost importance is that of the *Gaussian* fields. It should be remembered that a random field is *Gaussian* when each random variable of the field, *V*(*X*), has a probability density of the type:

$$f_V(v) = \frac{1}{\sqrt{2\pi}\sigma_V}\exp\left[-\frac{1}{2}\left(\frac{v-\mu_V}{\sigma_V}\right)^2\right] \tag{47}$$

and when the joint probability density of any set of n field variables is defined by the following equation (Mood and Graybill, 1963 [12]):

$$f_{V_1,\,\ldots,\,V_n}\left(v_1,\,\ldots,\,v_n;\,X_1,\,\ldots,X_n\right)=\frac{1}{\left|\mathbf{K}\right|^{\frac{1}{2}}\left(2\pi\right)^{\frac{n}{2}}}\,e^{-\frac{1}{2}\left(\mathbf{V}-\boldsymbol{\mu}\right)^{\mathrm{T}}\mathbf{K}^{-1}\left(\mathbf{V}-\boldsymbol{\mu}\right)} \tag{48}$$

for $-\infty < v_i < +\infty$ and $i = 1,\ldots,\mathrm{n}$

where **V** is the vector of the random variables $V(X_1)$, $V(X_2),\ldots$, $V(X_n)$; $\boldsymbol{\mu}$ is a vector of real values such that $\mu_i = E\{V(X_i)\}$ and **K** is the positive definite symmetric covariance matrix of the random variables that contains, in the principal diagonal, the respective variances of the different variables and, outside of the diagonal, the paired covariances.

An interesting property of Gaussian fields is that the linear estimators of minimal variance discussed in the previous paragraphs are exact. In other words, for a vector **V** of dimension *p* presenting a *p*-Gaussian distribution of expectation vector **U** and covariance matrix **K**, the conditional distribution of vector $\mathbf{V}_1$, of order *k*, knowing $\mathbf{V}_2$ is a *k*-Gaussian distribution of the expectation vector $\mathbf{V}_1{}^*$, defined by Eq. (41) and with a covariance matrix given by Eq. (42) (Mood and Graybill, 1963 [12]).

The central limit theorem allows for this type of field to develop naturally when the analyzed phenomenon results from adding the effects of multiple fields. In many cases, there is no particular reason to assume that this happens in the case of the geotechnical variables; however, this type of field can be used as a first approximation of more complex fields.

It should also be remembered that any field can be transformed into a Gaussian field. This transformation is known as *anamorphosis*. It can be performed by the classical *Jacobian* method. Transformation to a Gaussian field through anamorphosis may be necessary to ensure that the covariance matrices involved in the procedure described in 4.2 be positive definite and can be inverted, especially in the case of multiple fields.

### *II.4.5. Kriging*

The technique known as *kriging*, widely used in mining engineering (Matheron, 1965, [10]) consists, as in 4.2, of obtaining linear estimators of minimum variance (*Best Linear Unbiased Estimation* or *"BLUE"*). However, the technique has some variants that can be of interest and that are briefly discussed in what follows for the case of the point estimation.

#### *II.4.5.1. Simple kriging.*

The *simple* kriging is a technique that can be applied when the field expected value $E\,\{V(X)\}$ is a known function of $X$ (eventually a constant). It consists of obtaining the punctual estimators in the field having null mean, $V(X) - E\{V(X)\}$, rather than in $V(X)$. The elements of the vector $\mathbf{V}_1{}^*$ of Eq. (36), are then substituted by:

$$V^*(X) - E\{V(X)\} = \sum_{i=1}^{n} \lambda_i (V_i - E\{V_i\}) \tag{49}$$

where $V_i$ represents the known elements of vector $\mathbf{V}_2$ and $E\{V_i\}$ the elements corresponding to the expectation vector $\mathbf{U}_2$.

Coefficients $\lambda_i$ and the estimators sought for can be obtained by using equations of section 4.2. The *simple* kriging is in fact rigorously equivalent to the conditional estimation technique brought forward in sections 4.3 and 4.4.

### *II.4.5.2. Ordinary kriging*

When dealing with a stationary field, Eq. (43) of the *simple* kriging method can be expressed as follows:

$$V^*(X) = \sum_{i=1}^{n} \lambda_i V_i + \left[1 - \sum_{i=1}^{n} \lambda_i\right] \mu_V \tag{50}$$

where $\mu_V$ is the field's constant expected value.

It is possible to find an unbiased linear estimator with minimal variance that requires no knowledge of the mean $\mu_V$, by imposing the condition:

$$\sum_{i=1}^{n} \lambda_i = 1 \tag{51}$$

The estimation variance:

$$\sigma_E^2(X) = \mathrm{Var}\left[V(X) - V^*(X)\right] = E\left\{\left(V(X) - V^*(X)\right)^2\right\} \tag{52}$$

can be written as:

$$\sigma_E^2(X) = \mathrm{Var}\left[V^*(X)\right] + \mathrm{Var}\left[V(X)\right] - 2\,\mathrm{Cov}\left[V^*(X), V(X)\right] \tag{53}$$

but:

$$\mathrm{Var}\left[V^*(X)\right] = \mathrm{Var}\left[\sum_{i=1}^{n} \lambda_i V_i\right] = \sum_{i,j=1}^{n} \lambda_i \lambda_j C_V\left(X_i, X_j\right) \tag{54}$$

and:

$$\mathrm{Cov}\left[V^*(X), V(X)\right] = \mathrm{Cov}\left[\sum_{i=1}^{\mathrm{n}} \lambda_i V_i, V(X)\right] = \sum_{i=1}^{n} \lambda_i C_V\left(X, X_i\right) \tag{55}$$

Therefore:

$$\sigma_E^2(X) = \mathrm{Var}\left[V(X)\right] + \sum_{i=1}^{\mathrm{n}}\sum_{j=1}^{\mathrm{n}} \lambda_i\, \lambda_j\, C_V\left(X_i, X_j\right) - 2\sum_{i=1}^{\mathrm{n}} \lambda_i\, C_V\left(X, X_i\right) \tag{56}$$

It is possible to minimize $\sigma_E^2(X)$ respecting the unbiasedness condition by resorting to the technique of Lagrange's multipliers. The following system of linear equations is obtained:

$$\sum_{j=1}^{\mathrm{n}} \lambda_j C_V\left(X_i, X_j\right) - \nu = C_V\left(X, X_i\right) \quad i = 1 \text{ to n} \tag{57}$$

Including Eq. (49), there is a total of $n$+1 equations that allow the determination of the n coefficients, $\lambda_j$, and of Lagrange's multiplier, $\nu$.

The corresponding minimized estimation variance is:

$$\sigma_E^2(X) = \mathrm{Var}\left[V(X)\right] + \nu - \sum_{i=1}^{n} \lambda_i C_V\left(X, X_i\right) \tag{58}$$

The estimator provided by *ordinary* kriging has been said to be more *robust* than that obtained by *simple* kriging. Since it does not require the knowledge of the field´s expected value, it can adapt itself better to local variations. However, the fact that the method implies no knowledge of the expected value only constitutes a marginal advantage because this parameter is generally better known than the autocovariance function.

*II.4.5.3. Cokriging*

A solution to the multifield problem identified in 4.3 can also be obtained resorting to the *simple* and the *ordinary* kriging approaches (Wackernagel, 2003 [13]; Delgado Muñiz, 2017 [14]).

The general expression of the multivariate estimator is defined as follow:

$$V^*(X) = \sum\nolimits_{i=1}^{n} \lambda_i V(X_i) + \sum\nolimits_{j=1}^{m} \beta_i S(X_j) \tag{59}$$

where the left side of the equation represents the primary property $V(X)$ and the right side the secondary property $S(X)$, $\lambda$ and $\beta$ are the influence weights of the primary and secondary properties.

In cokriging, the variance of the estimate is reduced because it implicitly considers the spatial correlation between the two properties (Chiles and Delfiner, 2012). The variance of the estimate is:

$$\sigma^2{}_{ECK}(X) = \mathrm{Var}\left[V(X)\right] + \mu_1 - \sum\nolimits_{i=1}^{n} \lambda_i C_V(X_n - X_i) - \sum\nolimits_{j=1}^{m} \beta_i C_{VS}(X_m - X_j) \tag{60}$$

where Var[$V(X)$] is the variance of the primary variable, $C_V$ y $C_{VS}$ are the primary and cross covariances, $\mu_1$ is a Lagrange multiplier.

*II.4.6. Nonparametric estimation of the conditional distribution function*

When applying the techniques of linear estimation to the indicator function (Auvinet, 2002 [1]) of a field, it is possible to obtain a non-parametric estimation (i.e. not requiring estimating the expected value, variance or other parameters) of the probability distribution function of the field values at any point. In fact, the linear estimation applied to the indicator function provides the conditional expectation of this function, which, being a binary function in 0 and 1, is equal to the probability:

$$P\left[V(X) \leq v \,\middle|\, data\right] = F_{V\,|data}(v; X) \tag{61}$$

The distribution function can be obtained one point at a time for different values of $v$. This possibility is quite valuable, particularly when characterizing the field through an expected value and variance is insufficient.

*II.5. Simulation of random fields*

The *simulation* is the process by which a possible configuration of a random field is generated in a way compatible with its descriptive parameters (*unconditional* simulation) or with these parameters and, furthermore, with the available data (*conditional* simulation). Several realizations or images of the field can thus be generated to allow the appreciation, in particular, of potentially critical extreme values.

The easiest way to simulate a random field consists of considering that such a field is represented by $n$ points $X_1, X_2, \ldots, X_n$ where realizations of the set of random variables $V(X_1), V(X_2), \ldots, V(X_n)$ should be obtained, with the appropriate field structure in what refers to the expected value and covariance matrix. The simulation is generally carried out on a mesh of points in the domain of interest and it therefore suffices to generate a certain number of jointly distributed random variables. An introduction to this topic is presented below.

*II.5.1. General technique*

The most common technique to sample at random a representative value of a random variable $V(X)$ with a certain probability distribution function, $F_V(v, X)$ consists of adopting a value $v$ such that:

$$F_V^{-1}(v, X) = u \tag{62}$$

where $u$ is a random number with uniform probability density ranging between 0 and 1 (Mood and Graybill, 1963 [12]). The main algorithms that allow generating random numbers with these characteristics have been presented by Fogli (1980 [15]).

If $V(X_1), V(X_2), \ldots, V(X_n)$ is the set of n random variables representative of the field intended to be simulated, and these variables are statistically independent, then their joint density and probability distribution functions can be expressed as:

$$f_{V_1,\ldots,V_n}(v_1,\ldots,v_n; X_1,\ldots,X_n) = \prod_{i=1}^{n} f_{V_i}(v_i; X_i) \tag{63}$$

$$F_{V_1,\ldots,V_n}(v_1,\ldots,v_n;X_1,\ldots,X_n)=\prod_{i=1}^{n}F_{V_i}(v_i;X_i) \tag{64}$$

where $f_{V_i}(v_i\,;X_i)$ and $F_{V_i}(v_i\,;X_i)$ are, respectively, the marginal (individual) functions of density and probability distribution of $V(X_i)$.

In this case, the random values of each variable can be generated separately and independently by means of the technique described before (Eq. (62)).

For a set of dependent random variables $V(X_1)$, $V(X_2)$,…, $V(X_n)$, the joint density and probability distribution functions can be expressed as:

$$f_{V_1,\ldots V_n}(v_1,\ldots,v_n;X_1,\ldots,X_n)=f_{V_1}(v_1;X_1)f_{V_2}(v_2\mid v_1;X_2)\ldots f_{V_n}(v_n\mid v_1,\ldots v_{n-1};X_n) \tag{65}$$

$$F_{V_1,\ldots V_n}(v_1,\ldots,v_n;X_1,\ldots,X_n)=F_{V_1}(v_1;X_1)F_{V_2}(v_2\mid v_1;X_2)\ldots F_{V_n}(v_n\mid v_1,\ldots v_{n-1};X_n) \tag{66}$$

where functions $f_{V_i}(v_i|v_1,\ldots,v_{i-1};X_i)$ and $F_{V_i}(v_i|v_1,\ldots,v_{i-1};X_i)$ represent, respectively, the conditional probability density and distribution function of $V(X_i)$ given that $V(X_1)= v_1$, $V(X_2) = v_2$,…, $V(X_{i-1}) = v_{i-1}$.

Because the random variables are dependent, it is no longer valid to use directly a set of uniformly distributed and independent random numbers to generate the desired values. When the field is of the Gaussian type or it has been transformed by anamorphosis into a Gaussian field, it is possible to use the procedure indicated below.

### *II.5.2. Unconditional simulation*

This type of simulation requires initially the generation of a sequence of *normally distributed independent standard random variables* (with zero mean and unit variance), obtained from two random variables, $U_i$ and $U_{i+1}$, uniformly distributed between 0 and 1 (Fogli, 1980 [15]):

$$\begin{aligned} Z_i &= \sqrt{-2\ln(1-U_i)}\cos(2\pi U_{i+1}) \\ Z_{i+1} &= \sqrt{-2\ln(1-U_i)}\,\mathrm{sen}(2\pi U_{i+1}) \end{aligned} \tag{67}$$

Alternatively, uniformly distributed random numbers can be generated using integrated tools accompanying the computational environment in which the simulation process is implemented.

On the other hand, the correlation matrix, $\boldsymbol{\rho}$, constituted by elements:

$$\rho_V(X_i,X_j)=\frac{C_V(X_i,X_j)}{\sigma_V(X_i)\sigma_V(X_j)} \tag{68}$$

can be broken down in the product of a lower triangular matrix and its transpose:

$$\mathbf{L}\mathbf{L}^T=\boldsymbol{\rho} \tag{69}$$

This operation, known as *Cholesky's decomposition* (Alabert, 1987 [16]), evidences certain shortcomings: it cannot be carried out when some of the variables $V(X_i)$ are perfectly correlated among themselves; it is difficult to calculate when the number of points in the field is too large; and it tends to generate numerical rounding errors. However, efficient standard algorithms are available for its calculation.

From matrix **L** of Eq. (69), it is possible to obtain a *correlated normal standard random field*, as a linear combination of the normal independent standard variables, $Z_j$:

$$G(X_i) = \sum_{j=1}^{i} L_{ij} Z_j ; \quad i = 1, 2, ..., \text{ n} \tag{70}$$

Finally, the known values of the mean and the variance are introduced to generate realizations of $V(X_i)$, in order to obtain the field simulation:

$$V(X_i) = \mu_V(X_i) + \sigma_V(X_i) G(X_i) \tag{71}$$

When the random field $V(X)$ has already been simulated, the realization obtained can be used as a starting point for a deterministic analysis. The simulation process can then be repeated as many times as desired to evaluate the variability of the results as part of a *Monte Carlo* analysis.

### *II.5.3. Conditional simulation*

It is now assumed that the random field $V(X)$ has been observed at points $X_1, X_2, \ldots, X_p$ and that it will be simulated at points $X_{p+1}, X_{p+2}, \ldots, X_{p+n}$. It is intended to generate realizations of $V(X)$ that precisely equal the data at $p$ points and that are random in the remaining $n$ - $p$ points.

The *conditional* simulation of a random field can be directly performed by the method discussed in the previous section, but using conditional expected values, variances and covariances of the available data. Points can be generated one at a time or simultaneously in groups of convenient size. The former approach seems to be the most efficient (Shinozuka, 1996 [17]). The simulated values are then incorporated into the data and new points can be generated.

### *II.5.4. Conditional simulation by copulas*

In copula-based random field descriptions, the multivariate copula model accounts for the multivariate dependence of the random field explicitly and is parametrized through bivariate spatial copulas.

Consider the conditioning of the random field $V(X)$ at $N$ locations by the set $\alpha$ consisting of $n$ observations. This task can be completed using the sequential simulation approach. In terms of copulas, the simulation process is formulated as follows (Vázquez-Guillén and Auvinet, 2014 [3]):

$$F_V(X_1; v_1) = C_{X|\alpha}\left(u_1 = F_V\left(V(X_1) \le v(X_1)\right) \middle| u_\alpha = F_V\left(v(X_\alpha)\right), \alpha = 1, ..., n\right) \tag{72}$$

$$F_V\left(X_2;v_2\right)=C_{X|\alpha}\left(u_2=F_V\left(V\left(X_2\right)\leq v\left(X_2\right)\right)\middle|u_\alpha=F_V\left(v\left(X_\alpha\right)\right),\alpha=1,...,n+1\right) \tag{73}$$

$$F_V\left(X_3;v_3\right)=C_{X|\alpha}\left(u_3=F_V\left(V\left(X_3\right)\leq v\left(X_3\right)\right)\middle|u_\alpha=F_V\left(v\left(X_\alpha\right)\right),\alpha=1,...,n+2\right) \tag{74}$$

$$F_V\left(X_N;v_N\right)=C_{X|\alpha}\left(u_N=F_V\left(V\left(X_N\right)\leq v\left(X_1\right)\right)\middle|u_\alpha=F_V\left(v\left(X_\alpha\right)\right),\alpha=1,...,n+N-1\right) \tag{75}$$

where $F_V(\cdot)$ is the first-order distribution function and $C_{X|\alpha}(\ )$ is the conditional copula.

The simulation process is restricted to local neighborhoods $X_i$, for $i$=1,…, $n$ closest to the node to be simulated. This decision is supported by the fact that further away conditioning data is "screened" by the information content of nearest data. The values $u_\alpha$, include both original data (prior distribution) and previously simulated nodes. The simulation process can be performed by visiting unsampled locations at random over a mesh. After visiting all nodes of the mesh, the process is completed (Vázquez-Guillén and Auvinet, 2015 [6]).

## *References for Appendix II*


[1] Auvinet, G., (2002). "Uncertainty in Geotechnical Engineering/Incertidumbre en Geotecnia", Sixteenth Nabor Carrillo Lecture/Decimosexta Conferencia Nabor Carrillo. (English/Español), Sociedad Mexicana de Mecánica de Suelos, Mexico, 131p., ISBN: 968-5350 10-8.

[2] Deutsch, C. and Journel, A., (1992). GSLIB Geostatistical software library and user's guide: Oxford University Press, New York, 340p.

[3] Vázquez, F. y Auvinet, G., (2014). "Simulación de campos aleatorios con dependencia no multigaussiana empleando cópulas", Ingeniería, Investigación y Tecnología, FI-UNAM, Vol. XV, Núm 4, Mexico.

[4] Nelsen, R.B. (2006). "An introduction to copulas", Springer-Verlag, New York, 2nd Edition, pp. 269.

[5] Bárdossy, A. (2006). "Copula-based geostatistical models for groundwater quality parameters", Water Resour. Res., 42, W11416 (1 of 12).

[6] Vásquez-Guillén, F. y Auvinet, G., (2015). "Simulación de campos aleatorios espacio-temporales utilizando un filtro de Kalman modificado", Ingeniería, Investigación y Tecnología, FI-UNAM, Vol. XVI, Núm 1, 1-12, Mexico.

[7] Vázquez-Guillén, F. and Auvinet, G. (2017). "Identification of hydraulic conductivities via ensemble Kalman filtering with transformed data considering the risk of systematic bias", Geofísica Internacional, 56(4), pp. 317-333.

[8] Papoulis, A., (1985). Probability, Random variables and Stochastic Processes, McGrawHill, USA.

[9] Krige, D. G., (1962). "Statistical application in mine valuation", J. Institute Mine Survey, South Africa

[10] Matheron, G., (1965). "Les variables généralisées et leur estimation", Masson et Cie, France.

[11] Chiles, J.P. and Delfiner, P., (1999). "Geostatistics, Modeling spatial uncertainty", John Wiley and Sons, INC.

[12] Mood, A. M. and Graybill, F.A., (1963). "Introduction to the Theory of Statistics", Mc Graw-Hill Book Company, Inc., New York, USA.

[13] Wackernagel, H., (2003). Multivariate Geostatistics. An Introduction with Applications. Springer, 3rd Edition, Berlin, Germany, 387p.

[14] Delgado Muñiz, M., (2017). "Análisis geoestadístico multivariable de las propiedades geotécnicas del subsuelo lacustre del valle de México", Tesis de maestría, Programa de Maestría y Doctorado en Ingeniería, Ingeniería Civil, Geotecnia, UNAM, Ciudad de México, Mexico.

[15] Fogli, M., (1980). "L'approche de Monte Carlo dans les problèmes de sécurité: Application à l'estimation du risque de ruine des poutres hyperstatiques en béton armé soumises à des actions aléatoires statiques », Thèse de Docteur Ingénieur, INSA, Lyon, France, 217 p.

[16] Alabert, F., (1987). "The practice of fast conditional simulations through the LU decomposition of the covariance matrix". Mathematical Geology, Vol. 19, N° 5, pp. 369-386.

[17] Shinozuka, M., (1996). "Equivalence between Kriging and CPDF Methods for conditional simulation". Journal of Engineering Mechanics, ASCE, pp 530-538.

## Appendix III. Reduction of variance in a 1D random field with exponential autocorrelation coefficient

*III.1. Exponential autocorrelation coefficient*

A one-dimensional stationary random field *V*(*X*), where *X* is an abscissa in a one-dimensional domain is said to present an exponential autocorrelation coefficient function (normalized autocovariance), $\rho$ ,when for any interval such as $X_1$-$X_2 = \tau$ , this function can be expressed as:

$$\rho = e^{\frac{-\tau}{a}} ; \tau > 0 \tag{1}$$

where *a* is the area below the graph of the autocorrelation function:

$$\int_0^{\infty} e^{\frac{-\tau}{a}} d\tau = \left[ \frac{e^{\frac{-\tau}{a}}}{\frac{-1}{a}} \right]_0^{\infty} = a \tag{2}$$

Distance $\delta = 2a$ is known as the *correlation distance.*

*III.2. Variance of the average value of a random field in an interval with length L*

Taking into account Eq. (25) of Appendix II:

$$\mathrm{Var}\left[V_L\right] = \mathrm{Var}\left[V\right]\frac{1}{L^2}\int_0^L\int_0^L e^{-\frac{|y-x|}{a}} dxdy = 2\mathrm{Var}\left[V\right]\frac{1}{L^2}\int_0^L\int_0^y e^{-\frac{(y-x)}{a}} dxdy \tag{3}$$

$$\mathrm{Var}\left[V_L\right] = 2\mathrm{Var}\left[V\right]\frac{1}{L^2}\int_0^L e^{-\frac{y}{a}} dy \int_0^y e^{\frac{x}{a}} dx \tag{4}$$

$$\mathrm{Var}\left[V_L\right] = 2\mathrm{Var}\left[V\right]\frac{1}{L^2}\int_0^L e^{\frac{-y}{a}} \left( \frac{e^{\frac{x}{a}}}{\frac{1}{a}} - a \right)_0^y dy \tag{5}$$

$$\mathrm{Var}\left[V_L\right] = 2a\mathrm{Var}\left[V\right]\frac{1}{L^2}\int_0^L \left(1 - e^{\frac{-y}{a}}\right) dy = 2a\mathrm{Var}\left[V\right]\frac{1}{L^2}\left[ L - \left( \frac{e^{\frac{-y}{a}}}{-\frac{1}{a}} \right)_0^L \right] \tag{6}$$

$$\mathrm{Var}\left[V_L\right] = 2a\mathrm{Var}\left[V\right]\frac{1}{L^2}\left[L + \frac{e^{\frac{-L}{a}}}{\frac{1}{a}} - a\right] = \frac{2a^2}{L^2}\mathrm{Var}\left[V\right]\left[\frac{L}{a} + e^{\frac{-L}{a}} - 1\right] \tag{7}$$

*III.3. Covariance between average values defined on two non-overlapping segments*

The average values of the field are defined in two non-overlapping intervals ($x_1$, $x_2$), ($y_1$, $y_2$), with length $L_1$ and $L_2$ respectively and with ($y_1 > x_2$ ). The autocorrelation coefficient (normalized autocovariance) is:

$$\rho = e^{\frac{-\tau}{a}}; \tau > 0 \tag{8}$$

Calling $V_{L1}$ the average value of the field in interval ($x_1$, $x_2$) and $V_{L2}$ the average value in interval ($y_1$, $y_2$):

$$\mathrm{Cov}\left[V_{L1}, V_{L2}\right] = \mathrm{Var}\left[V\right]\frac{1}{L_1 L_2}\int_{y_1}^{y_2}\int_{x_1}^{x_2} e^{\frac{-|y-x|}{a}}\,dxdy \tag{9}$$

$$\mathrm{Cov}\left[V_{L1}, V_{L2}\right] = \mathrm{Var}\left[V\right]\frac{1}{L_1 L_2}\int_{y_1}^{y_2} e^{\frac{y}{a}}dy\int_{x_1}^{x_2} e^{\frac{x}{a}}dx \tag{10}$$

$$\mathrm{Cov}\left[V_{L1}, V_{L2}\right] = \mathrm{Var}\left[V\right]\frac{1}{L_1 L_2}\left[\frac{e^{\frac{-y}{a}}}{\frac{-1}{a}}\right]_{y_1}^{y_2}\left[\frac{e^{\frac{-x}{a}}}{\frac{1}{a}}\right]_{x_1}^{x_2} \tag{11}$$

$$\mathrm{Cov}\left[V_{L1}, V_{L2}\right] = \mathrm{Var}\left[V\right]\frac{a^2}{L_1 L_2}\left[e^{\frac{-y_1}{a}} - e^{\frac{-y_2}{a}}\right]\left[e^{\frac{x_2}{a}} - e^{\frac{x_1}{a}}\right] \tag{12}$$